Implementation of Human-Induced Pluripotent Stem Cell-Derived Cardiomyocytes to Model Excitation-Contraction Coupling in Health and Disease

By

Tromondae K. Feaster

Dissertation

Submitted to the Faculty of the

Graduate School of Vanderbilt University

in partial fulfillment of the requirements

for the degree of

DOCTOR OF PHILOSOPHY

in

Pharmacology

December, 2015

Nashville, Tennessee

Approved:

Joey V. Barnett, Ph.D.

Björn C. Knollmann, M.D., Ph.D.

Dan M. Roden, M.D.

H. Scott Baldwin, M.D.

Charles C. Hong, M.D., Ph.D.

This work is dedicated to my amazing wife, Patrice, your love and support have made this possible

and

To my mother, father, brother and sister for always encouraging, supporting and praying for me.

We made it.

ACKNOWLEDGMENTS

This would not have been possible without the help of many people. First, I would like to thank my mentor Dr. Charles C. Hong. Dr. Hong has been an amazing mentor. He has taught me the importance of being relentless and critical about my science. He has enabled me to explore my scientific curiosity, without restraint, and hone my critical thinking skills and ability to address complex questions.

Next, I would like to thank my co-mentor Dr. Björn C. Knollmann. Dr. Knollmann has been instrumental in my PhD training. He has shown me the importance of detailed hypothesis driven science and thoughtful experimental design, including appropriate controls. Dr. Knollmann has continually urged me to identify and perform key experiments, even if they appear challenging. I am especially indebted to him for the countless hours he has spent teaching me about cardiovascular physiology, grantsmanship and life in general.

I should also take this time to thank my Dissertation Committee chair Dr. Joey V. Barnett. Dr. Barnett has been deeply involved in my training as a positive role model, mentor and advocate, and encouraged me when needed. I would like to thank my entire Dissertation Committee including, Drs. Dan M. Roden and H. Scott Baldwin. You all have provided tremendous support and council throughout this process.

I am grateful for the many colleagues and collaborators who have contributed to my training over the years. A special thanks to Dr. Hyun Seok Hwang, Dr. Lili Wang, Mr. Adrian G. Cadar, Mr. Kevin Bersell, Dr. Young W. Chun, Dr. Jonathan E. Hempel, Dr. Joseph C. Wu, Mr. Charles H. Williams, Mrs. Audrey Frist, Dr. Lee E Limbird, Dr. Margaret Whalen, Mrs. Cynthia Merritt, Mrs. Cheryl Seneff and Mrs. Karen Gieg; as well as the entire Hong and Knollmann laboratories and personnel. Finally, I would like to thank the pharmacology and cardiovascular departments and personnel.

SOURCE OF FUNDING

This work was partly supported by the United States National Institutes of Health [HL88635, HL71670 & HL108173 to B.C.K.; NIH HL104040 to C.C.H.]; by the American Heart Association [13IRG13680003 to B.C.K., 12SDG12050597 to H.S.H., 12POST12080080 to D.K.], and by the Veterans Administration Merit Grant BX000771 to C.C.H.

Page

LIST OF TABLES

LIST OF FIGURES

LIST OF ABBREVIATIONS

AFM	Atomic force microscopy
Ca	Calcium
CM	Cardiomyocyte
cAMP	Cyclic adenosine monophosphate
CICR	Calcium induced calcium release
cTnI	Cardiac troponin I
DAD	Delayed afterdepolarization
DCM	Dilated cardiomyopathy
EAD	Early afterdepolarization
EB	Embryoid body
EC	Excitation-contraction
EC50	Half maximal effective concentration
ECG	Electrocardiograph
ECM	Extracellular matrix
EHT	Engineered heart tissue
HCM	Hypertrophic cardiomyopathy
hESC	Human embryonic stem cell

HF	Heart failure
hiPSC	Human induced pluripotent stem cell
HTS	High-throughput
HTS	High-throughput screen
ICa	L-type Ca channel
ICD	Implantable cardioverter defibrillator
IK1	Inward rectifier potassium ion channel
IKr	Rapid activating potassium ion channel
IKs	Slow activating potassium ion channel
INa	Sodium current
LAD	Left anterior descending artery
MOI	Multiplicity of infection
NCX	Na/Ca exchanger
OHT	Orthotopic heart transplantation
PDE	Phosphodiesterase
PKA	Protein Kinase A
PMCA	Plasma membrane ATPase
RCM	Restrictive cardiomyopathy

RyR2 Ryanodine receptor

SCD Sudden cardiac death

SERCA Sarcoendoplasmic reticulum Ca ATPase

SR Sarcoplasmic reticulum

SR Sarcoplasmic reticulum

ssTnI Slow skeletal troponin I

TdP Torsades de pointes

TFM Traction force microscopy

WT Wild type

Chapter 1

INTRODUCTION

1.1 Cardiac excitation-contraction coupling

Cardiac excitation-contraction (EC) coupling is a tightly regulated process, which is required for the heart to maintain proper functions [1]. These functions include pumping blood to the body, supplying oxygen and nutrients, eliminating waste and thermoregulation. These complex organ level processes can be broken down to the level of the individual cardiomyocyte (CM), the major structural and functional unit of the heart, responsible for contraction. This can be further broken down to the mechanisms that regulate CM physiology specifically EC coupling (Figure 1). EC coupling is the delicate balance between electrical excitation and mechanical contraction. This process is largely driven by the second messenger calcium (Ca) which links excitation and contraction and enables the heart to maintain adequate cardiac output to meet the needs of the body. However, in acquired and genetic situations in which the heart is not capable of supporting the needs of the body, heart failure ensues.

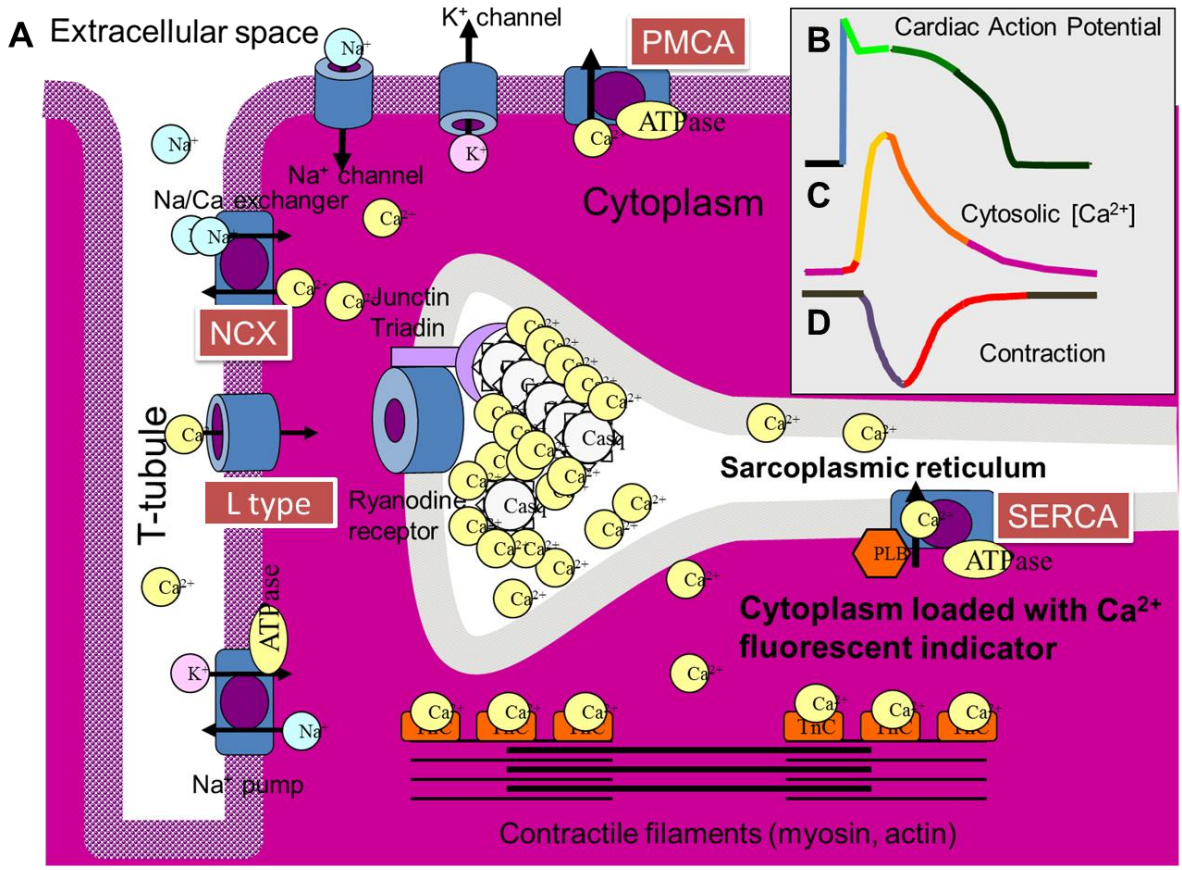

Figure 1. Schematic of human cardiac excitation-contraction coupling. A, Schematic of key EC coupling protein localization and function. Note the key sarcolemma Ca handling proteins: L-type Ca channel, NCX and PMCA as well as the intracellular SR calcium transporter SERCA. B, Cardiac action potential recording. C, Ca handling transient. D, Contraction trace. B – D demonstrates the temporal relationship between electrical depolarization, Ca flux and contraction. (Adapted from, Knollmann B., *Ph.D. Dissertation.* 1999).

Cardiomyocyte electrophysiology

Under physiological conditions each ventricular cardiac cycle is regulated by an array of ion channels and transporters that actively and passively regulate CM membrane potential (Figure 2) [2]. Changes in the membrane potential may result in CM depolarization, which during normal EC coupling is initiated by the fast inward sodium current (I_{Na}) (Figure 1 B and Figure 2 A and B). This rapid depolarizing current is responsible for Phase 0 of the human cardiac action potential morphology (Figure 2 B). Inactivation of the inward sodium current results in Phase 1 of the action potential producing a relatively small downward defection also referred to as the “notch”; that is driven by the outward potassium current including (I_{to}). Next, during Phase 2 of the action potential L-type Ca channels (I_{Ca}) open enabling the influx of Ca concurrent with potassium efflux through slow delayed potassium channels. This is indicated by the plateau of the action potential morphology (Figure 2 B). Once the L-type Ca channels close, the outward potassium channels (I_{Kr} and I_{Ks}) dominate the membrane potential resulting in repolarization represented as Phase 3. Finally, the CM membrane is returned to the resting state, Phase 4, which is largely driven by the CM conductance for potassium and inward rectifier potassium ion channels (I_{K1}) (Figure 2 B).

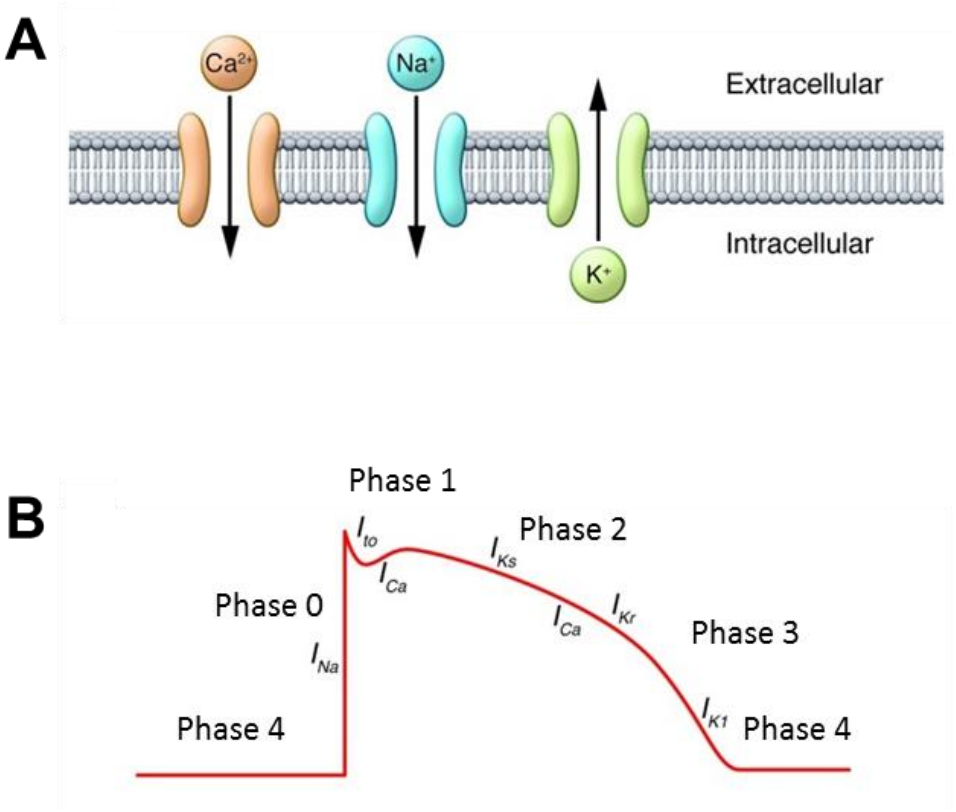

Figure 2. Human cardiac electrophysiological characteristics. A, Schematic of ion movement across CM membrane indicating calcium and sodium movement down their electrochemical gradient into the CM and potassium movement out of the CM. B, Action potential trace, depicting responsible currents for each phase of the action potential morphology. Phase 0 is initiated by depolarizing fast activating sodium current I_{na}. Next, the phase 1 transient activating potassium current I_{to} drives the relatively small downward notch. The balance between L-type calcium current I_{ca} and potassium currents I_{Kr} and I_{ks} is responsible for the phase 2 plateau. Finally, the potassium current I_{K1} dominates the membrane potential repolarizing the CM and returning it to Phase 4. (Adapted from, George A., *The Journal of Clinical Investigation.* 2013; 123(1):75-83).

Cardiomyocyte calcium handing

The change in CM electrical potential drives changes in CM Ca handling (Figure 1 C). At steady state the relatively small amount of free Ca in the cytoplasm is not sufficient to achieve threshold and initiate CM contraction [3]. After initial depolarization of the CM L-type Ca channels open producing a relatively small increase in intracellular Ca (Figure 1 C); this Ca is responsible for activating receptors in the sarcoplasmic reticulum (SR), the intracellular Ca store, in a mechanism known as calcium induced calcium release (CICR). This enables the SR to release a relatively large amount of free Ca into the cytoplasm resulting in the upward spike of the Ca transient morphology (Figure 1 C). This Ca is then free to bind to intracellular Ca binding sites (e.g., troponin C) to effect contraction. There are two primary Ca removal pathways responsible for Ca efflux (Figure 1) from the cytoplasm, the sarcoendoplasmic reticulum Ca ATPase (SERCA) and the Na/Ca exchanger (NCX) with other non-NCX and non-SR removal pathways such as the plasma membrane Ca ATPase (PMCA) and mitochondria contributing less than 5%. These removal pathways are responsible for returning the CM to the resting Ca concentration [4] resulting in Ca decay as indicated by the decline of the Ca transient morphology (Figure 1 C).

Cardiomyocyte contractility

The interaction between Ca and the myofilament regulates sarcomere and cell shortening, resulting in contraction of the CM. Ca released from the SR binds to intracellular Ca sites including the troponin complex of the thin filament (Figure 1). The troponin complex is composed of three subunits: troponin C, which directly binds Ca acting as a Ca dependent regulator of contraction [3]. Troponin I the inhibitory subunit, which inhibits the actin and myosin interaction, acting as a negative regulator of contraction, and the troponin T subunit which binds tropomyosin stabilizing the troponin-tropomyosin complex. The majority of free Ca binds to troponin C resulting in a conformation change in the troponin I subunit. This conformation

change moves troponin I out of an inhibitory positon and enables myosin within the thick filament to interact with actin, of the thin filament, enabling cross bridge formation resulting in cell shortening and contraction (Figure 1 D).

1.2 Induced pluripotent stem cell technology

Human induced pluripotent stem cells

In 2007 two seminal papers were published in the journals *Cell* and *Science* that represented a significant scientific advance in stem cell technology. Yamanaka and colleagues [5] and Thomson and colleagues [6] demonstrated that stem cells with similar characteristics as human embryonic stem cells (hESC) could be generated from human fibroblasts by expressing specific pluripotency genes (e.g., Oct4, Sox2, Klf4, and C-Myc/L-Myc). These cells were termed human induced pluripotent stem cells (hiPSCs) (Figure 3). HiPSCs, like hESCs, are capable of self-renewal and pluripotency. For decades, since the establishment of hESCs in 1998 [7], by James Thomson, researchers have been working to unlock the full potential of hESCs. However, efforts have been hampered by ethical, political and legal controversy surrounding hESC use.

The establishment of hiPSCs represents a cell source with similar promise as hESCs, however, with the added benefits of avoiding the negative issues surrounding their use. In addition hiPSCs have the unique attribute of being derived from healthy or patient's somatic cells, representing disease-specific stem cells, a major advance for regenerative medicine and disease modeling. Initial hiPSC reprogramming strategies, while sufficient, were limited by low efficiency (< 1 %), dependence on mouse embryonic fibroblasts as feeder layer and retrovirus or lentivirus reprogramming strategies (Figure 3 A) that may result in transgene integration in

the host genome and potential adverse effects, such as tumor formation. Since then additional reprogramming strategies have been developed to address these pitfalls. For instance feeder-free and integration-free based methods such as sendai virus and plasmid (i.e., 7 F2 and Epi 5) (Figure 3 A and Figure 4 B and D). These methods typically express similar pluripotency genes and have enabled many groups in basic science and industry to generate hiPSC from various somatic cell sources. Most notably fibroblasts (Figure 5 A) from skin punch biopsy and peripheral blood mononuclear cells from routine blood draw. Plasmid-based reprogramming factors are introduced into somatic cells by transfection systems that have become standard at many institutions (Figure 4 A and C). For standardization, each of the hiPSC lines is validated by demonstration of key hESC-like features such as morphology (Figure 5 B) and expression of pluripotency markers (Figure 5 C and D). The implementation of hiPSC technology has enabled the development of novel directed differentiation protocols to transform hiPSC to various cell types; such as neurons, hepatocytes, endothelial cells and cardiomyocytes.

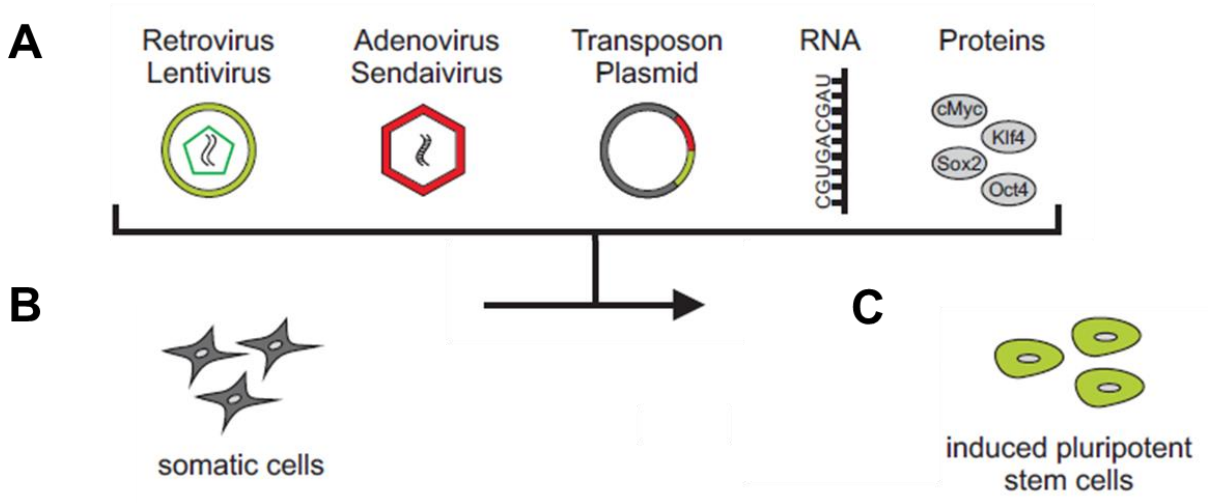

Figure 3. hiPSC reprogramming. A, Reprogramming strategies including integrating and non-integrating viral based methods and non-integrating plasmid, RNA and protein based methods. B, Isolated somatic cells (e.g., fibroblast or peripheral blood mononuclear cells) expanded in culture and reprogrammed by exposing the somatic cells to reprogramming factors (see figure 4) to generate induced pluripotent stem cells, C. (Adapted from, Friedrichs et al, TCM 2012).

A

B

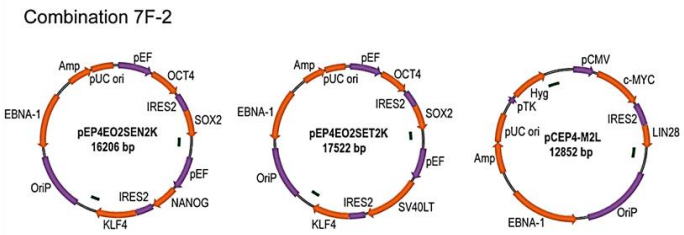

C

D

Component*	Vectors	Genes
Epi5™ Reprogramming Vectors	pCE-hOCT3/4	Oct4
	pCE-hSK	Sox2, Kfl4
	pCE-hUL	L-Myc, Lin28
Epi5™ p53 & EBNA Vectors	pCE-mP53DD	mp53DD
	pCXB-EBNA1	EBNA1

Figure 4. Reprogramming systems and plasmids. A, Amaxa biosystems nucleofector II ("Nucleofector™ 2b Manual." Lonza. Web. 2015). B, Combination 7F-2 plasmids expressing factors OCT4, SOX2, c-MYC, NANOG, KFL4 and LIN28 (Junying Y. et al., *PLoS ONE.* 2011; doi:10.1371/journal.pone.0017557). C, ThermoFisher Scientific neon transfection system ("Neon® Transfection System. *Product Information*. Web. 2015). D, Epi5 episomal iPSC reprogramming vectors expressing reprogramming factors OCT4, SOX2, KFL4 L-MYC, LIN28. Epi5 plasmids are 2nd generation plasmids that benefit from the addition of a p53 suppressor gene, which improves reprogramming efficiencies. And contain L-MYC instead of the highly tumorigenic c-MYC (Episomal IPSC Reprogramming Kit." Life Technologies. Web. 2013.)

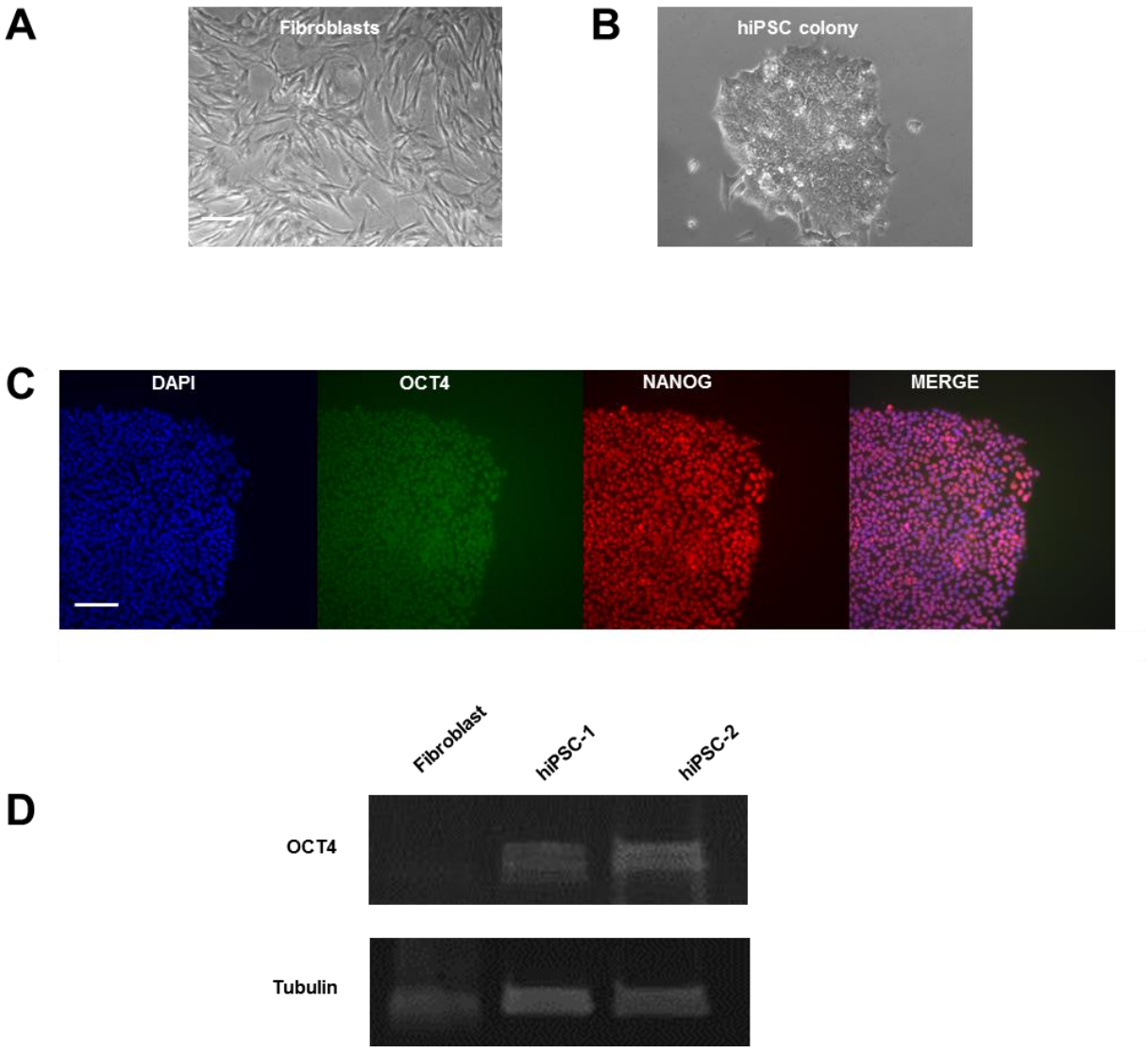

Figure 5. hiPSC validation. Bright field images of A, Somatic cells (cardiac fibroblast) expanded in culture. And B, typical morphology of reprogrammed hiPSC colony. C, Immunofluorescence images of hiPSC for DAPI (blue) and pluripotency markers OCT4 (green) and NANOG (red) demonstrating successful reprogramming and generation of hiPSC. Scale bar 100 µm. D, PCR analysis for pluripotency marker OCT4 in two independently generated hiPSC lines, fibroblast included as negative control. (Representative hiPSCs images A – C and example PCR analysis D shown are from Vanderbilt hiPSCs).

Human induced pluripotent stem cell derived cardiomyocytes

Substantial progress has been made in hiPSC-CM cardiac differentiation protocols, evolving from the inefficient and variable aggregation-based method (i.e., embryoid body (EB)). Traditional EB based methods generate spontaneously beating CMs by forced aggregation of hiPSCs, thought to mimic the environment of the early embryo, under high serum conditions. This method resulted in low yields of hiPSC-CMs (< 1 %). However, since then more robust monolayer-based methods (i.e., > 80 % hiPSC-CMs) such as the Matrigel sandwich method (Figure 6 A) have been developed, which benefit from the defined sequential application of growth factors and cytokines targeting distinct signaling pathways implicated in human cardiomyogenisis (e.g., transforming growth factor – β (TGFβ), activin A and BMP4). This method provides a significant advance in cardiac differentiation methodology by greatly increasing hiPSC-CM yield for most laboratories. However, the Matrigel sandwich method was limited by the undefined chemical nature of the reagents and high cost of Matrigel. For these reasons a small molecule method (Figure 6 B) [8-10] was developed, based on the temporal modulation of the Wnt signaling pathway, and a completely chemically defined monolayer-based method [10]. To characterize and validate cardiac differentiation efficiency hiPSC-CMs are evaluated for cardiac phenotype (Figure 7 A) such as spontaneous beating and expression of cardiac specific markers (Figure 7 B and C).

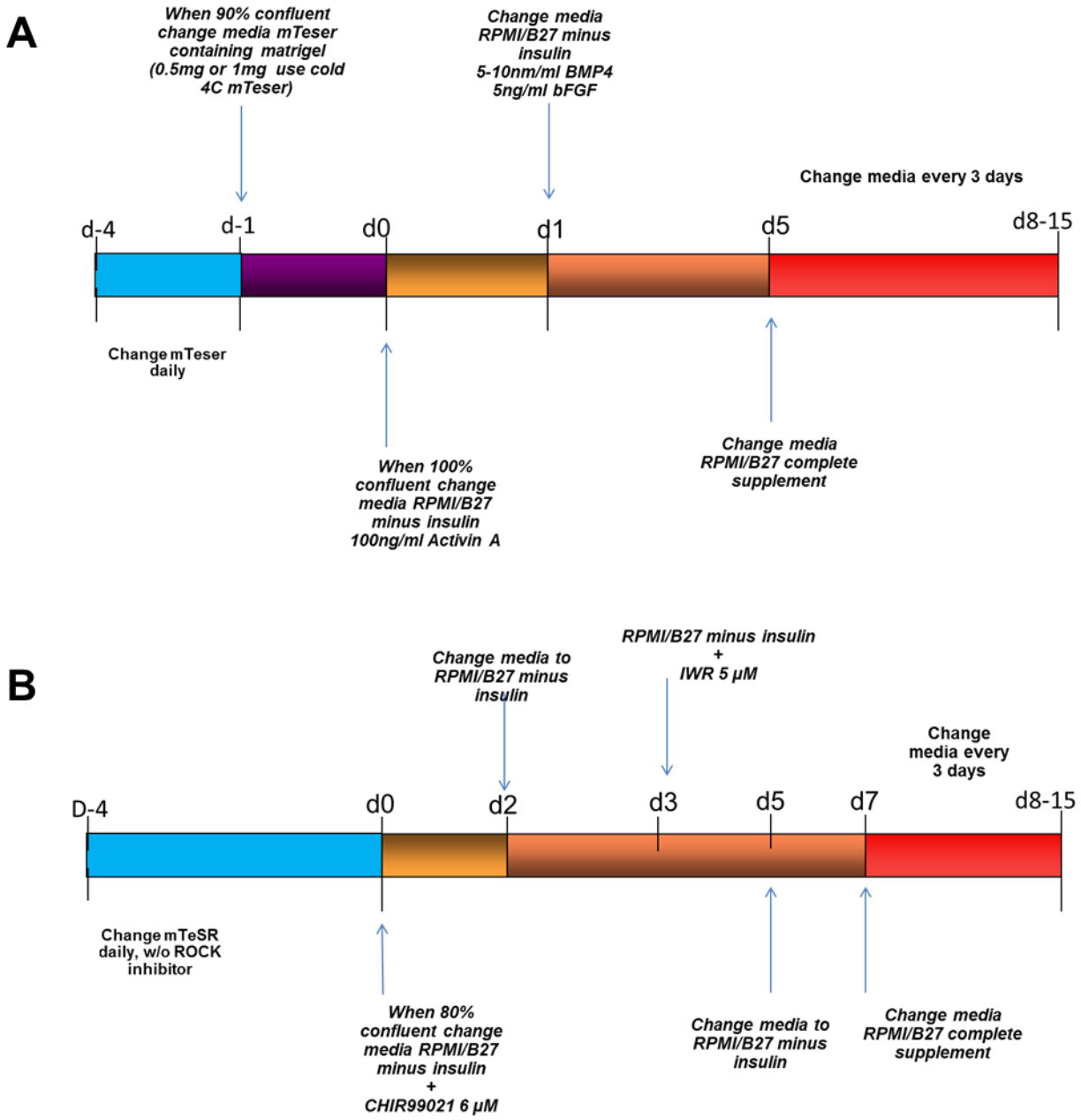

Figure 6. Monolayer cardiac differentiation methods. A, Matrigel sandwich method. Work flow demonstrating the stage specific sequential application of growth factors and proteins, including the addition of a thin layer of ECM (i.e., matrigel). (Adapted from Zhang J et al., *Circulation Research.* 2012; 111(9):1125-36)B, Small molecule based method. Work flow displaying the temporal modulation of the Wnt signaling pathway. Early (day 0) activation with the small molecule Wnt agonist, CHIR99021, and late (day 3) inhibition with Wnt antagonist, IWR-1. (Burridge P. et al., *Nature Methods.* 2014; 11(8): 855–860).

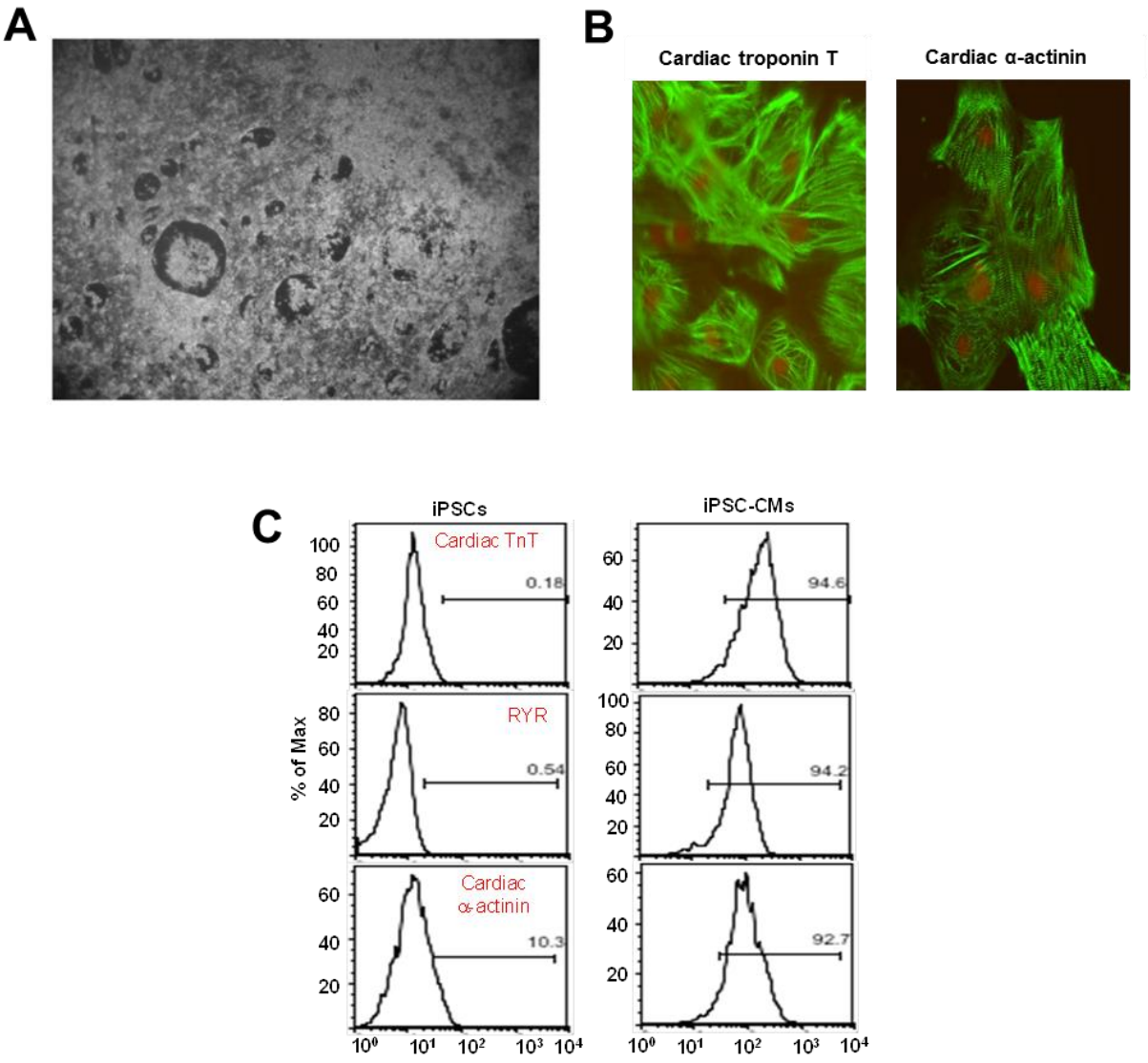

Figure 7. hiPSC-CM validation. A, Bright field image of a 2D monolayer sheet of hiPSC-CMs. Courtesy of Mr. Calvin Sheng B, Immunofluorescence staining of hiPSC-CMs for cardiac markers (green) troponin T (left panel) and α-actinin (right panel), and nucleus DAPI (red). Scale bar 20 µm. C, FAC analysis demonstrating greater than 90 % pure population of hiPSC-CMs, cardiac markers troponin T (TnT), ryanodine receptor (RYR) and α-actinin. (Representative hiPSC-CM images A – B and example FAC analysis C shown are from Vanderbilt University hiPSC-CMs derived from hiPSC line CC2). Panel B and C courtesy of Dr. Young Wook Chun.

State of hiPSC-CM E-C coupling

HiPSC-CMs recapitulate key aspects of human CM biology. For example hiPSC-CMs contain the appropriate machinery to contract *in vitro* and respond appropriately to electrical stimulation. HiPSC-CMs express key sarcomeric and Ca handling proteins, similar to native myocardium [9, 11] and recapitulate several inherited heart disease phenotypes [12, 13]; thus representing a theoretically unlimited source of human CMs for experimental studies. The utility of these cells has reproducibly been demonstrated for basic research, drug discovery, and preclinical cardiotoxicty. However, there remains a major hurdle which is the clinical translatability of these cells and results obtain from them. The majority of reports suggest that hiPSC-CMs, while useful, represent a relatively immature phenotype. For example (Table 1) [11] compares immature CMs to adult CMs and highlights key structural, molecular and functional differences in hiPSC-CMs and their adult counterparts. Structurally, like immature CMs, hiPSC-CMs are circular and small relative to adult ventricular CMs and display unorganized sarcomeres with decreased sarcomere length. In addition hiPSC-CMs lack T-tubules, which are deep invaginations in the CM membrane, necessary for uniform EC coupling properties. Molecularly several isoforms present in adult-CMs are poorly expressed in immature CMs and hiPSC-CMs. For example, hiPSC-CMs primarily express the fetal slow skeletal troponin I (ssTnI) instead of the mature adult cardiac troponin I (cTnI), even with extended time in culture (e.g., 9 months) [14].

Functionally the EC coupling of hiPSC-CMs have not been investigated in great detail. However, it is accepted that hiPSC-CM electrophysiological properties include significantly reduced upstroke velocity and depolarized resting membrane potentials characteristic of immature CMs. With respect to Ca handling properties hiPSC-CMs generated by EB-based cardiac differentiation methods, at various ages (e.g., day 7 – 60), display either lack of caffeine releasable SR Ca stores [11] or their presence only in a sub-population of CMs [12, 15-17],

suggesting immature or underdeveloped Ca handling properties. A recent report characterized Ca handling of hiPSC-CMs generated by the monolayer-based Matrigel Sandwich method [9]. However, this study only evaluated twitch Ca handling properties in response to different pacing rates, while SR content and function were not evaluated. Moreover, Ca fluorescence measurements were obtained from clumps or clusters of cells, not single cells. These cases highlight the need for a detailed systematic evaluation of these properties in single hiPSC-CMs.

The contractile properties of hiPSC-CMs remain among the least studied parameters of EC coupling. Various methods have been attempted to assess contractility of hiPSC-CMs however single cell measurements have been notoriously difficult to obtain. Hence, many researchers have transitioned to multicellular preparations (e.g., EHTs, BioWire or XCELLigence). These methods provide high-content readout of contractile function and when coupled with a Ca sensitive dye, enable simultaneous Ca and contractile measurements [18]. However, as these are multicellular preparations they are inherently heterogeneous, which may mask the individual CM properties and are extremely costly. To elucidate what makes the hiPSC-CM contractile phenotype, single cell analyses are required.

Traditionally, the method of choice for measuring single rod shaped adult-CM contractile properties has been video-based microscopy, evaluating changes in cell or sarcomere length [19]. However, this method has not been routine for hiPSC-CMs, which exhibit relatively immature sarcomere architecture including circular shape and unaligned myofilament alignment. In addition, under standard culture condition, hiPSC-CMs, do not display a dominant contraction axis, as their edges are firmly attached to the culture substrate and do not move with each contraction cycle. Instead the inside of the cell (i.e., nuclear region) displays observable movement [20, 21].

For these reasons single cell contractility methods (e.g., traction force microscopy (TFM), atomic force microscopy (AFM) or image-based rhythmic methods) have been used [19] however these methods have certain caveats. For example; AFM is highly invasive and not fitting for long term measurements. In addition several methods have been developed focusing on image or pixel based analysis of non-shortening hiPSC-CMs (i.e., no change in cellular geometry). These measurements are not ideal as they represent intracellular movement instead of whole cell movement which may hinder detailed studies of hiPSC-CM mechanical properties [7, 9]. Moreover, impedance changes and changes in beat frequency are *not* representative of hiPSC-CM mechanical properties.

Previous attempts to evaluate single hiPSC-CM contraction, using video edge-detection, to evaluate changes in cellular shortening, of "early-stage" hiPSC-CM, (i.e., day 20 – 40) suggest that these hiPSC-CMs, display contractions of approximately 5 % of their resting cell length. In addition the same report suggests late-stage hiPSC-CMs (i.e., day 100 – 120) contract approximately 10 % and exhibit slowed contractile kinetics, relative to the early stage hiPSC-CMs [22]. The authors conclude that late stage hiPSC-CMs display "matured" contractile properties however these results have yet to be reproduced. The lack of reliable user-friendly contractility methods limits the study of hiPSC-CM contractility in most laboratories thus limiting our understanding of hiPSC-CM EC coupling.

To the best of our knowledge no report has compared hiPSC-CM E-C coupling properties (i.e., electrophysiology, Ca handling and contractility) to adult human CMs under identical experimental conditions. Currently there is little available information regarding the human CM *in vitro* phenotype this due to the quality of human samples and harsh isolation protocols that may alter CM physiology. For this reason a side-by-side comparison of hiPSC-CMs and human adult-CMs would be of great use to the field. However, because of the lack of

available human adult cardiac tissue for such comparison animal adult CMs (e.g., rabbit-CMs) are the next logical step.

Table 1. Comparison between immature and adult CMs

	Parameter	Immature CMs	Adult CMs
Morphology	Cell Shape	Circular	Rod Shaped
Sarcomere	Structure	Disarrayed	Organized
	Length	1.6 µm	2.2 µm
Myofibrillar isoform	Troponin I	ssTnI/TNNI1	cTnI/TNNI3
	MHC	β > α	β >> α
E-C Coupling			
Electrophysiological Properties	Upstroke Velocity	50 V/s	250 V/s
	Resting Membrane Potential	-60 mV	-90 mV
Calcium Handling		Partially Developed	Mature
Contractile Properties	Force	nN	µN
β adrenergic response	Chronotropic	Yes	Yes
	Inotropic	No	Yes

Table 1. Comparison between immature and adult CMs. (Adapted from Yang X. et al., *Circulation Research* 2014; 114(3):511-23).

1.3 Heart failure

Heart failure (HF) is a leading cause of morbidity and mortality in the developed world, affecting 5.7 million Americans (Figure 8) and accounting for over 280,000 US deaths annually [1]. This creates an enormous financial burden that is projected to result in 77 billion dollars of direct cost, in the US alone by the year 2030 (Figure 8 B). Primary cardiomyopathy, defined as abnormal heart muscle structure and function in the absence of significant coronary artery disease is increasingly recognized as an important cause of severe HF, particularly in the young. Moreover, because most primary cardiomyopathy cases have a genetic root cause in sarcomere components, it is widely accepted that a better understanding of their molecular pathophysiology will elucidate the pathogenesis of HF in general, and guide development of future therapies and treatments. For example studies in transgenic mice carrying various mutations indicate autosomal dominant sarcomere mutations are a causal factor. However, these mutations have yet to be investigated in intact human CMs.

Primary *sarcomeric* cardiomyopathy (Figure 9) can be subdivided into three categories hypertrophic cardiomyopathy (HCM), dilated cardiomyopathy (DCM) and restrictive cardiomyopathy (RCM). HCM is clinically characterized by preserved systolic function with impaired diastolic function and affects 1 in 500 people. Classically HCM is accompanied by thickening of the heart muscle, typically the septum (Figure 9 C). However, this is not a dependent factor for sudden cardiac death (SCD) as there have been rare reports of arrhythmia without CM hypertrophy. At the level of the CM, HCM displays inherent defects such as myofilament disarray associated with causal mutations, in both thick and thin sarcomere components, such as β-myosin heavy chain encoded by,*MYH7*, and cardiac troponin T encoded by *TNNT2*. DCM is characterized by impaired systolic function and linked to sarcomere mutations in the thick and thin filament, for example, proteins such as titin encoded by *TTN,* α-cardiac actin encoded by *ACTC1* and tropomyosin encoded by *TPM1*. Structurally DCM hearts

are enlarged with thin walls including the septum (Figure 9 B). RCM is characterized by restrictive diastolic filling of non-hypertrophied, non-dilated ventricles (Figure 9 D); normal or reduced diastolic volumes; and normal or near normal systolic function. RCM in particular carries a poor prognosis, with 50% mortality within 2 years of diagnosis. RCM is linked to sarcomeric proteins including cardiac troponin T encoded by *TNNT2* and cardiac troponin I encoded by *TNNI3.*

Attempts to separate cardiomyopathies into distinct categories have failed. It is becoming increasingly clear that there is considerable overlap and in some cases one form may progress to another. For example HCM can transition to DCM in end stage HF. Nevertheless each form of sarcomeric cardiomyopathy can dramatically increase the risk of progressive HF, arrhythmia and SCD.

In principle, hiPSCs are an attractive platform to meet the need for cultured human CMs. HiPSC-CMs have many potential application including drug screening and toxicology, disease modeling and regenerative medicine. For instance hiPSC-CMs derived from hiPSCs of patients with inherited cardiomyopathies have permitted examination of the effects of specific genetic mutations at the cellular level [12, 13]. Current HF treatments, including surgery transplant or implantable cardioverter defibrillator (ICD), are not ideal as they require rare donor hearts or invasive procedures. Current pharmacological treatments are largely palliative and focus on reducing blood pressure (e.g., ACE inhibitors) and water retention (e.g., Diuretic) (Figure 10) to reduce the work load of the heart. As an additional treatment agents that directly target the CM and modulate key components of EC coupling are approved. For example, positive inotropic agents such as β-adrenergic agonists, phosphodiesterase inhibitors and cardiac glycosides (Figure 10 and Figure 11) have all been used to treat HF but primarily for symptomatic relief. Hence, drug discovery efforts would benefit from an *in vitro* human CM model with better translatability.

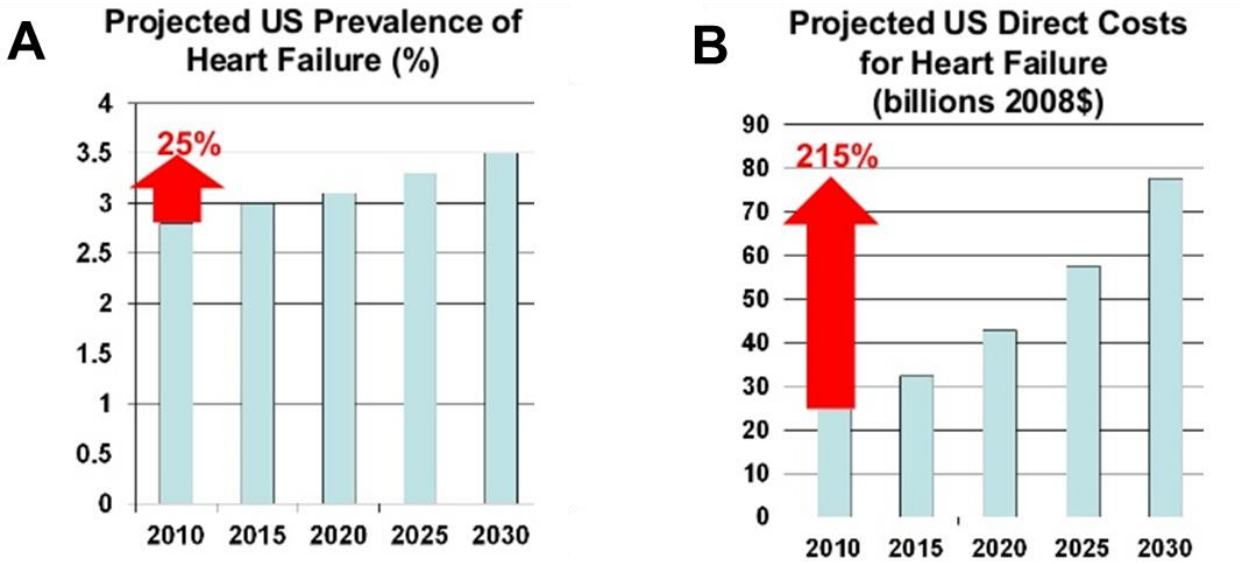

Figure 8. Heart failure projections. A , Graph depicting a 25 % projected increase of heart failure cases in the US, by the year 2030. B, Graph demonstrating 215 % projected increase in direct cost. (Projected increased indicated by the red arrows). (Modified from Heidenreich PA. et al., *Circulation.* 2011; 123:933-944).

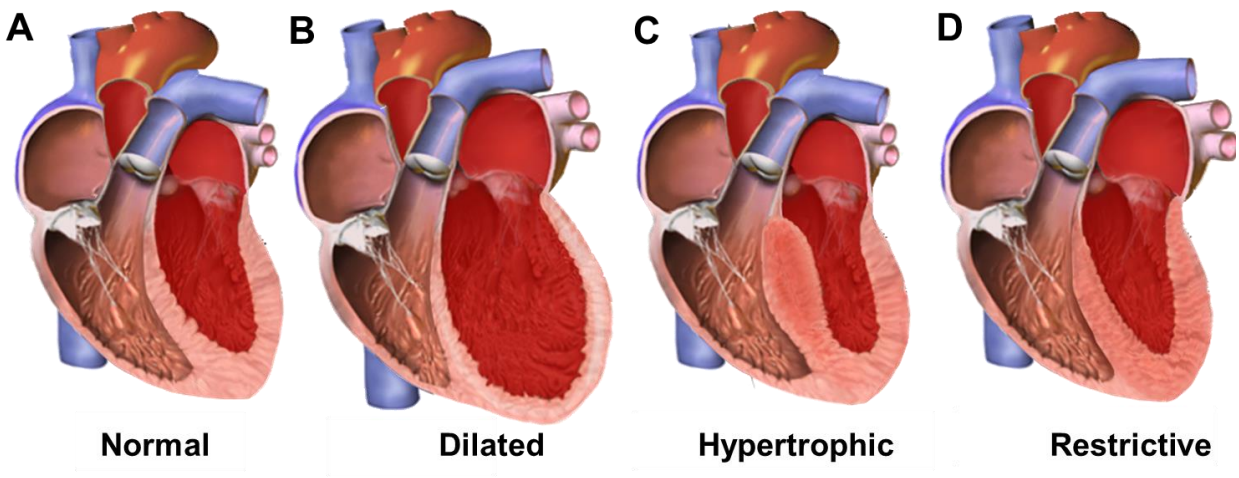

Figure 9. Sarcomeric cardiomyopathy structural characteristics. A, Normal heart. B, Dilated cardiomyopathy (DCM) heart displaying hallmark dilated left ventricle including septum and free wall and enlarged chamber size. C, Hypertrophic cardiomyopathy (HCM) heart displaying characteristic thickening of the left ventricle septum and free wall including reduced chamber size. D, Restrictive cardiomyopathy (RCM) heart displaying moderate to mild hypertrophy and normal chamber size. (Modified from, Blausen Medical Communications, *Journal of Medicine.* 2014 doi:10.15347/wjm/2014.010. ISSN 20018762).

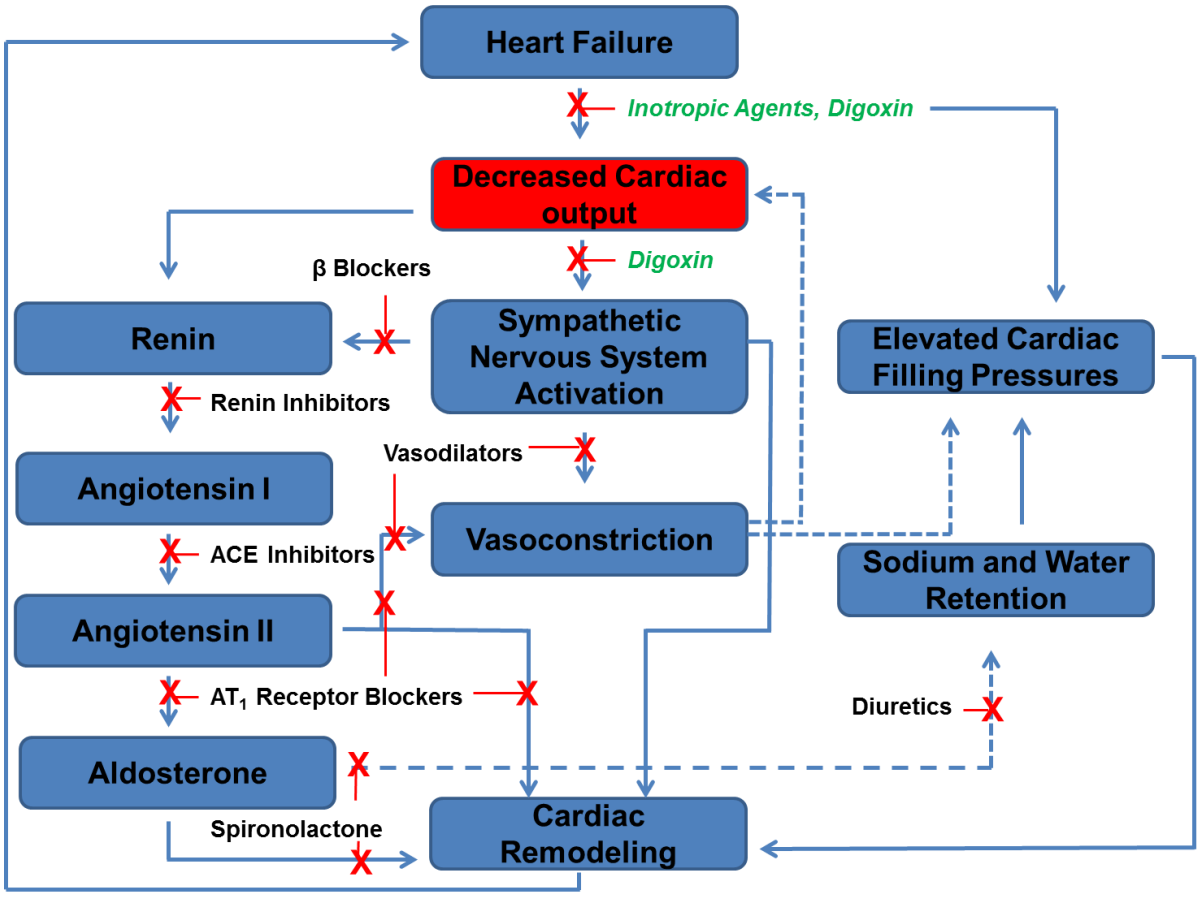

Figure 10. Heart failure therapies. Flow chart depicting key nodes and interventions for heart failure. HF is clinical defined as decreased cardiac output (indicated in red). Decreased cardiac output activates feedback pathways that increase cardiac preload and blood pressure. Chronic stimulation of these processes ultimately increases the work demand of the heart and worsens the condition. Inhibition of the renin-angiotensin system, to decrease blood pressure and diuretic to reduce sodium and water retention are traditional first line therapies. Therapies that directly affect the cardiomyocyte include inotropic agents and digoxin (indicated in green) these agents provide little benefit for mortality. AT_1 (angiotensin receptor) and β (β adrenergic receptor). (Adapted From, Bruton LL, Chabner BA, Knollmann BC*; Goodman & Gilman's The Pharmacological Basis of Therapeutics*, 12th Edition: www.accessmedicine.com).

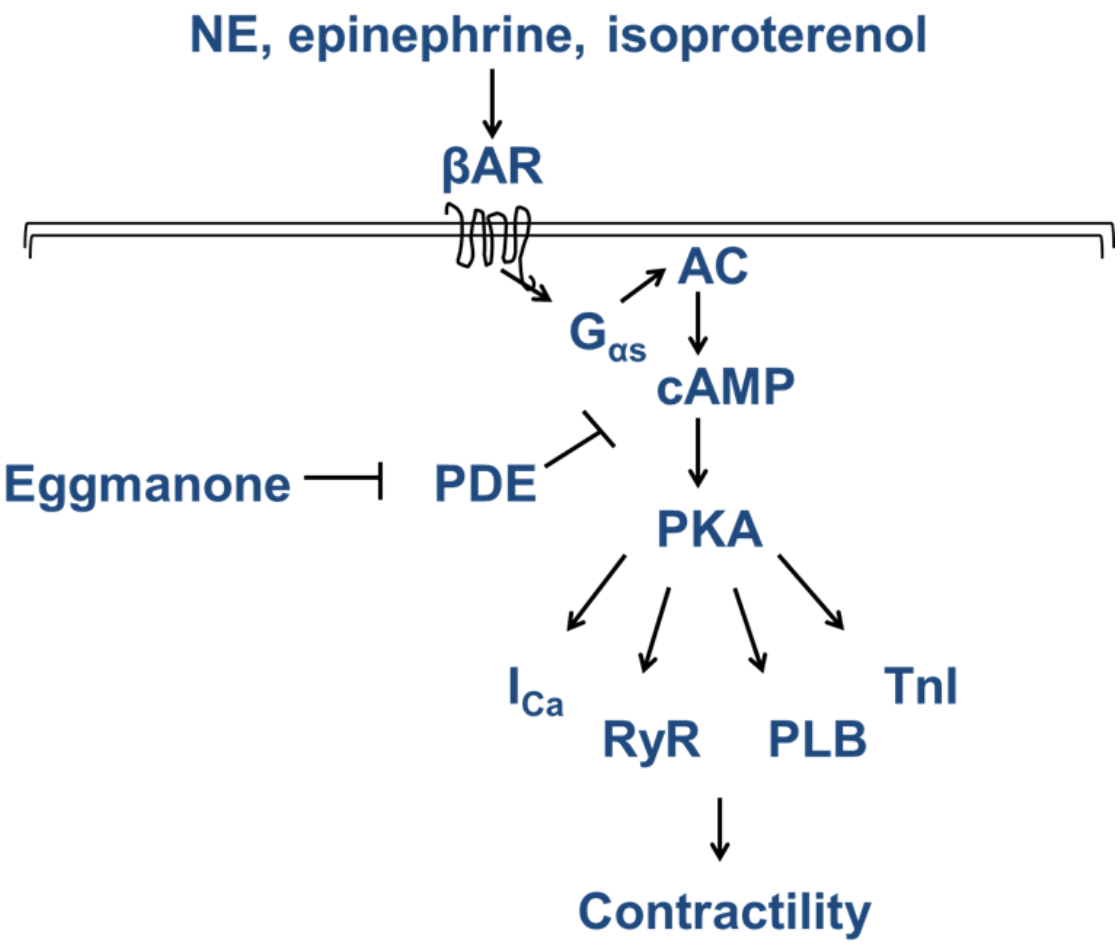

Figure 11. β- Adrenergic signaling pathway. Upon ligand binding to the G protein–coupled receptor a conformation change occurs which enables the Gα subunit to dissociate from the Gβ and Gγ. The dissociated Gα then activates the enzyme adenylate cyclase (AC) which then activates the second messenger cyclic adenosine monophosphate (cAMP). Activation of cAMP leads to activation of protein kinase A (PKA) which then phosphorylates targets that ultimately enhance contractile properties. Phosphorylation of phospholamban (PLB) results in increased SR Ca content. Phosphorylation of the L-type calcium channels result in increased intracellular Ca and enhanced CICR, during each contraction cycle. Phosphorylation of ryanodine (RYR) increases the amount of Ca that extrudes from the SR during each beat. And phosphorylation of TnI increases the rate of CM relaxation.

1.4 Objective

Here, I set out to characterize the EC coupling properties of single hiPSC-CMs including contractile performance with the goal of better understanding the utility of these cells for basic research and drug discovery purposes. I elucidate the steady-state EC coupling properties of control “healthy” hiPSC-CMs. In these experiments, I focused on detailed characterization of EC coupling parameters; electrophysiology, Ca handling [23] and contractility (i.e., cell shortening). To achieve this, I developed and implemented a novel culture method that enables assessment of single hiPSC-CM contractile properties *in vitro* [24]. For standardization, and assessment of hiPSC-CM maturation status I elucidate these properties under identical experimental conditions with hiPSC-CMs generated at different institutions and adult ventricular animal-CMs (i.e., rabbit and mouse). To the best of our knowledge this work represents the first systematic detailed characterization of hiPSC-CM EC coupling properties.

Next, I demonstrate the utility of hiPSC-CMs for disease modeling and drug discovery and provide support for a potential HCM *MYH7* mechanism. These findings, along with the detailed studies defining normal hiPSC-CM properties will aid future functional characterization of disease specific hiPSC-CMs as well as the effect of novel and known pharmacological agents.

Chapter 2

EXCITATION - CONTRACTION COUPLING OF HIPSC-CM

2.1 Chapter Abstract

The lack of reliable *in vitro* methods to evaluate human cardiomyocyte biology, contributes to high mortality and drug attrition rates for heart diseases. In addition, inconsistencies in cellular reprogramming and cardiac differentiation, as well as lack of available methods to assess hiPSC-CM EC coupling parameters have resulted in conflicting reports, thus limiting our understanding of hiPSC-CMs and the utility of these cells for modeling heart diseases. Here, I set out to characterize EC coupling properties of single "healthy" hiPSC-CMs. Focusing on three EC coupling parameters [electrophysiology, Ca handling and contractility (i.e., cell shortening)] in an effort to compare hiPSC-CMs generated independently from different hiPSC lines, at different institutions and correlate these results with that obtained from acutely isolated primary adult-CMs (i.e., rabbit-CM and mouse-CM), under identical experimental conditions. We found that hiPSC-CMs have relatively comparable electrophysiological properties as do adult CMs. Likewise the Ca handling comparison revealed mature Ca handling properties. With the implementation of a novel culture method termed the, "Matrigel mattress," I quantify the contractile properties of single hiPSC-CMs, as well as demonstrate reproducibility across groups. I further demonstrate hiPSC-CMs have comparable contractile properties as adult-CMs including contractile kinetics comparable to that of adult rabbit-CMs. Taken together, these data demonstrate hiPSC-CMs display relatively mature EC coupling properties including electrophysiology, Ca handling and contractility. And implementation of a novel culture method enables rapid generation of robustly contracting hiPSC-CMs and enhances maturation.

2.2 Introduction

Excitation-contraction (EC) coupling is essential for heart function [1]. However, detailed mechanistic studies of human cardiomyocyte (CM) EC coupling in both basic science and drug discovery have been limited by lack of an appropriate *human* CM model. The use of acutely-isolated primary human CMs is hampered by rare availability and technical limitations. Coupled with increasing prevalence of heart failure, lack of current therapies, rising drug attrition rates and cardiac toxic adverse effects, there is a great need for *in vitro* human CM evaluation.

The recent establishment of human induced pluripotent stem cells (hiPSCs) has provided a new approach for obtaining human CMs [5, 25]. hiPSCs, generated from mature somatic cells harvested from patients, are analogous to human embryonic stem cells (hESCs); while avoiding the ethical controversies surrounding their use [26]. Hence, hiPSCs represent a renewable cell source of patient- or disease-specific tissue, potentially avoiding immune rejection [27]. Additionally, hiPSCs can be differentiated to cells of all three germ layers, including cardiac muscle [25] thus enabling generation of CMs from different genetic backgrounds.

In mature ventricular CMs, EC is initiated by membrane depolarization followed by influx of Calcium (Ca) via L-type Ca channels. Entering Ca triggers Ca-induced Ca release (CICR) from the sarcoplasmic reticulum (SR) via ryanodine receptor Ca release channels [3]. The ensuing rise in intracellular Ca binds to the troponin complex and activates myofilament resulting in cellular contraction and shortening [28]. For relaxation to occur, Ca is removed from the cytoplasm, by two primary removal pathways: the sarcoendoplasmic reticulum Ca ATPase (SERCA) and the Na/Ca exchanger (NCX), with other, non-NCX non-SR removal pathways such as plasma lemma Ca ATPase and mitochondria contributing less than 5%, returning the CM to the resting cell length [4]. Given Ca's central role in linking electrical activation, through

cellular depolarization, and contraction, dysfunctional CM Ca handling has been associated with contractile dysfunction, arrhythmia and other heart diseases [29, 30].

Earlier studies of the functional properties of hiPSC-CMs have largely focused on electrophysiological properties, hiPSC-CMs express all ion channels naturally found in adult human left ventricular tissue, albeit at various levels [31, 32]. Additionally, hiPSC-CMs, generated using the monolayer Matrigel sandwich method display human-like action potential morphology and robust L-type Ca currents [9]. However, the Ca handling properties and contractile properties remain not well understood; moreover EC coupling parameters have not been compared to adult-CMs under identical experimental conditions. To date, immature Ca handling and SR function have been associated with hiPSC-CMs [12, 13, 15, 31]. And while contractile properties have been studied, in hiPSC-CMs generated by monolayer based methods, these studies are limited as they evaluate beat frequency as a surrogate of cellular contractility.

A major concern for use of hiPSC-CMs is their relatively "immature" phenotype which may result in substantial differences in their physiology when compared to native CMs. With respect to EC coupling, earlier reports have indicated that hESC-CMs and hiPSC-CMs depend primarily on trans-sarcolemmal Ca entry for contraction [3, 11, 28]. Moreover, the usefulness of hiPSC-CMs depends, in part, on their contractile properties which in turn relies on the Ca handling of these cells [28]. This highlights the need for direct comparison of EC coupling properties of hiPSC-CMs and adult-CMs under identical experimental conditions.

Here, I characterize EC coupling of single hiPSC-CMs. I specifically focus on comparison of electrophysiological, Ca handling and contractile properties of hiPSC-CMs generated from multiple hiPSC lines, independently by different laboratories, to that of acutely-isolated adult rabbit and mouse ventricular-CMs. To the best of our knowledge, this is the first

report of a comprehensive, systematic evaluation of EC coupling in single normal hiPSC-CMs derived by monolayer-based cardiac differentiation methods. We find that hiPSC-CMs display relatively mature electrophysiological properties including comparable amplitude and resting membrane potential. We further show hiPSC-CMs from different laboratories exhibit comparable and reproducible intracellular Ca handling including robust and functional SR Ca stores. Finally, I present the development and implementation of a novel culture method to evaluate hiPSC-CM contractility. I elucidate the contractile properties of single hiPSC-CMs and demonstrate reproducibility across laboratories and comparable properties to that of acutely-isolated adult rabbit-CMs. Taken together, our results suggest hiPSC-CMs generated by monolayer-based methods exhibit relatively mature EC coupling properties *in vitro*.

2.3 Materials and methods

The University Committee on Use and Care of Animals at Vanderbilt University Medical Center approves all animal protocols. All animal protocols conformed to the *Guiding Principles in the Care and Use of Animals* of the American Physiological Society. Data averaged from multiple days were used for analysis. All chemicals, unless otherwise specified, were obtained from Sigma (St. Louis, MO). All Protocols were approved by Vanderbilt University Medical Center Institutional Review Board.

Human iPSC derivation and culture

Human induced pluripotent stem cells (hiPSCs) from healthy volunteers were independently generated, as previously described, by three laboratories Stanford University [33], Vanderbilt University [34], and University of Wisconsin [9, 35]. All protocols were approved by the respective institutions Institutional Review Board. Three different methods of reprogramming were used. Briefly, Stanford hiPSC lines, 13FLVN0C1 and SCVI13 were derived from adult fibroblast using lentivirus based reprogramming [20]. Vanderbilt hiPSC line,

CC2 was derived from dermal fibroblast by non-integrating episomal based reprogramming, and CJ1-001 was derived from peripheral blood mononuclear cells by non-integrating episomal based reprogramming [36]. Wisconsin hiPSC line, DF19-9-11T, was derived from neonatal foreskin fibroblast by vector and transgene free episomal based reprogramming [22]. For all reprogramming individual colonies with typical hESC morphology were picked at day 17 to 30 and clonally expanded. All hiPSCs exhibit normally karyotype. hiPSC lines were routinely maintained on Matrigel, growth factor-reduced 1:200 (Corning) or on Synthemax II-SC coated plates in mTeSR1 medium (Stemcell Technologies) or E8 medium (Stanford University). Cells were passaged every 4 days using 0.5 mM EDTA (Life Technologies) in D-PBS without $CaCl_2$ or $MgCl_2$ (Life Technologies). 2 µM thiazovivin (Selleck Chemicals) or 10 µM Rho kinase inhibitor Y-27632 (CalBiochem) was added for the first 24hrs after passaging. Cells were maintained at 37ºC, with 5% CO_2 and 5% O_2.

Monolayer-based cardiac differentiation

Two protocols were used for induction of cardiac differentiation at the three institutions. Both protocols yield 80-95% troponin T positive cells that spontaneously contract from day 7:

1. *Matrigel Sandwich Induction (University of Wisconsin* [9] *& Vanderbilt University [34]).*

Briefly, hiPSCs (>p20) were incubated with Versene solution (Invitrogen) (1 mL/well 6-well plate) at 37ºC for 5 minutes to dissociate cells. Cell were seeded on Matrigel growth factor-reduced (Corning) coated plates at a density of 100,000 cells/cm^2 in mTeSR1 medium (Stemcell Technologies) supplemented with 10 µM Rho kinase inhibitor Y-27632 (CalBiochem). The mTeSR1 medium was changed daily for 4 days at which point the monolayer reached ~80% confluence. A thin layer of Matrigel 0.5 mg was overlaid in ice-cold mTeSR1 medium. When cells reached 100% confluence, medium was changed to basal medium RPMI 1640 (11875, Life Technologies)

supplemented with B-27 without insulin (Invitrogen) containing Activin A (100 ng/mL, R&D Systems) and Matrigel (0.5 mg Matrigel/6-well plate); this is referred to as day 0. On day 1, medium was changed to RPMI 1640 medium plus B-27 without insulin supplement (Invitrogen) without Matrigel and supplemented with BMP4 (5-10 ng/mL, R&D Systems) and (bFGF 5-10 ng/mL, Invitrogen) for 4 days. At day 5, RPMI 1640 medium plus B27 complete supplement (Invitrogen) was added and medium changed every 3 days until dissociation.

2. *Small Molecule Induction (Stanford University [10, 37]).* Briefly, hiPSCs (>p20) cultured in E8 medium were split at 1:12 ratio. Cells were grown for 4 days at which time they reached ~80% confluence. This is referred to as day 0; medium was changed to cardiac differentiation medium consisting of RPMI 1640 (11875, Life Technologies) and B-27 minus insulin supplement (A1895601, Life Technologies) supplemented with 10 μM or 6 μM CHIR99021 (LC Laboratories) for day 0 to day 1. On day 1 medium was changed to cardiac differentiation medium. On day 3 medium was changed to cardiac differentiation medium supplemented with 5 μM IWR-1 (Sigma). On day 5 medium was changed to cardiac differentiation medium. Medium was changed on day 7 to cardiac medium consisting of RPMI1640 (11875, Life Technologies) and B-27 supplement (17504, Life Technologies). At day 10 medium was changed to metabolic selection medium consisting of RPMI 1640 without glucose (11879, Life Technologies) plus B27 without insulin. On day 12 medium was changed to RPMI 1640 medium (11875, Life Technologies), 2 % B-27 supplement (Invitrogen), and 1 % Pen-Strep (Life Technologies) until dissociation.

hiPSC-CM dissociation, storage and plating

HiPSC-CMs were dissociated and plated as described [23]. Briefly hiPSC-CMs were washed with D-PBS without $CaCl_2$ or $MgCl_2$ (Life Technologies) and incubated with TrypLE Express (Life Technologies) for 10 to 15 minutes at 37ºC to dissociate cells. For

cryopreservation hiPSC-CMs were suspended in 90% FBS, 10% DMSO and stored in liquid nitrogen at day 30 after cardiac differentiation. Prior to plating hiPSC-CMs were filtered (100 µm) (Falcon) and plated at low density (40,000 cells) on either control substrate (Matrigel growth factor-reduced 1:60 in DMEM F12) or Matrigel mattress coated dish, as described below) in approximately 200 µl solution containing: RPMI 1640 medium (11875, Life Technologies), 2 % B-27 supplement (Invitrogen), and 1 % Pen-Strep (Life Technologies). hiPSC-CMs were maintained at 5 % CO_2 and 21 % O_2. Medium was changed every day and experiments were performed 3 - 7 days after plating.

For contractility experiments cryopreserved hiPSC-CMs, SCVI13 (Stanford), were thawed and plated on Matrigel (1:200 dilution) for 4 days to allow CM contractile machinery to recover from cryopreservation prior to plating on Matrigel mattress.

Primary myocyte isolation

Ventricular myocytes from mouse and rabbit were isolated by a modified collagenase/protease method as previously described [38]. All the experiments conducted in Tyrode's solution containing (in mM): $CaCl_2$, NaCl 134, KCl 5.4, $MgCl_2$ 1, glucose 10, and HEPES 10, pH adjusted to 7.4 with NaOH. Final concentration of Ca was 2 mM.

Measurement of intracellular Ca

Myocytes were loaded with Fura-2 acetoxymethyl ester, Fura-2 AM (Molecular Probes Inc, Eugene, OR) as described previously [38]. Briefly, myocytes were incubated with 2 µM Fura 2 AM for 8 minutes at room temperature to load the indicator in the cytosol. Myocytes were washed twice for 10 minutes with Tyrode's solution containing 250 µM probenecid to retain the indicator in the cytosol. A minimum of 30 min were allowed for de-esterification before imaging the cells. Fura 2-AM loaded myocyte Ca transients recorded during 0.5 Hz field stimulation in 2 mM Ca Tyrode's solution for 20 second at room temperature. Then stimulation

was switched off followed by application of caffeine 10 mM for 5 seconds to estimate SR Ca content. A subset of cells were exposed to 0Ca0Na Tyrode's solution for 10 second then caffeine 10 mM applied for 30 second to estimate non-NCX Ca extrusion. For each cell and each experimental condition, tau (τ), amplitude and baseline values were averaged from 3 consecutive Ca transients. Ca transients were recorded and analyzed using commercially available data analysis software (IonOptix, IonWizardTM Milton, MA). All experiments were conducted at room temperature.

Western blot analysis

Western blot analysis was carried out as in [39]**.** Briefly, hiPSC-CMs were seeded on mattress or non-mattress (1:60 Matrigel) for 5 days. hiPSC-CMs were lysed with RIPA buffer supplemented with protease inhibitor and phosphatase inhibitor cocktail (Sigma). To remove excess Matrigel from mattress lysates, all lysates were centrifuged at 16,000 rpm for 15 minutes at 4°C. Protein was quantified using Bio-Rad DC Protein Assay. 5 µg of protein lysates were resolved on 12 % mini-Protean TGX gels (Bio-rad) and transferred onto nitrocellulose membranes for immunoblotting. Membranes were incubated with primary antibodies α-tubulin (rabbit monoclonal, Abcam), ssTnI (rabbit polyclonal, Sigma), cTnI (rabbit polyclonal, Abcam) overnight at 4°C. LI-COR. LI-COR secondary antibody were used and detected by Odyssey CLX (LI-COR) per manufacturer's protocol. Protein band intensities were quantified and normalized to alpha-tubulin band intensities using Li-COR Image Studio software.

Preparation of Matrigel mattress substrates

Matrigel mattress platforms were prepared on the same day as CM dissociation and seeding. Briefly, mattresses were arrayed on a glass coverslip (Corning) or Delta TPG Dish (Fisher Scientific). Application of 1 µL lines of completely thawed, ice cold, undiluted growth factor-reduced Matrigel [8 - 12 mg/mL] (Corning) were arrayed in parallel. Matrigel was evenly

pipetted at a 45 degree angle (Figure 18) with a P2 pipet and corresponding 10 µL tip. The mattresses were allowed to incubate for 8 - 10 minutes at room temperature at which point 200 µL of RPMI 1640 medium, 2 % B-27 supplement (Invitrogen), and 1 % Pen-Strep (Life Technologies), with the addition of 40,000 CMs were immediately added, halting mattress polymerization. Each mattress had a width of approximately 0.85 mm. The thickness of each mattress was 0.40 - 0.88 mm and each line was approximately 23 mm long in detail below.

Prepare before beginning mattress experiments:

- 24 hours before plating thaw Matrigel (Basement Membrane Matrix Growth Factor Reduced [8 - 12 mg/mL] (Corning Catalog # CB-40234)) aliquot on ice.

  Note: Typical aliquot is 250 uL of Matrigel in Eppendorf tube. In case of time constraints Matrigel can be thawed based on manufactures recommendations (on ice ~ 1 hour until completely thawed).

- Prepare P 2 pipet set at 1 uL
- Prepare P 2 pipet tips (10 uL)
- Prepare dishes ((Fisher Scientific Delta TPG DISH (50/Pack) 0.17mm black) / coverslip (Corning #12-542-C 25X25-1) for experiments (typically 3 dishes/coverslips per group)
- M3 media (Cardiomyocyte (CM) media) RPMI 1640 with glucose (Invitrogen, cat# 11875), B27 with insulin (Invitrogen, cat#17504-044) and 1 % Pen-Strep (Invitrogen, cat#17504-044).
- TrypLE Express (Life Technologies) store at room temperature.
- Timer

For cryopreserved hiPSC-CMs:

1. Thaw day 30 – 35 cells using standard thawing protocol. Plate cells in 6 well Matrigel coated plates (1:200 diluted in DEM F12). Culture for 4 days to allow cell to recover from cryopreservation. Change M3 at 24 hours and 72 hours post thaw.
2. Skip to dissociation and counting section

For hiPSC-CMs already in culture:

1. From standard small molecule based cardiac induction culture cells until day 30 – 35.
2. Skip to dissociation and counting section

Dissociation and counting

1. Check status of cultured CMs before dissociation. Evaluate health of CMs make sure cells are viable and beating. The purity of the population is very important some form of selection (e.g., metabolic selection or sorting) should be used to reduce experimental contamination of other cell types. Non CMs may disrupt mattress substrate.
2. Wash CMs with 2 ml per well D-PBS without CaCl2 or MgCl2 (Life Technologies).
3. Remove D-PBS add 1 ml per well TrypLE Express (room temperature) incubate at 37 C for 15 minutes.
4. Prepare 15 mL conical tube by adding 10 mL fresh M3.
5. Use 5 mL serological pipette and pipettor to lift CMs by gently spraying 3 mL of fresh M3 onto cells.
6. Add the 4 mL (3mL fresh media + 1 mL TrypleE including and CMs) to the conical tube.
7. Take one mL fresh M3 add to well and scrape cells to get any remaining CMs.
8. Add the 1 mL M3 + CMs to the conical tube (Final volume 15 mL).
9. Spin CMs for 5 minutes at 200g to pellet.
10. Remove supernatant to 2 mL mark.

11. Re-suspend by adding 3 mL fresh M2 with 5 mL serological pipette and pipettor. To a final volume of 5 mL.
12. Count cells using trypan blue in duplicate.
13. Allow cells to remain at room temperature during mattress preparation process (10 minutes).

Matrigel mattress preparation: All steps carried out in tissue culture hood

1. Mix Matrigel by flicking tube, immediately place back on ice.
2. Start timer counting up, immediately before the first mattress is plated (time zero).
3. Pipet 1uL Matigel up and down 3 times to chill pipet tip.
4. Evenly pipette 1 uL undiluted Matrigel at 45 degree angle **(Figure 18)** onto dish/coverslip. Each 1 uL line is one mattress (4 lines or mattresses per dish/coverslip). Typically timing ~ 2 minutes to prepare 3 dish/coverslips or 12 mattresses. Plate all mattresses in the same orientation on each dish/coverslip; this will help when performing experiments at 40X.

   Note: Be sure to go the entire length of dish/coverslip ~ 23mm. Short mattresses (10 mm) will be too thick reducing mattress stability and may be outside the focal plane when viewing at 40X. Do not allow Matrigel to dry in pippet tip. If this occurs quickly switch tips, pipette Matrigel up and down to chill tip and immediately continue. Try to work quickly. When starting out it is recommended to prepare a low number of plates (3) until proper timing is established, at which time you may scale up. In addition practicing mattress preparation in advance is encouraged.

Depending on imaging set up mattress near the edge of the dish/coverslip may be outside working area. For this reason it is recommended to localize mattresses to the center of dish/coverslip.

5. Allow Mattress to incubate at room temperature for 8 – 10 minutes.

   Note: The timing is critical, incubation for longer than 10 minutes will result in stiff substrate and no shortening, incubation for shorter than 8 minutes will result in unstable mattress that may implode.

6. Immediately plate CMs drop wise directly on mattress ~ 40,000 cells per dish in low volume ~ 200 uL in M3 with P1000 **(Figure 18)**. This will halt mattress polymerization.

7. Allow cells to sit undisturbed at room temperature for 5 minutes. This allows cell to adhere properly to mattress.

   Note: At this point visually inspect plates on microscope 5-20 X to ensure CMs are on the mattress and the density is appropriate (single cells). If plates are too dense quickly make more mattress as above and plate fewer cells.

8. Gently add 1 mL fresh M3 to each dish/coverslip.

9. Place cells at 37 C for 5 days changing media daily.

   Note: visually inspect cells for correct morphology, immediately after plating cell should appear round **(Figure 20)***, at ~ 24 hour post plating distinct morphological changes and small cell shortening may be observed. By day 3 posts plating robust cell shortening should be observed.*

Common mattress mistakes:

1. High serum/FBS in media will result in networks of CMs no single cells (similar to endothelial cell assay).
2. Preparing too many mattresses at one time.
3. Plating CM or changing media harsh. Gently change media from the edge of dish/coverslip as not to disrupt Mattresses.
4. Plating CMs at high density. For these experiments few cells are used, want to ensure cells are spread out for single cell analysis.
5. Perfusion or suction to strong, this will tear cells off Mattress.
6. Making Mattress to thick or thin.
7. Not visually inspecting cells to confirm they are on mattresses.
8. Preparing sloppy mattresses, while it is important to work quickly the integrity of each mattress is important.
9. Plating too many Mattresses on a dish, it is important to be able to clearly distinguish between the mattress and the glass. This is especially important for diseased CMs where contractile dysfunction may be a phenotype.
10. Not using a timer.
11. Culturing mattress cells to long. 14 days is the maximum it is recommended to perform experiments from 5 to 7 days.
12. Not setting smoothness to 10 on IonWizard acquisition software (IonOptix)

Measurement of cell volume

Measurements of hiPSC-CM volume were obtained as previously descried [23], Z-stacks were obtained using a confocal microscope (LSM 510, 25X oil immersion Plan-Neofluar lens) as described. Briefly, hiPSC-CMs were loaded with 5 µM Calcein AM (Molecular Probes, Eugene,

OR), for 30 min at room temperature; to label intracellular space. HiPSC-CMs were washed twice to remove extracellular Calcein with no Ca Tyrode solution. Fluorescence was excited at 488-nm with 1% argon laser power. 25-46 images (1.5 µm sections) were obtained for each hiPSC-CM. Images were reconstructed in three-dimensions and surface area and volume analyzed using the three-dimensional image analysis program IMARIS (Bitplane, South Windsor, CT).

Immunohistochemistry

Immunostaining of CMs was carried out as before [13]. Briefly, CMs were fixed in 2% paraformaldehyde for 5 minutes at room temperature, permeabilized with 0.2% Triton X-100 (Sigma) for 10 minutes at 4 C. Samples were blocked with 1% BSA in PBS solution and incubated for 1 hour at room temperature. Primary antibody, a-actinin (mouse monoclonal, Sigma), was added in 0.1% Triton X-100 1% BSA in PBS solution and incubated overnight at 4 C. Samples were washed with 0.2% Tween 20 in PBS, secondary antibodies specific to the primary IgG isotype were diluted (1:1000) in the same solution as the primary antibodies and incubated at room temperature for 1 hour. Samples were washed with 0.2% Tween 20 in PBS twice and mounted. Slides were examined with Olympus IX81 microscope coupled to Slidebook software. For morphometric analysis images were imported into Image J and analyzed using standard plugins.

Cardiac gene quantitative PCR screen

A panel of cardiac genes was screened by qPCR. Briefly, total RNA was isolated from Day 30-35 mattress and non-mattress hiPSC-CMs via TRIzol Reagent and Dnased treated via DNA-free DNA removal kit per manufacturer's instructions (Ambion). cDNA was generated using high-capacity cDNA reverse transcription Kit (Life Technologies). qPCR arrays were performed using Taqman ViiA7 Fast Real-Time RT-PCR System according to the

manufacturer's instructions (Applied Biosystems, Foster City, CA, USA). All TaqMan probes were obtained from Applied Biosystems (Table A-1). Transcripts were normalized to housekeeping gene 18S rRNA and differential fold changes were presented as heat map.

Action potential measurement

Cardiac action potentials were measured from single cardiomyocytes with ruptured whole cell patch-clamp technique [40]. Briefly, cells were superfused with Tyrode's solution containing (in mmol/L) 137 NaCl, 5.4 KCl, 10 HEPES, 10 Glucose, 1 MgCl2, 1.8 CaCl2; pH was adjusted to 7.4 with NaOH. The glass pipette had access resistance of 3-6 MΩ after filling with the internal pipette solution containing (in mmol/L) 110 KCl, 5 Mg-ATP, 0.5 MgCl2, 5 EGTA, 10 HEPES, pH adjusted to 7.2 with KOH. Action potential was recorded using Axopatch 200B, Digidata 1322A and pClamp 8.0 software (Axon Instruments, Foster City, CA, USA) for data amplification and acquisition. A 2ms current pulse at approximately 20% above threshold was provided to evoke action potentials at a cycle length of 2s (0.5Hz). Electrophysiological data were analyzed using Clampfit 9.0 and the figures were prepared by using Origin 7.2.1. All experiments were performed at room temperature.

Measurements of sodium current

Sodium currents (I_{Na}) were measured using external solution contained (in mmol/L): 135 CsCl, 10 NaCl, 10 HEPES, 10 Glucose, 1.8 CaCl2, 1 MgCl2, pH 7.4 (CsOH). To eliminate L- and T-type calcium currents, 1 µmol/L nisoldipine and 200 µmol/L NiCl2 were added to the external solution. The internal pipette solution contained (in mmol/L): 5 NaCl, 135 CsCl, 5 EGTA, 10 HEPES, 5 Mg-ATP, 2 CaCl2, pH 7.2 (CsOH). I_{Na} densities were measured by applying 40 - ms test pulse between -80mV and 60mV in 10mV increments from a holding potential of -120mV. Steady-state inactivation was measured by varying the conditioning holding potential from -140 mV to -20mV, followed by a 40-ms test pulse to -20mV

Video based edge detection

Video edge detection was used to assess cellular contraction (i.e., cell shortening) of contracting CMs. Briefly; CMs were visualized using Nikon Ellipse T5100 coupled to IonOptix video microscopy system (IonOptix). Spontaneous or field stimulated contraction traces were recorded in 2 mM Ca Tyrode solution. For each cell and each experimental condition typical contraction parameters including percent cell shortening (i.e., percent of resting cell length) and contractile kinetics (i.e., time to peak 90% and time to baseline 90%) values were averaged. Contraction traces were recorded and analyzed using commercially available data analysis software (IonOptix, IonWizardTM Milton, MA). Only isolated hiPSC-CMs with aspect ratio greater than or equal to 4 were used, non-shortening cells were excluded from analysis.

Traction force microscopy

Traction force maps were generated using the traction force microscopy method [39]. Briefly, contraction cycle of isolated hiPSC-CMs maintained on Matrigel mattress containing 0.75 μm (Polysciences) fluorescence beads 1:50 were tracked by phase-contrast for contractile motion and fluorescence microscopy for substrate deformation; videos of individual hiPSC-CMs, cultured on mattress containing beads, were captured and particle image velocimetry (PIV) used to assess displacement deformation of hiPSC-CMs. Fourier transform traction cytometry (FTTC) was used to access force using ImageJ plugin [19, 41]. For traction force microscopy experiments spontaneous beating hiPSC-CMs in 2 mM Ca Tyrode were evaluated at room temperature.

Contraction force and contraction stress measurements

Contraction force and stress measurements were calculated based on the following equation.

$$F = \left(\frac{E\mathrm{Ao}\Delta L}{Lo}\right)$$

Where, F is the force exerted on an object

E is the Young's modulus (modulus of elasticity) of the substrate

A_0 mean hiPSC-CM cross-sectional area

ΔL is the amount by which the length of the hiPSC-CM changes

L_0 is the resting length of the hiPSC-CM

Briefly, the resting cell length, L_0, was determined by video based edge detection (IonOptix). Mean modulus, E, of the Matrigel mattress, 5.8 kPa, was determined by Atomic Force Microscopy. ΔL, the change in cell length (i.e., peak cell shortening amplitude) of each cell was determined using video based edge detection (IonOptix). The mean cross sectional area, A_0, was calculated from Z stack images as described [23]. Assumptions for this analysis: as hiPSC-CMs shorten equal force is applied to the Matrigel mattress (i.e., that Matrigel mattress moves as CM contracts). This is shown in our traction force analysis, by displacement of embedded florescent beads (Figure 26 A)

Time-lapse microscopy

Differential Interface Contrast (DIC) time lapse images were acquired using a Zeiss LSM Meta 710 confocal microscope. Briefly, day 30 hiPSC-CMs were dissociated and re-plated on Matrigel mattress on MatTek 35mm petri dishes (P35G-1.5-14-C). hiPSC-CMs were maintained

at 37° C with 5% CO2 and imaged every 15 minutes for 10 hours. Images were exported into ImageJ for processing.

Statistical analysis

Data are mean ± SD unless indicate otherwise. Statistical differences between two groups were tested with two-tailed Student's t test. Statistical differences among more than two groups were assessed using one-way ANOVA followed by tukey or bonferroni correction. Results were considered statistically significant if the p-value was less than 0.05. Statistical analysis was performed using Graphpad Prism 6.

2.4 Results

Elucidating the electrophysiological properties of single hiPSC-CM

Single hiPSC-CMs were plated at low density on control substrate (<0.1 mm thick 1:60 diluted matrigel, "control hiPSC-CM") and cell surface area, cell volume and EC coupling parameters (action potential and Ca handling) measured 3 – 7 days after plating. We first measured CM shape and volume from Z-stacks of confocal images after loading cells with calcein to label intracellular space [26]. The shape of hiPSC-CM was highly variable, ranging from circular to elongated to triangular morphology (Figure 12 A). HiPSC-CMs were smaller (cell volume 3.96 ± 0.25 pL, n = 44) compared to mouse ventricular CM (cell volume 29 ± 2 pL, n = 34). On the other hand, cell surface area to volume ratio was significantly larger in hiPSC-CMs compared to adult-CMs (Figure 12 B). Circular hiPSC-CM had lower surface area and volume compared to elongated and triangular, but surface to volume ratio was not statistically different among the three control hiPSC-CM cell shapes (Figure 12 B).

Electrophysiological properties have been the most studied parameters of hiPSC-CM EC coupling. However, the majority of reports have not correlated results with adult-CM properties

under identical experimental conditions. Therefore as a first step in characterizing the EC coupling of hiPSC-CMs; we assessed the electrophysiological properties including action potential and ion channels. Despite the differences in cell size and shape, hiPSC-CM display relatively mature electrophysiological properties including amplitude, maximum diastolic potential and APD50/90 (Figure 13 and table 2) comparable to that of adult rabbit-CMs. In addition hiPSC-CMs generated independently from multiple hiPSC lines exhibit robust L-type Ca currents that were not statistically different from L-type Ca current measured in mouse-CM (Figure. 14). To the best of our knowledge this represents the first comparison of the electrophysiological properties of hiPSC-CMs and adult-CMs under identical experimental conditions.

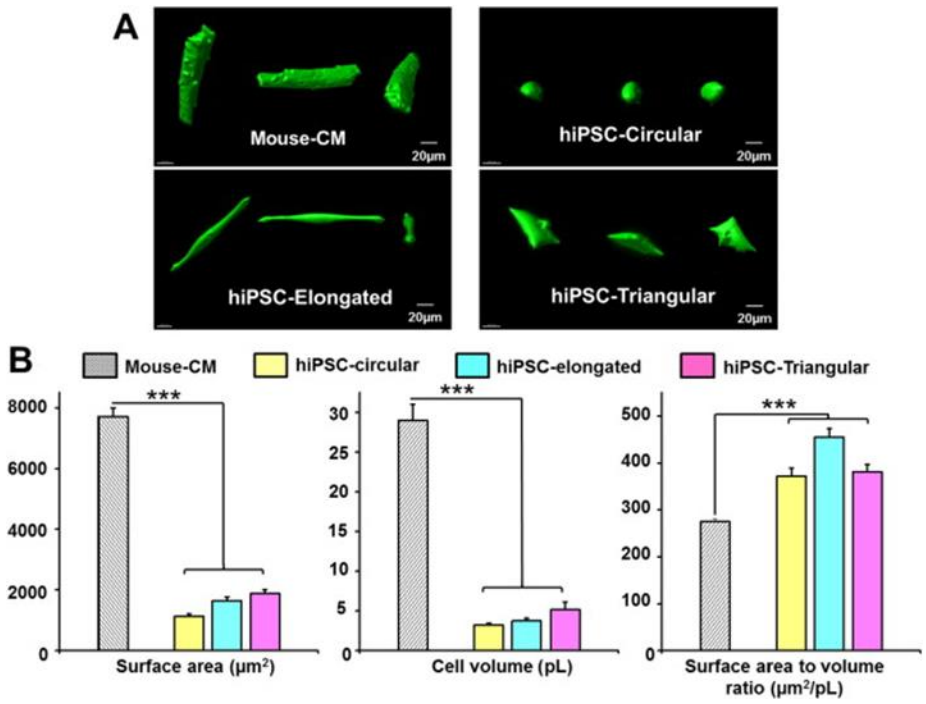

Figure 12. Surface area and volume of mouse-CMs and hiPSC-CMs. A, representative examples of three-dimensional reconstruction of mouse-CM and hiPSC-CMs. B, averaged data. Data are mean ± SEM. N=13-34 per group. ****P*<0.001 vs mouse-CM. (Hwang, Kryshtal and Feaster et al., *Journal of Molecular and Cellular Cardiology*. 2015; 85, 79-88).

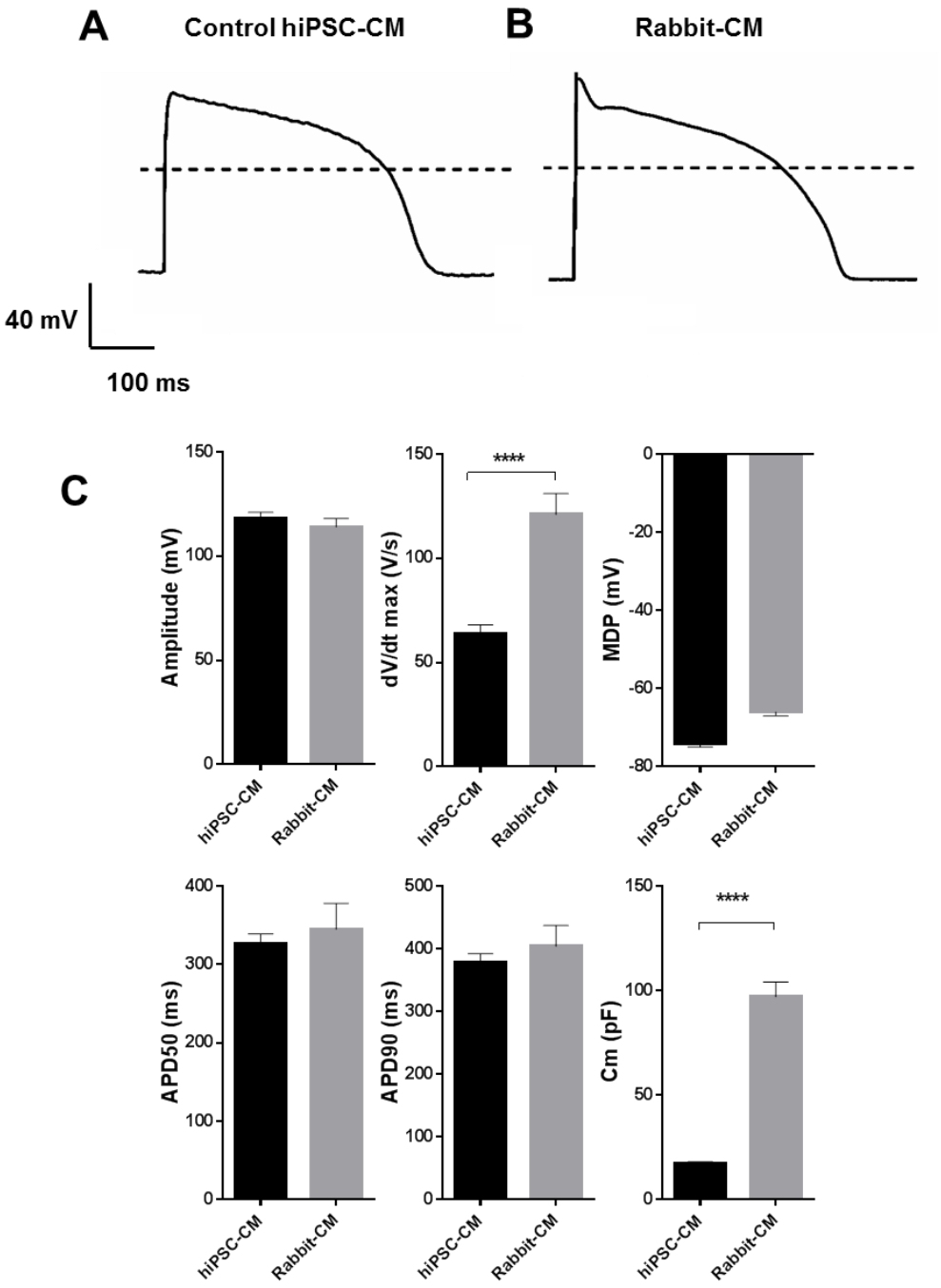

Figure 13. Electrophysiological characterization of hiPSC-CMs. Representative action potential recordings of A, control hiPSC-CM and B, Rabbit-CM. Dotted line indicates 0 mV. C, Data are mean ± SEM n = 11 - 53 per group indicating relatively comparable electrophysiological properties as adult rabbit CMs. ****P*<0.001 vs mouse-CM. Courtesy of Dr. Lili Wang. (Adapted from Feaster T. et al., *Circulation Research* 2015; doi: 10.1161/CIRCRESAHA.115.307580).

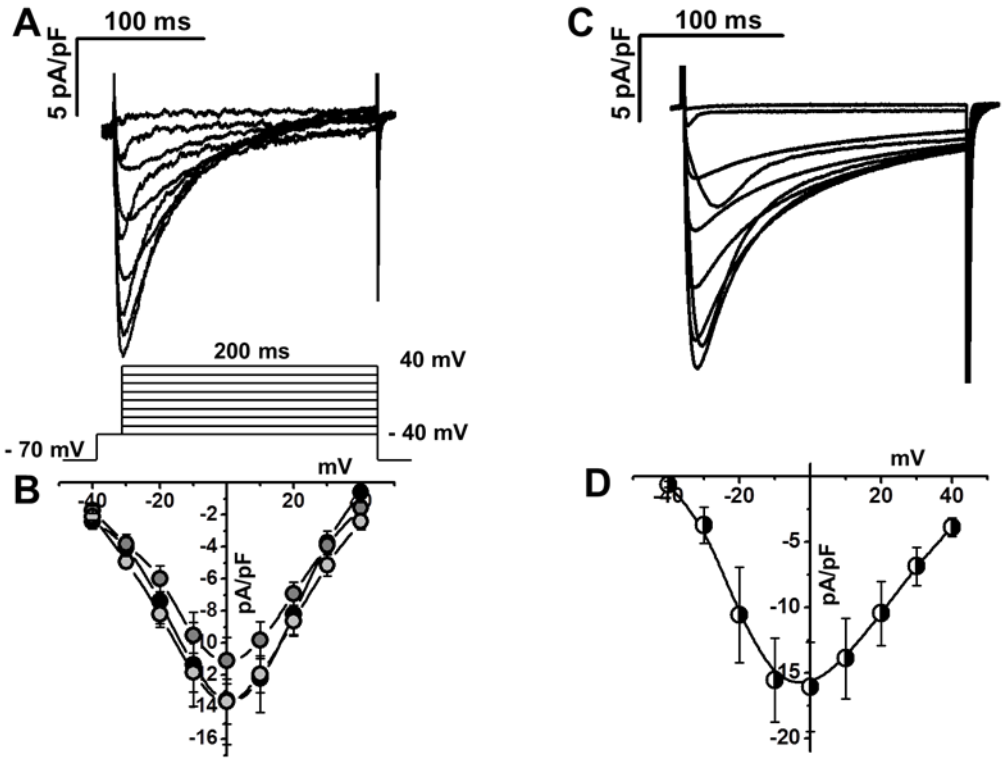

Figure 14. L-type Ca currents of hiPSC-CM and mouse-CM. A, C, representative example of Ca currents from hiPSC-CM (Stanford, A) and mouse-CM B, Voltage protocol shown below current records. B, D current–voltage relationships of peak Ca currents from hiPSC-CM (Stanford (light gray), n=6; Vanderbilt (gray), n=6; Wisconsin, black, n=5) and from mouse CM (n=6), respectively. Courtesy of Dr. Dmytro O. Kryshtal. (Hwang, Kryshtal and Feaster et al., *Journal of Molecular and Cellular Cardiology*. 2015; 85, 79-88).

Table 2. Electrophysiological characterization

Parameter	Control hiPSC-CM	Mattress hiPSC-CM	Rabbit - CM
Amplitude (mV)	118.0 ± 3.0	124.0 ± 4.0	114.0 ± 4.0
dV/dt max (V/s)	64.0 ± 4.0	84.0 ± 8.0*	121.0 ± 10.0****
MDP (mV)	-74.0 ± 1.0	-74.0 ± 2.0	-66.0 ± 1.0
APD50 (ms)	326.0 ± 13.0	318.0 ± 15.0	345.0 ± 33.0
APD90 (ms)	378.0 ± 14.0	376.0 ± 16.0	404.0 ± 33.0
Cm (pF)	17.0 ± 1.0	17.0 ± 1.0	97.0 ± 7.0****
n	53	46	11

Table 2. Electrophysiological characterization. Summary data are mean ± SEM. *P<0.05 vs control . ***P<0.001 vs mouse-CM. Courtesy of Dr. Lili Wang. (Feaster T. et al., *Circulation Research* 2015; doi: 10.1161/CIRCRESAHA.115.307580).

Elucidating the calcium handling properties of single hiPSC-CMs

Although the cell shape and size of the nucleus of single hiPSC-CMs and adult mouse CMs differ drastically, staining with the low-affinity Ca sensitive indicator Mag Fluo-4 demonstrates that both hiPSC-CMs and adult mouse-CMs have robust intracellular Ca stores (Figure 16 A). We next compared the Ca handling of field-stimulated (0.5Hz) control hiPSC-CMs generated independently from multiple hiPSC lines (i.e., Stanford University, Vanderbilt University and University of Wisconsin-Madison) to that of adult primary ventricular rabbit and mouse-CMs under identical experimental conditions using the ratiometric Ca indicator, Fura 2-AM. For these experiments frozen aliquots were shipped, recovered from cryopreservation, plated at low density on control substrate and compared 3–5 days after plating.

Typical Ca handling parameters (diastolic [Ca], Ca transient amplitude, time to peak, Ca decay rate) (Figure 15 and 16 A) were not significantly different among all three hiPSC-CM lines. Compared to adult rabbit and mouse CMs, only time to peak and Ca transient decay rates were significantly prolonged in hiPSC-CM, whereas all other Ca handling parameters were not different (Figure 16 C).

We next tested for the presence of functional sarcoplasmic reticulum (SR) Ca stores using caffeine, an agonist of ryanodine receptor (RyR2) Ca release channels (Figure 16 B). Analogous to adult primary CMs, all hiPSC-CMs tested exhibited robust caffeine-releasable SR Ca stores (Figure 16 B and C). Caffeine-induced Ca transients and hence SR Ca content were of similar magnitude and not significantly different from rabbit or mouse-CMs. These results are consistent with the presence of intracellular Ca stores stained with Mag Fluo-4 (Figure 16 A) Taken together; these data demonstrate that single hiPSC-CMs exhibit intracellular Ca transients comparable to that of adult animal-CMs, and that the presence of functional SR in hiPSC-CMs derived using monolayer-based methods is consistent across multiple laboratories.

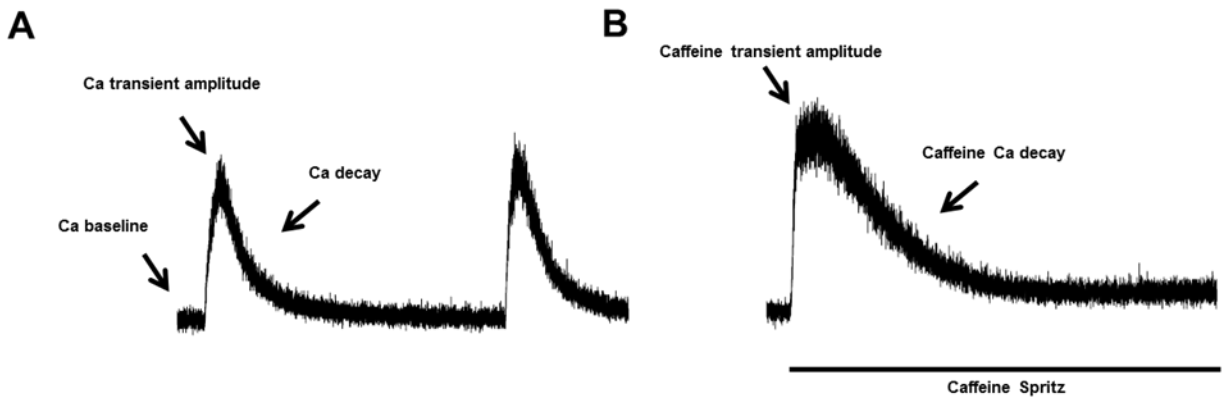

Figure 15. Representative cytosolic calcium transients and typical parameters. A, Twitch Ca transient parameters: Ca baseline (diastolic Ca), Ca transient amplitude (peak cytosolic Ca) and Ca decay (Ca removal from the cytoplasm, primarily by SERCA). B, Caffeine Ca transient [10 µM] parameters: Caffeine transient amplitude (SR Ca content or SR Ca load) and caffeine Ca decay (Ca removal from the cytoplasm, primarily by NCX). hiPSC-CMs loaded with Fura 2-AM [2 µM].

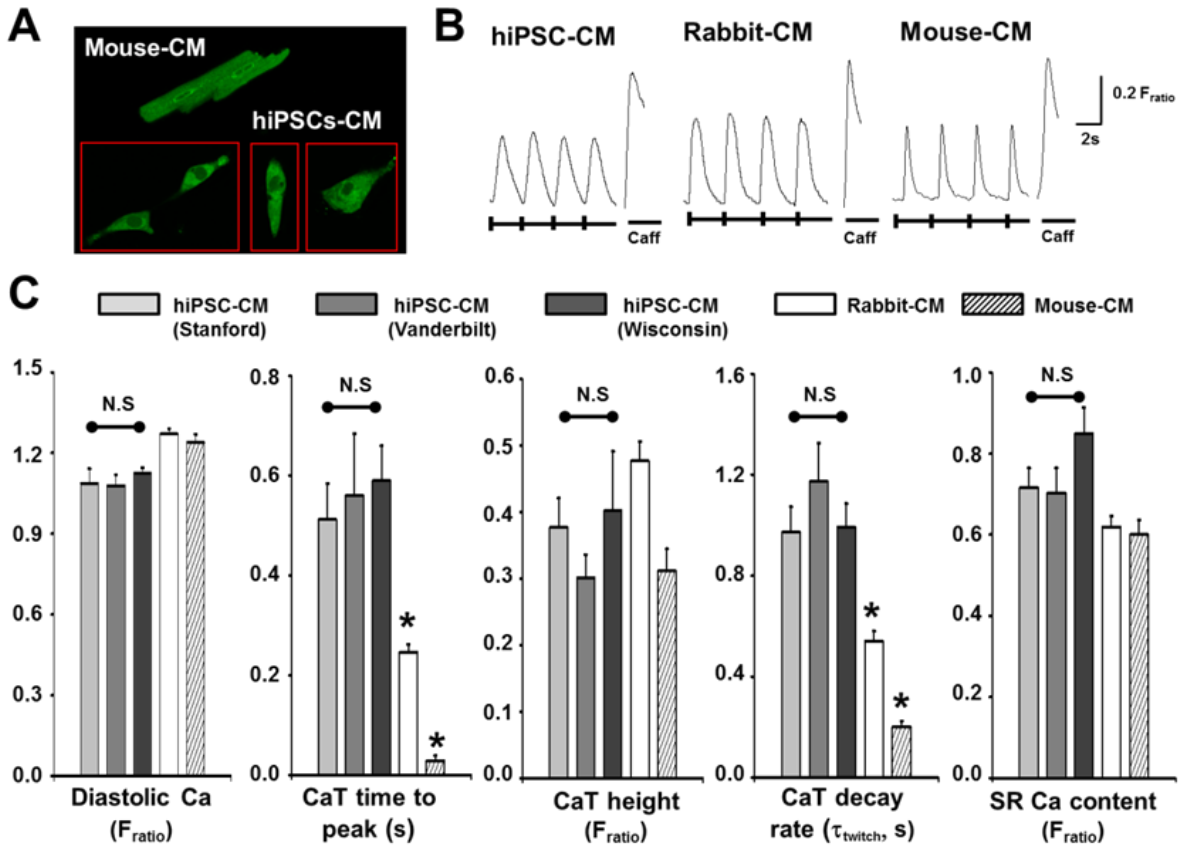

Figure 16. Ca handling of hiPSC-CMs and animal CMs. A, confocal images of a mouse-CMs and hiPSC-CMs loaded with low-affinity Ca indicator, Mag-Fluo-4AM 5μM to label intracellular Ca stores (i.e. SR). B-C, representative Ca transients B and averaged data C recorded in hiPSC-CMs and acutely isolated adult ventricular rabbit and mouse CMs. Cells were field-stimulated (0.5Hz, 20s train) in 2mM Ca Tyrode's solution followed by caffeine spritz (10mM, 5s) to estimate SR Ca content. Data are mean ± SEM. N=22-27 per group. **P*<0.05 vs. hiPSC-CM. (hiPSC-CM images A and example Ca transient records B shown are from Vanderbilt hiPSC-CMs). Courtesy of Dr. Hyun Hwang. (Hwang, Kryshtal and Feaster et al., *Journal of Molecular and Cellular Cardiology* 2015; 85, 79-88).

Development of an in vitro method to assess contractility of hiPSC-CMs

The matrigel mattress method

Current methods to evaluate cellular contractile properties of individual hiPSC-CMs are lacking. For this reason, many laboratories have moved to multicellular preparations such as 2D monolayer (e.g., XCELLigence) [42] or 3D multicellular (e.g., EHT). While useful, these methods make detailed hiPSC-CM contraction studies challenging for most laboratories.

For single hiPSC-CMs studies hiPSC-CMs are routinely plated on tissue culture substrates such as gelatin or Matrigel (<0.1 mm thick 1:60 diluted matrigel, "control hiPSC-CMs") a commercially available extracellular matrix (ECM) preparation, (Figure 17 A and Figure 18 A) [33]. However, such substrates do not enable detailed assessment of contractile properties as the majorly of the cells are circular displaying unaligned myofilaments (Figure 17) with no relevant shortening (i.e., little or no contractile work) [11][18]. As such methods including atomic force microscopy (AFM), traction force microscopy (TFM) and image-based rhythmic methods have been used [19] (Figure 17 B - D). As discussed earlier these methods have their limitations.

I sought to develop a simple, rapid, low-cost contractility platform, which would enable robust reproducible hiPSC-CM cell shortening and hence evaluation of contraction performance. I report the Matrigel mattress method [24] for routine evaluation of contractile performance (Figure 18). I hypothesized that, provided a substrate with appropriate properties such as stiffness and composition, hiPSC-CMs would shorten as is commonly observed with acutely isolated adult animal-CMs. Hence, enabling contractile assessment with standardized equipment typically used for adult-CMs. A broad substrate screen [39] revealed that undiluted Matrigel (0.4 - 0.8 mm thick, “mattress hiPSC-CMs”), which we have termed the Matrigel

mattress, supported elongation, alignment and robust hiPSC-CM shortening (Figure 19 A). For these experiments day 30 - 35 hiPSC-CMs were dissociated and re-plated on either control or mattress (Figure 19 A and D) and evaluated 5 - 7 days after plating. We took advantage of the inherent properties of Matrigel, its substrate modulus and its ability to adhere cells without additional functionalization [43].

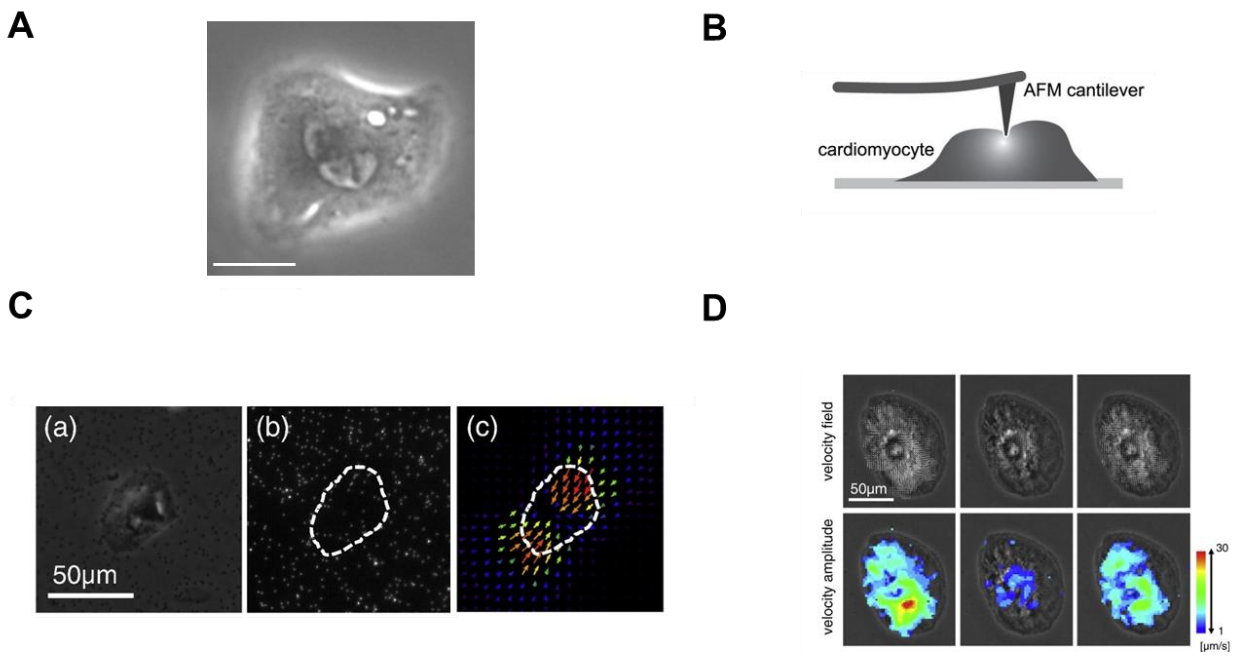

Figure 17. Current single hiPSC-CM contractility assays. A, Typical control hiPSC-CMs morphology (i.e., Matrigel diluted 1:60 in DMEM F12). Scale bar, 25 µm. B, Schematic of atomic force microscopy set up. (Liu J. et al., *PLoS*. 2012; doi: 10.1371/journal.pone.0037559). C, Representative traction force microscopy and analysis and D, image-based pixel analysis. (Panels C and D adapted from, Hayakawa T. et al., *Journal of Molecular and Cellular Cardiology*. 2014; 77:178-91). Representative hiPSC-CM image A is from Vanderbilt University, derived from hiPSC line CC2).

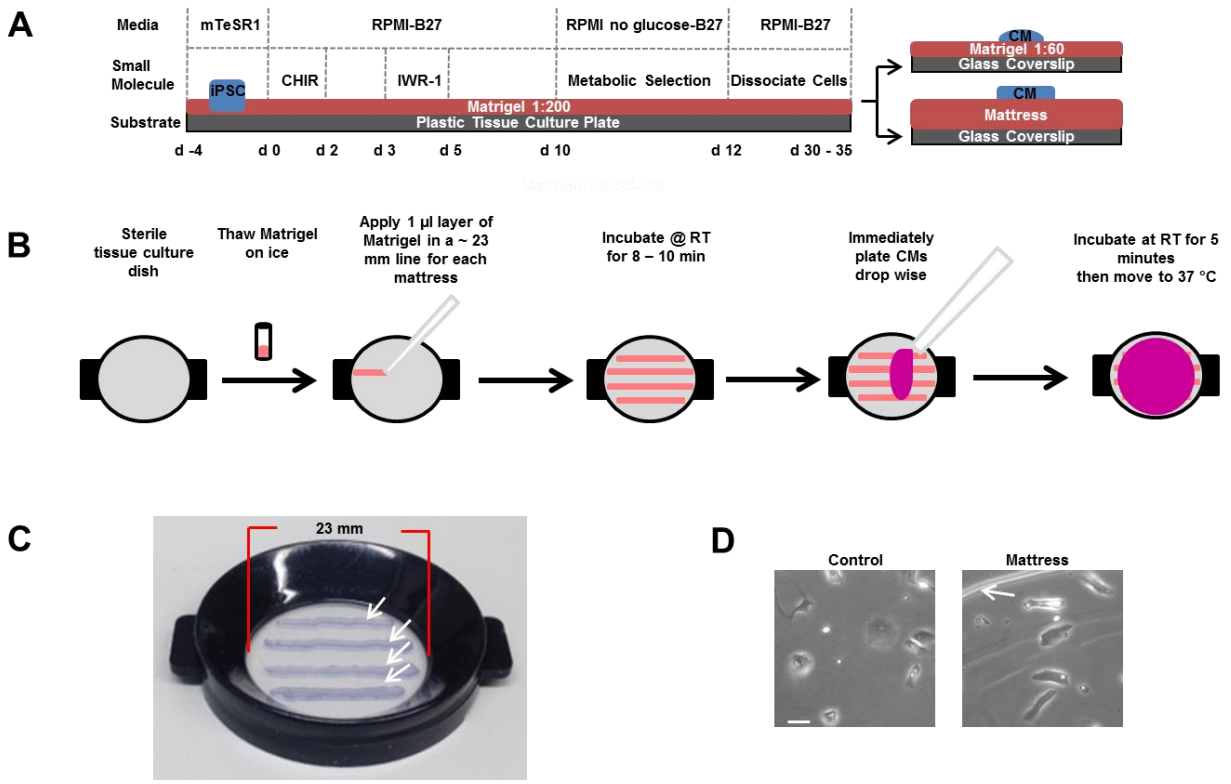

Figure 18. Overview of Matrigel mattress method. A, Schematic of cardiac induction and Matrigel mattress method plating protocol. B, Matrigel mattress method work flow. C, Matrigel mattresses plated on Delta TPG Dish (Fisher Scientific), white arrows indicate edge of each mattress, blue dye included to visualize mattress. D, hiPSC-CMs plated on control (left panel) and mattress (right panel). Scale bar 50 µm. White arrows indicate edge of mattress platform. (Feaster T. et al., *Circulation Research* 2015; doi: 10.1161/CIRCRESAHA.115.307580).

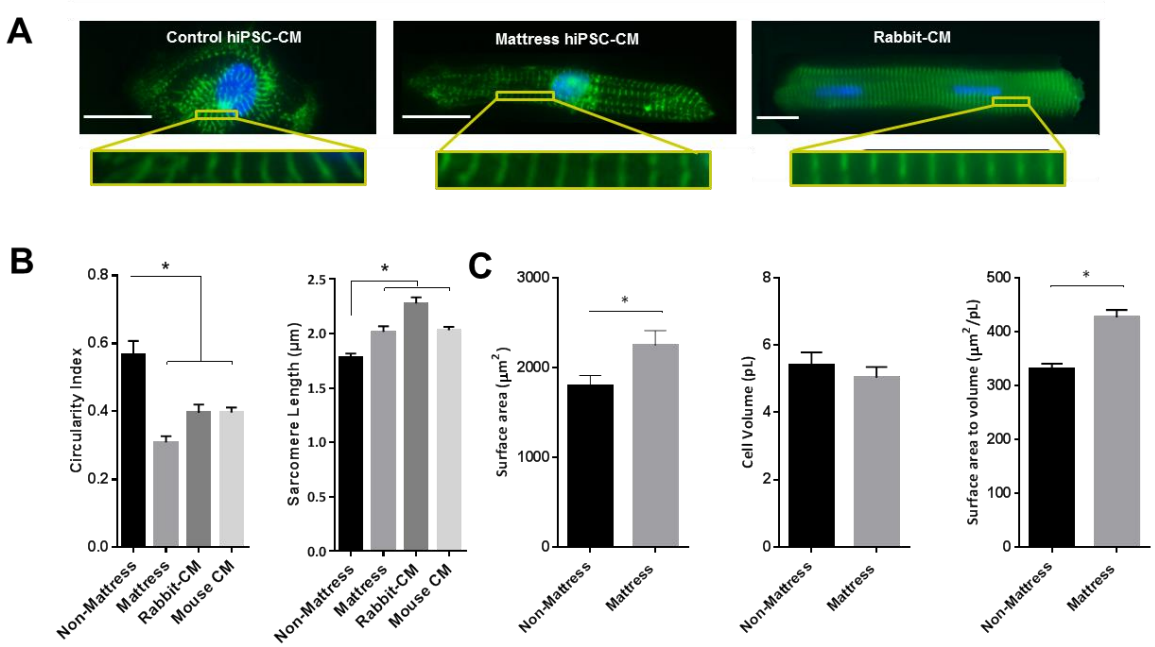

Figure 19. Matrigel mattress morphometry. A, Immunofluorescence staining of cardiomyocyte (CM) structural marker α-actinin (green) and nucleus (blue, DAPI) for control human induced pluripotent stem cell-derived cardiomyocytes (hiPSC-CM) (left), mattress hiPSC-CM (center) and rabbit-CM (right). Scale bar 20 μm. 63X. B, Cell morphometry measuring circularity index (left) and sarcomere length (right) are plotted for indicated CMs. C, Surface area (left), cell volume (center) and surface area to volume ratio (right) are plotted. Data are mean ± SEM. (n = 9 – 48 cells per group). **P*<0.05 vs control. (Feaster T. et al., *Circulation Research* 2015; doi: 10.1161/CIRCRESAHA.115.307580).

Mattress hiPSC-CMs display aligned myofilaments

Modulation of substrate stiffness has been shown to effect CM morphology [19]. Current cardiac induction strategies generate hiPSC-CMs, of similar age (i.e., day 30), with relatively immature structure exhibiting circular shape and unaligned myofilament architecture. I assessed morphology of mattress hiPSC-CMs using quantitative immunofluorescence staining (Figure 19 A and B) and Z stacks of confocal images (Figure 19 C). First, CMs were immunostained with α-actinin, Z-disk protein and dapi, nuclear marker. I found that mattress hiPSC-CMs display hallmarks of adult CMs that were missing in control hiPSC-CMs. Mattress hiPSC-CMs were more elongated, with increased anisotropy and aspect ratio, calculated as the length of the long axis divided by the length of the short axis [19] [20] and decreased circularity [11] (Figure 19 B) relative to control hiPSC-CMs. In addition, mattress hiPSC-CMs display increased sarcomere length more comparable to that of freshly isolated adult ventricular-CMs (Figure 19 B) and increased surface area. However, there was no change observed in cell volume which confirmed a quantitative geometric transition for mattress hiPSC-CMs, as shown in time-lapse images (Figure 20), along with increased surface area to volume ratio (Figure 19 C). These data demonstrate that while the Matrigel mattress does not enhance hiPSC-CM size it does enhance key morphological characteristics of hiPSC-CMs. In addition to the significant differences in morphology, I discovered that mattress hiPSC-CMs display visible cellular contraction (i.e., cell shortening) relative to control hiPSC-CMs (Figure 21) as demonstrated by percent of single hiPSC-CMs visibly shortening.

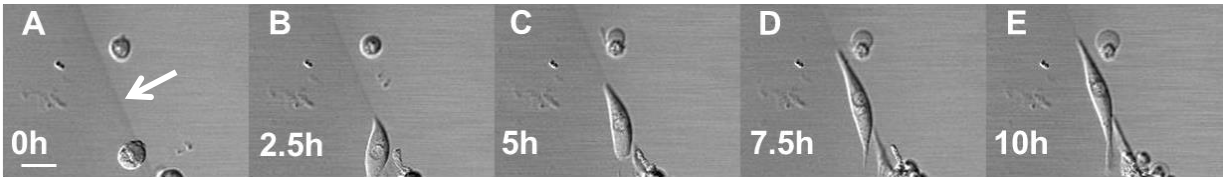

Figure 20. Sequential montage of hiPSC-CMs on Matrigel mattress. Scale bar 20 µm. Day 30 hiPSC-CMs were plated on Matrigel mattress and imaged every 15 minutes for 10 hours. White arrow indicates edge of Matrigel mattress. Images show mattress hiPSC-CM elongating in culture. Courtesy of Mr. Adrian C Gadar. (Feaster T. et al., *Circulation Research* 2015; doi: 10.1161/CIRCRESAHA.115.307580).

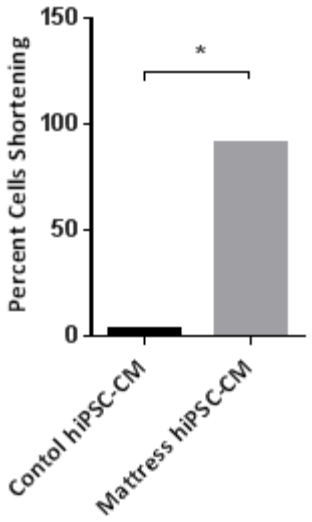

Figure 21. Robust shortening of Mattress hiPSC-CMs. Percent of hiPSC-CMs shortening on control substrate (i.e., Matrigel 1:60 and Matrigel mattress) cells are non-paced. *$P < 0.0001$ vs control. N = 407 – 547 per group. (Adapted from Feaster T. et al., *Circulation Research* 2015; doi: 10.1161/CIRCRESAHA.115.307580).

Mattress calcium handling assessment

To elucidate the mechanisms responsible for difference in contractile performance, I evaluated intracellular Ca handling, as Ca is directly upstream of contraction. I found that typical twitch Ca handling parameters (i.e., baseline, amplitude, decay) (Figure 22) were not significantly different in both groups suggesting changes in global Ca are not responsible for increased contractile performance (Figure 22 A and Table 3) of mattress hiPSC-CMs. However there was a significant increase in maximum return velocity of mattress hiPSC-CM twitch Ca transient which suggests enhanced EC coupling. Next, I evaluated the contribution of sarcoplasmic reticulum (SR) Ca stores using caffeine, an agonist of ryanodine receptor (RyR2) Ca release channels. Analogous to control, mattress hiPSC-CMs exhibited robust caffeine-releasable SR Ca stores (Figure 22 B and Table 3). Both caffeine-induced Ca transients and hence SR Ca content were of similar magnitude and not significantly different in both groups. However, the caffeine-induced Ca decay rate was faster in mattress hiPSC-CMs, which largely represents enhanced sodium calcium exchanger (NCX) activity. Taken together, these results are consistent with negligible effect of the Matrigel mattress on intracellular twitch Ca handling. The result that hiPSC-CMs maintained on Matrigel mattress exhibit robust cellular shortening and have comparable twitch Ca handling as control hiPSC-CMs suggest that the mattress does not negatively affect Ca handling properties. Further, these data suggest that Ca handling differences are not the primary mechanism responsible for the enhanced contractile performance and suggest that other interactions (e.g., substrate stiffness, integrins or myofilament alignment) are responsible.

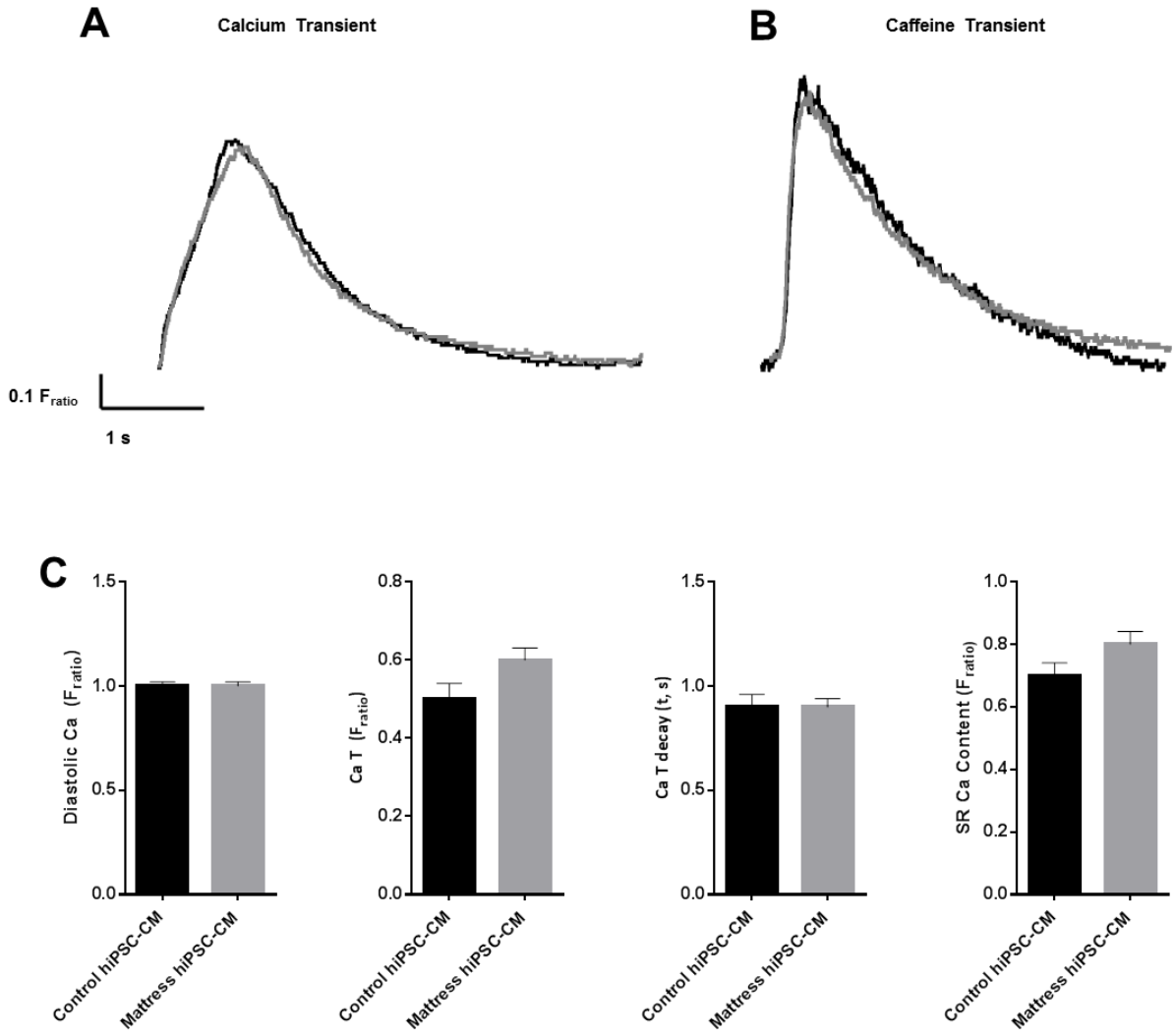

Figure 22. Mattress hiPSC-CM Ca handling. A, Representative Control (Black) and Mattress (Grey) hiPSC-CM Twitch Calcium transient. B, Representative Control (Black) and Mattress (Grey) hiPSC-CM Caffeine [10mM] Calcium transient. C, Data are mean ± SEM. N=25-35 per group. Date indicate negligible effect of the mattress culture method on twitch Ca handling. (Adapted from Feaster T. et al., *Circulation Research* 2015; doi: 10.1161/CIRCRESAHA.115.307580).

Table 3. Matrigel mattress calcium handling properties

Parameter	Control	Mattress	P - value
Diastolic Ca (F_{ratio})	1.0 ± 0.02	1.0 ± 0.02	0.6
CaT Amplitude (F_{ratio})	0.5 ± 0.04	0.6 ± 0.03	0.1
CaT Decay (t_{twitch}, s)	0.9 ± 0.06	0.9 ± 0.04	1.0
Time to Peak 90% (s)	0.3 ± 0.03	0.4 ± 0.04	0.2
Time to Baseline 90% (s)	2.0 ± 0.2	1.9 ± 0.1	0.8
SR Ca Content (F_{ratio})	0.7 ± 0.04	0.8 ± 0.04	0.09
Caff Tau (t_{Caff}, s)	3.0 ± 0.1	2.7 ± 0.1*	0.04
Vmax Upstroke (F_{ratio}/s)	4.1 ± 0.6	5.5 ± 0.7	0.2
Vmax Decay (F_{ratio}/s)	0.5 ± 0.4	0.7 ± 0.1*	0.03
n	25	35	

Table 3. Mattress Ca handling properties (non-paced). Summary data are mean ± SEM. **P*<0.05 vs control. (Feaster T. et al., *Circulation Research* 2015; doi: 10.1161/CIRCRESAHA.115.307580).

Elucidating the contractile properties of single hiPSC-CMs

Robust cellular shortening of isolated hiPSC-CMs

hiPSC-CM contractile properties have not been well described, greatly limiting our understanding of EC coupling. Hence, I set out to elucidate the baseline contractile properties (i.e., contraction, rates and kinetics) (Figure 23), of day 30 - 35 hiPSC-CMs, using the novel culture method. When quantitated with video-based microscopy, un-paced, mattress hiPSC-CMs contracted ~9.0 % of their resting cell length as compared to ~ 0.4 % for control (Figure 24 and Table 4). For comparison, contractions of this magnitude have only been reported for late-stage hiPSC-CMs after 80-120 days in culture [21], suggesting the mattress method accelerates this process, thus validating the significant contribution of the Matrigel mattress method to assessment of early hiPSC-CM contractility *in vitro* and demonstrates significant improvement over standard conditions.

As there is an expected inherent variability in hiPSC-CMs studies I evaluated the reproducibility of hiPSC-CMs contractile properties. To do this I quantified cellular contraction parameters of hiPSC-CMs independently generated at a different institution from an independently generated hiPSC line (Figure 24 and Table 4) as well as post recovery from cryopreservation. I found that all hiPSC-CMs plated on the mattress have comparable contractile properties including kinetics and beat frequency (Figure 24 and Table 4). These results demonstrate that mattress hiPSC-CM cellular contractile measurements are consistent and reproducible across lines.

The result that mattress hiPSC-CMs exhibit robust cellular shortening relative to control hiPSC-CMs suggest that the Matrigel mattress enables detailed quantifiable cell shortening, using standard microscopy techniques commonly used to assess adult-CMs. As such

implementation of the Matrigel mattress provides a robust platform for simultaneous evaluation of cellular contractile properties and other functional readouts including Ca handling of single hiPSC-CMs.

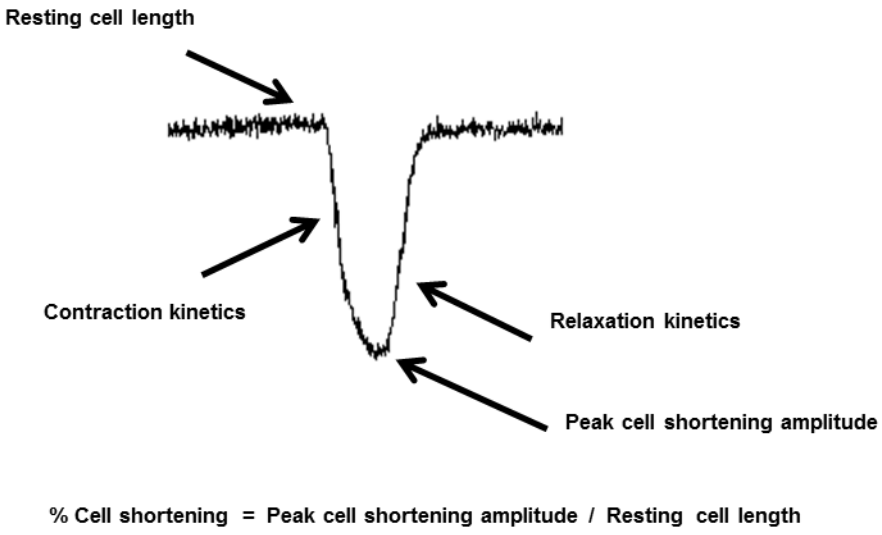

Figure 23. Diagram of typical cell shortening parameters: Resting cell length (cell length during diastole), peak cell shortening (cell length when maximally contracted, during systole), % cell shortening (cellular contraction normalized to the resting cell length) and contraction and relaxation kinetics (time to peak and time to baseline, respectively).

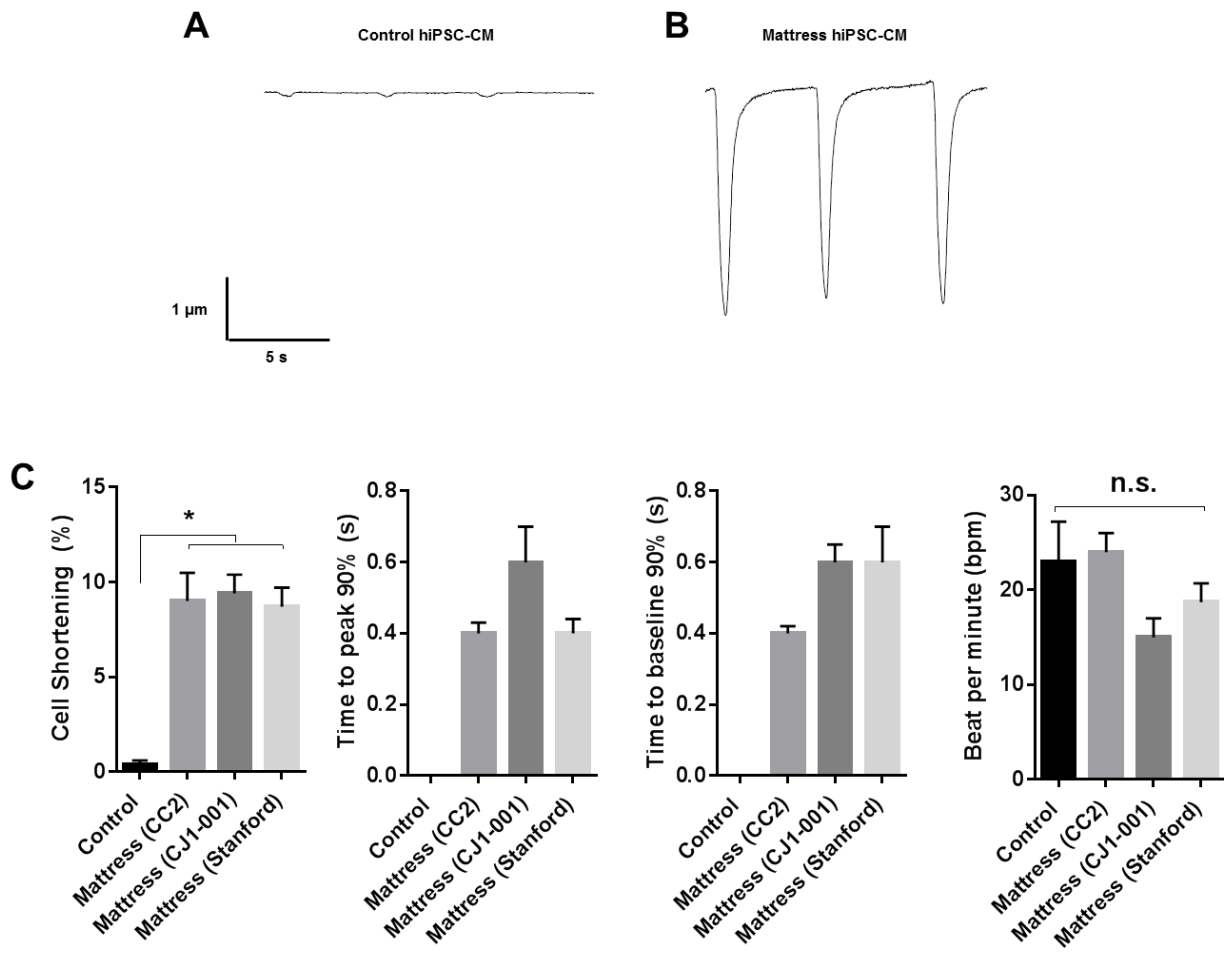

Figure 24. Matrigel mattress cell shortening measurements. A, Representative non-mattress and B, mattress hiPSC-CM contraction traces. C, Data are mean ± SEM. N=6-17 per group. Data indicate robust quantifiable contractile properties of mattress hiPSC-CMs. **P* < 0.05 vs control. Spontaneously beating hiPSC-CMs. Control hiPSC-CM contraction and relaxation kinetics were not measureable. (Adapted from Feaster T. et al., *Circulation Research* 2015; doi: 10.1161/CIRCRESAHA.115.307580).

Table 4. hiPSC-CM contractile properties

Parameter	Control	Mattress (CC2)	Mattress (CJ1 – 001)	Mattress (Stanford)
Peak Cell Shortening Amplitude (μm)	0.2 ± 0.1	5.1 ± 1.0**	7.0 ± 1.0***	7.0 ± 1.0***
Cell Shortening (% resting length)	0.4 ± 0.2	9.0 ± 1.5***	9.4 ± 1.0**	8.7 ± 1.0**
t to peak 50% (s)	n.m.	0.2 ± 0.02	0.3 ± 0.05	0.2 ± 0.02
t to peak 90%(s)	n.m.	0.4 ± 0.03	0.6 ± 0.1	0.4 ± 0.04
t to baseline 50% (s)	n.m.	0.3 ± 0.02	0.3 ± 0.03	0.3 ± 0.04
t to baseline 90% (s)	n.m.	0.4 ± 0.02	0.6 ± 0.05	0.6 ± 0.1
Beats per minute (bpm)	23.0 ± 4.2	24.0 ± 2.0	15.0 ± 2.0	18.7 ± 2.0
n	9	17	6	9

Table 4. hiPSC-CM contractile properties. Summary data are mean ± SEM *P < 0.05 vs control. (Feaster T. et al., *Circulation Research* 2015; doi: 10.1161/CIRCRESAHA.115.307580).

Mattress hiPSC-CMs display mature contractile properties

It remains unclear whether hiPSC-CMs accurately recapitulate characteristics of native-CMs. Therefore I directly compared contractile properties of hiPSC-CMs to that of freshly isolated adult ventricular CMs (i.e., rabbit and mouse) under identical experimental conditions (Figure 25). To determine the physiological relevance and provide context for the hiPSC-CM contractile properties, field-stimulated (0.2Hz) hiPSC-CMs and adult rabbit and mouse ventricular CMs were evaluated. While hiPSC-CMs were significantly shorter than adult-CMs (Figure 25 B left panel), consistent with the morphometric assessment. Cellular contraction and peak shortening amplitude (data not shown) were not significantly different and of similar magnitude among groups (Figure 25 B right panel). I also discovered mattress hiPSC-CMs exhibit contractile kinetics (i.e., time to peak and time to baseline) more comparable to that of rabbit-CMs (Figure 25 C), which are thought to be more comparable to human CMs [2], and significantly slower compared to that of mouse-CMs. These data suggest hiPSC-CMs are capable of producing cellular contractions and kinetics comparable to adult-CMs, displaying mature cellular contraction *in vitro*.

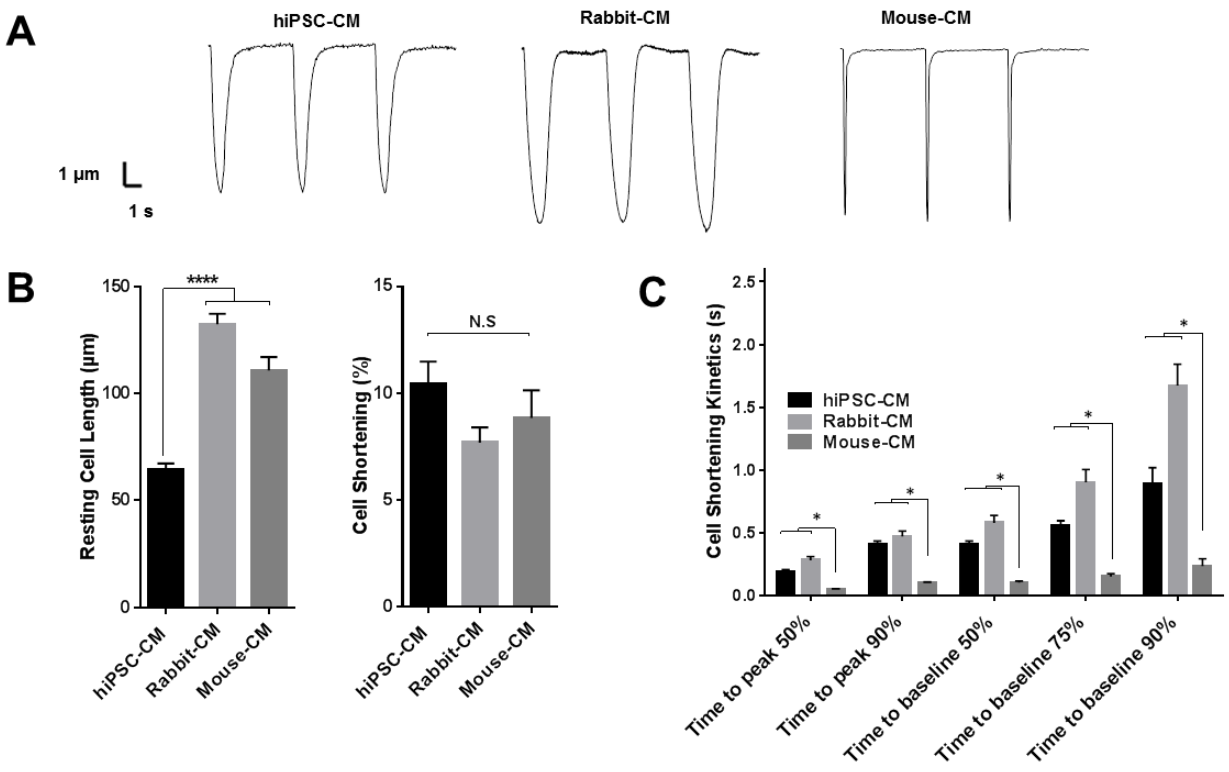

Figure 25. hiPSC-CM and adult-CM contractile comparison. A, Representative contraction traces of indicated CMs, 0.2Hz. B, and C, data are mean ± SEM. N = 6 – 20 cells per group. Data indicate mattress hiPSC-CMs display comparable contractile properties as adult rabbit-CMs. **** *P*< 0.0001 vs hiPSC-CM. **P*<0.05 vs mouse-CM. n.s, Not significant. (Feaster T. et al., *Circulation Research* 2015; doi: 10.1161/CIRCRESAHA.115.307580).

Contraction force and traction force of hiPSC-CMs

CM force is decreased in end-stage HF as such methods to evaluate and modulate this parameter are sought after. Here, I set out to determine if the contraction force produced by mattress hiPSC-CMs could be obtain from the Matrigel mattress platform analysis. HiPSC-CM contraction force was calculated based on the area of each hiPSC-CM, the deflection (i.e., peak shortening amplitude) and the mean modulus of the Matrigel mattress platform. To account for differences in cell size and enable experimental comparison, total force was normalized to cross sectional area and is presented as (mN/mm2). I found the average contraction force of hiPSC-CMs to be 0.3 ± 0.1 mN/mm2 (Figure 26).

Next, we evaluated how well the Matrigel mattress force compared with the established traction force microscopy (TFM) method (Figure 26 A and B) [7, 10] we found Matrigel mattress force correlated well with the established TFM method, exhibiting a positive correlation. These results demonstrate that hiPSC-CMs contraction forces can be evaluated with the data obtain from the Matrigel mattress platform.

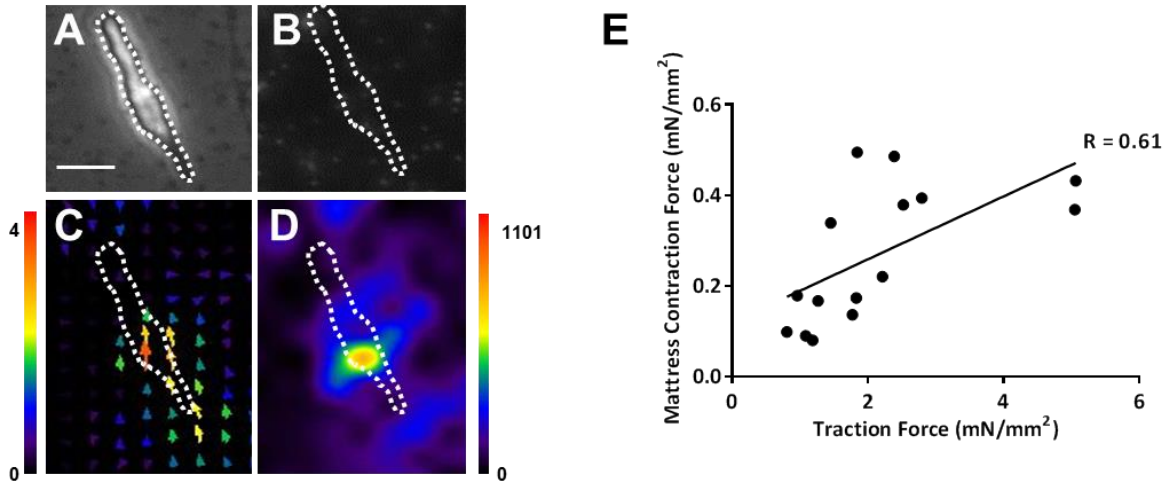

Figure 26. Traction Force correlation. A, Phase contrast image of hiPSC-CMs on Matrigel mattress with embedded fluorescence beads (0.75 µm diameter). B, Fluorescent image of A, C. Representative displacement field image of fluorescent beads calculated with particle image velocimetry (PIV) algorithm. D, Fourier transform traction cytometry (FTTC). (A – D). Scale bar, 20 µm. E, Correlation between Matrigel mattress platform calculated contraction stress and traction force estimated with the FTTC algorithm (n = 15 cells). Courtesy of Mr. Charles H. Williams. (Feaster T. et al., *Circulation Research* 2015; doi: 10.1161/CIRCRESAHA.115.307580).

Enhanced maturation of hiPSC-CMs

Cardiac molecular profile of mattress hiPSC-CMs

In an attempt to correlate functional differences of mattress hiPSC-CMs with molecular expression and to provide mechanistic insight, we performed transcriptional profiling of a subset of cardiac genes involved in EC coupling (Figure 27 A). We observed differential expression of genes including *TNNI3*, encoding cardiac troponin I. Cardiac troponin I is minimally expressed in hiPSC-CMs on standard substrates. However, it is required for a mature molecular signature [25]. Western blot analysis confirmed transcriptional alteration associated with the mattress (Figure 27 B and C), and thus, we have validated the ability of the Matrigel mattress to modulate not only hiPSC-CM morphology and contractility but also underlying molecular profile.

Enhanced electrophysiological properties of hiPSC-CMs

To determine if the Matrigel mattress enhances electrophysiological properties we evaluated action potential morphology and sodium current density of mattress and control hiPSC-CMs. (Figure 28). We found mattress hiPSC-CMs have increased upstroke velocity (84 ± 8.0 V/s $P < 0.05$) relative to control hiPSC-CMs, consistent with both increased sodium current density (Figure 28 B and C) and increased SCN5A transcript (Figure 27 A).

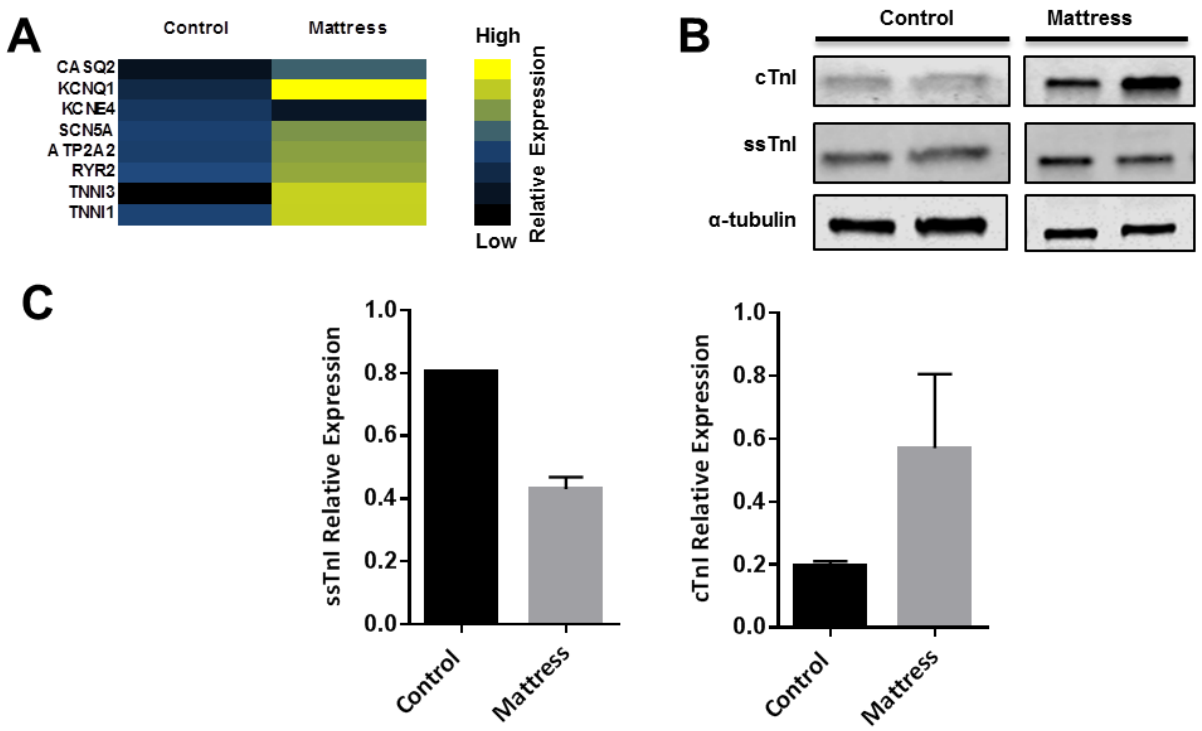

Figure 27. Mattress hiPSC-CM molecular characterization. A, Heat map from gene expression screen, non-mattress and mattress hiPSC-CMs, measured by real-time qPCR. Low expression (Black) and high expression (Yellow). B, Western blot confirmation for indicated proteins (n = 2 independent biological replicates). C, Summary bar graphs of relative ssTnI and cTnI expression, data are mean ± SEM. Courtesy of Mr. Adrian C Gadar. (Feaster T. et al., *Circulation Research* 2015; doi: 10.1161/CIRCRESAHA.115.307580).

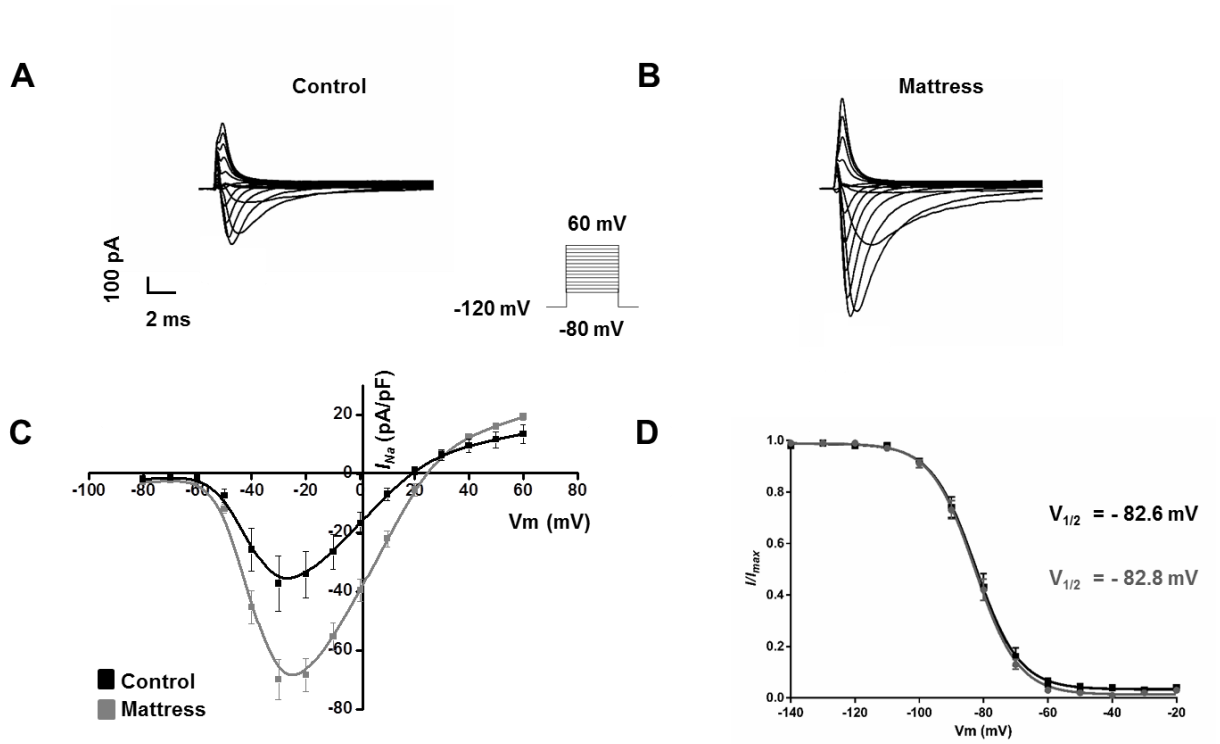

Figure 28. Characteristics of mattress sodium (I_{Na}) current. A, Representative I_{Na} current of control hiPSC-CMs and B, mattress hiPSC-CMs. Traces were elicited be voltage protocol shown below current recording. C, Current-voltage relationship of peak I_{Na} current from control hiPSC-CMs and Mattress hiPSC-CMs. D, I_{Na} Steady-state inactivation for control hiPSC-CMs and mattress (hiPSC-CMs). (Control hiPSC-CMs, black, n = 13) and (mattress hiPSC-CMs, grey, n = 15). $V_{1/2}$, half activation voltage. Courtesy of Dr. Lili Wang. (Feaster T. et al., *Circulation Research* 2015; doi: 10.1161/CIRCRESAHA.115.307580).

2.5 Discussion

hiPSC-CMs could become a powerful tool for basic biology and drug discovery. However, for the full potential of this technology to be realized, detailed characterization of EC coupling is required. This includes multiple functional read outs (i.e., electrophysiology, Ca handling and contractility) under identical experimental conditions however this is rarely done. I systematically evaluate key aspects of EC coupling properties of hiPSC-CMs, at the single cell level.

Major new findings are that hiPSC-CMs generated by the latest monolayer based cardiac differentiation protocols display relatively mature electrophysiological properties (Figure 13). Along with robust and functional SR Ca handling that is not statistically different from that of acutely-isolated adult rabbit ventricular CMs (Figure 16), a species that is generally thought to exhibit cardiac Ca handling similar to humans [3]. We further demonstrate that independently generated hiPSC-CM lines from healthy donors exhibit comparable and reproducible Ca handling. In addition the establishment and implementation of our novel culture method enables robust hiPSC-CM cellular shortening of single hiPSC-CMs (Figure 21). I demonstrate hiPSC-CM exhibit relatively mature contractile properties that are comparable to adult rabbit-CMs and reproducible across laboratories (Figure 24 and 25). Moreover, the mattress platform enhances maturation of hiPSC-CMs including morphology, molecular expression and action potential waveform.

Comparison of hiPSC-CMs and acutely-isolated adult CMs EC coupling.

Lacking access to acutely-isolated healthy human ventricular CMs – a common problem for the field – we compared hiPSC-CMs with adult rabbit and mouse CMs. Rabbit-CMs have been widely used to model human heart diseases [3]. We found that hiPSC-CMs have twitch EC coupling properties comparable to that of rabbit-CMs. This includes Ca transient

amplitude, % cell shortening and action potential amplitude. This is in direct contrasts with previous reports indicating that hiPSC-CMs have smaller relatively “immature” electrophysiology, Ca handling and contractile properties [28] [22]. On the other hand there are several EC coupling differences between hiPSC-CM and adult rabbit-CMs. For instance there are electrophysiological differences such as significantly slower upstroke velocity (Figure 13 and table 2). This could be the result of decreased I_{Na} relative to rabbit-CMs. HiPSC-CMs also display markedly smaller cell capacitance (Figure 13 C) consistent with previous reports [11] and our morphometric analysis (Figure 12) of their cell size. This may be the result of the perceived unloaded culture conditions. As for Ca handling we observed differences between hiPSC-CM and rabbit CM including: significantly slower SERCA and NCX Ca transport (Table 3) slower time to peak Ca transient (Figure 16). Morphological factors such as the lack of t-tubules of hiPSC-CMs leading to an inefficient Ca induced Ca release and hence impaired Ca-dependent inhibition of L-type Ca current during the action potential plateau may contribute to the slower time to peak of hiPSC-CM Ca transients. While the differences in SERCA and NCX function could be due to species differences between human and rabbits, a more likely explanation is that Ca transport remains somewhat immature in hiPSC-CMs compared to adult CMs.

With respect to contractile properties despite the fact that hiPSC-CMs display significantly shorter resting cell length they are capable of producing contractions comparable to adult-CMs (Figure 25). Moreover, their contractile kinetics are comparable to those of adult rabbit-CMs. Thus, I provided the first direct comparison of isolated hiPSC-CM contractile properties and adult-CMs, a comparison that has been lacking in the field. In addition the direct comparison to freshly isolated adult-CMs studied under identical experimental conditions further demonstrates the utility of this platform.

Advantages of the matrigel mattress culture method

The culture method we describe here has a number of significant advantages: (1) the commercial availably of Matrigel, (2) the simple logistics of the Matrigel mattress platform preparation, (3) the noninvasive and non-lethal nature of the experiments which widens the scope of potential studies, (4) the mattress is label free this is particular important for Ca handling experiments enabling multiple fluorophores to be used simultaneously without substrate interference, (i.e., embedded fluorescent beads), as is the case with traction force microcopy, (5) this platform does not require functionalization as Matrigel provides an inherent adhesive substrate for attachment unlike other hydrogel based platform (e.g., polyacrimide), (6) the moduli of Matrigel mattress used in this study, ~ 5.8 kPa, is physiologically relevant recapitulating cardiac tissues which provide stiffness of 4.0 to 46.2 kPa [12][41] this in contrast to the perceived preload of glass (i.e., GPa range) [44]. Taken together these advantages demonstrate how the proposed platform will prove useful by making cellular mechanical measurements translatable to most laboratories.

Implications for future hiPSC studies

The results of our experiments have a number of implications for using hiPSC-CMs as experimental models. First, monolayer-based methods of cardiac differentiation are capable of generating hiPSC-CM with robust and functional SR Ca stores. In addition the mattress method enables quantifiable and robust cell shortening. The results presented here provide a foundation for future disease modeling studies by elucidating “healthy” hiPSC-CM EC coupling properties. In this method hiPSC-CMs can be recovered from cryopreservation demonstrating that these cells exhibit robust reproducible properties. And culturing hiPSC-CMs on mattress enhances key characteristics of maturation. Moreover, as there is limited contractile movement on standard substrates the Matrigel mattress may be able to systematically unmask disease

phenotypes not present under standard culture conditions [18]. And hiPSC-CMs made from different hiPSC lines that were derived from different somatic tissue sources by different methods of reprogramming have comparable Ca handling and contractile properties. This result is reassuring, since there is concern in the field that starting cell source (e.g. neonatal or adult fibroblast) and reprogramming methodology (e.g. integrating or non-integrating) may impact differentiated cell progeny (e.g., alter EC coupling) our results demonstrate starting somatic cell source does not clearly impact E-C coupling functional readouts.

Finally, the methods of cryopreservation and recovery described here could serve as a first step of standardization, which is greatly needed in the field. Having frozen stocks of hiPSC-CMs that can be reproducibly recovered, as shown here, opens up a number of possibilities. Cells can be shared between laboratories, saved for future experiments, or for doing larger experiments such as screening compound libraries and regenerative medicine.

Limitations

There are several limitations for the Ca handling comparison. To ensure identical study conditions, all hiPSC-CMs were frozen at specific dates after cardiac differentiation, then thawed and re-plated prior to study. We cannot exclude that the freezing and thawing process has altered the phenotype of the hiPSC-CMs. However, the advantage of this approach is that multiple batches of re-plated cells from different labs can be readily compared, which is why we chose this approach here. This is also the reason why we could not examine hiPSC-CMs older than 30 days, because the viability of older cells decreases substantially after freezing. Another limitation is that we did not differentiate hiPSC-CM subtype (i.e., nodal, atrial, and ventricular-like). However, previous studies have shown that the cardiac induction protocols used here produce approximately 80% ventricular-like CMs. Importantly, the cell to cell variability of Ca handling parameters (i.e., twitch transient amplitude) of hiPSC-CMs was comparable to that of

acutely-isolated adult CMs (approximately a 30% coefficient of variation). As such methods to enrich for a desired subtype will be useful, to characterize the chamber specific properties of hiPSC-CMs and for chamber specific diseases such as atrial fibrillation

In addition there are several limitations to our hiPSC-CM contractility studies, most notably hiPSC-CM maturity. The immature phenotype, relative to adult primary CMs, is based on several structural and functional endpoints, previously reported. Here we report external factors, namely substrate stiffness, can enhance hiPSC-CM morphometry. Further work will need to be done to fully understand these mechanisms, currently may researchers are exploring additional methods including, biochemical and electrical stimulation, to accelerate hiPSC-CM maturation *in vitro*.

While unlikely, the dependence on Matrigel, a chemically undefined substrate, may be a limitation. Whereas Matrigel is routinely used for hiPSC maintenance and hiPSC-CM functional studies, there may be unknown effects of undiluted Matrigel on contractile properties. For this reason we and others are working to develop chemically define substrates. If these substrates are capable of capturing contractile properties of isolated hiPSC-CMs they will be a nice addition to this approach.

Here, our major findings focus on cellular contractility (i.e., cell shortening), instead of sarcomere length. While sarcomere length can also be measured with the Matrigel mattress platform we focused on changes in total cell length. It has previously been demonstrated that changes in hPSC-CM cell length and sarcomere length correlate well with each other [21]. Additionally, the limited throughput of the Matrigel mattress platform makes large scale primary screening assays unrealistic. While in the future the Matrigel mattress may be extend to medium throughput, in its current form it will prove useful as a secondary screening assay, early

in candidate identification, providing mechanistic insight in a human background. Indeed, we are currently developing such high throughput format.

I also present a calculated contraction force measurement. This mathematically derived contraction force is not a direct measurement and does not represent an absolute measurement. The contraction force presented takes into account the area of each hiPSC-CM making it possible to compare results across laboratories. However, it should be noted that edge detection is a two point analysis based on lateral movement that may underestimate total force produced as axial modes of force may not be accounted for. Additionally the cross sectional area used only applies to hiPSC-CMs in this study and age.

Chapter 3

hiPSC-CM DISEASE MODELING

3.1 Chapter Abstract

Sarcomeric cardiomyopathy, encompassing hypertrophic cardiomyopathy (HCM), dilated cardiomyopathy (DCM), and restrictive cardiomyopathy (RCM), is an important cause of morbidity and mortality. While human genetic studies have provided lists of causal sarcomeric gene mutations, the pathobiology of human sarcomeric cardiomyopathies remain generally poorly understood. A major hindrance to detailed study of sarcomeric cardiomyopathies in humans has been lack of an appropriate *in vitro* cardiac tissue models. Here, I use hiPSC-CM technology to study the functional consequence of sarcomeric cardiomyopathies specifically Ca handling and contractility. HiPSC-CMs were generated through reprogramming of somatic cells of two cardiomyopathy patients, one carrying a HCM *MYH7* R633H mutation and one with DCM but no known mutation. In addition I use genetic engineering strategies to evaluate the RCM *TNNI3* R204C mutation. I found HCM *MYH7* R633H hiPSC-CMs display abnormal twitch Ca handling properties including significantly slower Ca decay rates and prolonged Ca handling kinetics (i.e., time to peak and time to baseline) concurrent with contractile dysfunction and I provided evidence supporting an enhanced myofilament Ca sensitivity mechanism. Next, I recapitulate *in vitro* DCM phenotypes, in a *novel* DCM hiPSC-CM line, including myofilament disarray, altered Ca handling kinetic and increased SR Ca content. Finally I provide a reagent to evaluate the *novel* RCM cardiac troponin I mutation. I conclude that patient specific hiPSC-CMs exhibit classic clinical phenotypes, and that the implementation of the mattress platform facilitates elucidation of previously undiscovered defects of diseased hiPSC-CM.

3.2 Introduction

The lack of human heart samples has been a major barrier to detailed understanding of the pathophysiology of human cardiomyopathies. However, this spectrum of diseases is thought to be multifactorial, primarily involving complex interplay between genetic sarcomere mutations and acquired events or compensatory mechanisms. As such typical disease progression involves maladaptive phenotypic alterations in myocardial structure and function. Despite the depth of knowledge, surrounding the genetic association little is known of the pathophysiology and underling mechanisms of cardiomyopathies.

To study heart failure pathology and pathophysiology I use hiPSC-CMs, as an intact *human* heart cell model. Through collaboration with the Vanderbilt Center for Inherited Heart Disease I have obtained dozens of explanted cardiac tissue samples to generate hiPSC lines. We have also collaborated with other institutions to obtain diseased hiPSC-CMs carrying specific mutations.

Here, I study the hypertrophic cardiomyopathy (HCM) line, SCVI6-CM, derived at Stanford University (Joseph Wu Laboratory) from a patient carrying an autosomal dominant missense mutation Arg663His in the gene *MYH7* which encodes the sarcomere component β-myosin heavy chain. Patients with this disease causing mutation present with abnormal thickening of the heart muscle and progress to a HF phenotype. Lan and colleagues showed HCM hiPSC-CMs display key structural features of HCM such as cellular hypertrophy and increased multinucleation [13]. HCM hiPSC-CMs displayed key functional features such as contractile arrhythmias evaluated by pixel quantification analysis (as disused above), and Ca handling abnormalities such as increased diastolic Ca and decreased SR Ca content however no change was reported in Ca handling decay rate or kinetics. Detailed assessment of contractile properties was not performed due to current methodological limitation.

Dilated cardiomyopathy (DCM) is the most common form of cardiomyopathy. Here we derived hiPSC from a DCM patient (6 months old) by plasmid-based reprogramming from left ventricular cardiac fibroblasts. Genetic testing of a panel of cardiomyopathy associated genes revealed no known mutation. Sun and colleagues demonstrated DCM hiPSC-CMs derived form a patient carrying *TNNT2* mutation, which encodes cardiac troponin T, recapitulate DCM phenotypes *in vitro* such as disorganized myofilaments, Ca handling abnormalities and using AFM show mechanical dysfunction [12].

Restrictive cardiomyopathy (RCM) is the most devastating form of cardiomyopathy with a high risk of disease progression and death for which there are few animal models and no hiPSC-CMs model to date. While mutations in the desmin, α-cardiac actin, cardiac troponin T and cardiac troponin I (*TNNI3*) genes have been associated with RCM, how specific mutations alter human cardiomyocyte (CM) structure and function, and ultimately cause the RCM phenotype, are largely unknown.

I identified a RCM patient with a *de novo* R204C mutation in *TNNI3*, which encodes the cardiac troponin I (Figure 38). The patient initially presented with aborted SCD, and no observable hypertrophy. However, symptoms progressed to a point necessitating cardiac transplantation. Here I use genetic engineering strategies to evaluate the structural and functional consequences of this novel mutation in *TNNI3*, which is otherwise not expressed in hiPSC-CMs, providing the first hiPSC-CM RCM model and demonstrating feasibility for evaluating the physiological consequences of the RCM mutation in hiPSC-CMS.

3.3 Materials and methods

Primary myocyte isolation

Ventricular myocytes from mouse and rabbit were isolated by a modified collagenase/protease method as previously described [38]. All the experiments conducted in

Tyrode's solution containing (in mM): $CaCl_2$, NaCl 134, KCl 5.4, $MgCl_2$ 1, glucose 10, and HEPES 10, pH adjusted to 7.4 with NaOH. Final concentration of Ca was 2 mM.

Human iPSC derivation and culture

Human induced pluripotent stem cells (hiPSCs) were generated, as described above. Briefly, HCM line SCVI6-CM (HCM; MYH7 Arg663His) and control SCVI13-CM (Family member; WT unaffected) were derived from skin fibroblast by lentivirus with the 4 Yamanaka factors at Stanford University. DCM line LVIP4 was generated from left ventricular cardiac fibroblast by episomal based reprogramming. All protocols were approved by the respective institutions Institutional Review Board. For all reprogramming individual colonies with typical hESC morphology were picked at day 17 to 30 and clonally expanded. All hiPSCs exhibit normally karyotype. hiPSC lines were routinely maintained on Matrigel, growth factor-reduced 1:200 (Corning) or on Synthemax II-SC coated plates in mTeSR1 medium (Stemcell Technologies) or E8 medium (Stanford University). Cells were passaged every 4 days using 0.5 mM EDTA (Life Technologies) in D-PBS without $CaCl_2$ or $MgCl_2$ (Life Technologies). 2 µM thiazovivin (Selleck Chemicals) or 10 µM Rho kinase inhibitor Y-27632 (CalBiochem) was added for the first 24hrs after passaging. Cells were maintained at 37ºC, with 5% CO_2 and 5% $O_{2.}$.

Generation of Adenoviral Vectors

Recombinant adenovirus vectors were engineered as previously described [45] by transfecting shuttle plasmids containing cardiac troponin I (cTnI) cDNAs and Ad-5-derived plasmid into HEK 293 cells. Each shuttle plasmid had a CMV promoter, along with WT or mutant cTnI and a bicistronic mCherry cassette. Each virus was titered, plaque-purified and stored at – 80 C until use.

Measurement of intracellular Ca

Myocytes were loaded with Fura-2 acetoxymethyl ester, Fura-2 AM (Molecular Probes Inc, Eugene, OR) as described previously [38]. Briefly, myocytes were incubated with 2 μM Fura 2 AM for 8 minutes at room temperature to load the indicator in the cytosol. Myocytes were washed twice for 10 minutes with Tyrode's solution containing 250 μM probenecid to retain the indicator in the cytosol. A minimum of 30 min were allowed for de-esterification before imaging the cells. Fura 2-AM loaded myocyte Ca transients recorded during 0.5 Hz field stimulation in 2 mM Ca Tyrode's solution for 20 second at room temperature. Then stimulation was switched off followed by application of caffeine 10 mM for 5 second to estimate SR Ca content. A subset of cells was exposed to 0Ca0Na Tyrode's solution for 10 seconds then caffeine 10 mM applied for 30 second to estimate non-NCX Ca extrusion. For each cell and each experimental condition, tau (τ), amplitude and baseline values were averaged from 3 consecutive Ca transients. Ca transients were recorded and analyzed using commercially available data analysis software (IonOptix, IonWizardTM Milton, MA). All experiments were conducted at room temperature. Briefly, myocytes were incubated with 2 μM Fura 2 AM for 8 minutes at room temperature to load the indicator in the cytosol. Myocytes were washed twice for 10 minutes with Tyrode's solution containing 250 μM probenecid to retain the indicator in the cytosol. A minimum of 30 min were allowed for de-esterification before imaging the cells. Fura 2-AM loaded myocyte Ca transients recorded during 0.5 Hz field stimulation in 2 mM Ca Tyrode's solution for 20 second at room temperature. Then stimulation was switched off followed by application of caffeine 10 mM for 5 second to estimate SR Ca content. A subset of cells was exposed to 0Ca0Na Tyrode's solution for 10 second then caffeine 10 mM applied for 30 second to estimate non-NCX Ca extrusion. For each cell and each experimental condition, tau (τ), amplitude and baseline values were averaged from 3 consecutive Ca transients. Ca

transients were recorded and analyzed using commercially available data analysis software (IonOptix, IonWizardTM Milton, MA). All experiments were conducted at room temperature.

Video based edge detection

Video edge detection was used to assess cellular contraction (i.e., cell shortening) of contracting CMs. Briefly; CMs were visualized using Nikon Ellipse T5100 coupled to IonOptix video microscopy system (IonOptix). Spontaneous or field stimulated contraction traces were recorded in 2 mM Ca Tyrode solution. For each cell and each experimental condition typical contraction parameters including percent cell shortening (i.e., percent of resting cell length) and contractile kinetics (i.e., time to peak 90% and time to baseline 90%) values were averaged. Contraction traces were recorded and analyzed using commercially available data analysis software (IonOptix, IonWizardTM Milton, MA). Only isolated hiPSC-CMs with aspect ratio greater than or equal to 4 were used, non-shortening cells were excluded from analysis.

Hysteresis loop analysis

Hysteresis loops were constructed as described before [46]. Briefly, representative HCM and control, Ca transient and cell shortening trace were selected by highlighting in IonWizardTM software (IonOptix, Milton, MA). Both Ca transient amplitude data (F_{ratio}) and cell shortening trace data (um) were exported and pasted into Microsoft Excel. In Microsoft Excel duplicated were removed, this function is found under the data tab, by highlighting both time and length or time and ratio then selecting only the time variable. Such that for each time point there was a corresponding cell length measurement and Ca transient amplitude ratio. Cell shortening values were multiplied by -1 to convert all values to positive numbers and were plot on the Y-axis as a function of Ca transient amplitude values on the X-axis.

Potential hysteresis loop characteristics:

- Positive inotrope, increased area and upward shift of the hysteresis loop
- Negative inotrope, decreased area and downward shift of the hysteresis loop
- Myofilament Ca sensitizer, upward leftward shift of the hysteresis loop
- Myofilament Ca desensitizer, downward rightward shift of the hysteresis loop
- Larger loop area, indicated higher contractile function

Western blot analysis

Western blot analysis was carried out as described [39]. Briefly, hiPSC-CMs were seeded on mattress or non-mattress (1:60 Matrigel) for 5 days. hiPSC-CMs were lysed with RIPA buffer supplemented with protease inhibitor and phosphatase inhibitor cocktail (Sigma). To remove excess Matrigel from mattress lysates, all lysates were centrifuged at 16,000 rpm for 15 minutes at 4°C. Protein was quantified using Bio-Rad DC Protein Assay. five µg of protein lysates were resolved on 12 % mini-Protean TGX gels (Bio-rad) and transferred onto nitrocellulose membranes for immunoblotting. Membranes were incubated with primary antibodies α-tubulin (rabbit monoclonal, Abcam), ssTnI (rabbit polyclonal, Sigma), cTnI (rabbit polyclonal, Abcam) overnight at 4°C. LI-COR. LI-COR secondary antibody were used and detected by Odyssey CLX (LI-COR) per manufacturer's protocol. Protein band intensities were quantified and normalized to alpha-tubulin band intensities using Li-COR Image Studio software.

Immunohistochemistry

Immunostaining of CMs was carried out as before [13]. Briefly, CMs were fixed in 2% paraformaldehyde for 5 minutes at room temperature, permeabilized with 0.2% Triton X-100 (Sigma) for 10 minutes at 4 C. Samples were blocked with 1% BSA in PBS solution and incubated for 1 hour at room temperature. Primary antibody, a-actinin (mouse monoclonal, Sigma), was added in 0.1% Triton X-100 1% BSA in PBS solution and incubated overnight at 4

C. Samples were washed with 0.2% Tween 20 in PBS, secondary antibodies specific to the primary IgG isotype were diluted (1:1000) in the same solution as the primary antibodies and incubated at room temperature for 1 hour. Samples were washed with 0.2% Tween 20 in PBS twice and mounted. Slides were examined with Olympus IX81 microscope coupled to Slidebook software. For morphometric analysis images were imported into Image J and analyzed using standard plugins.

Electron micrograph

A ten cm dish of day 30 control hiPSC-CMs and DCM hiPSC-CMs were washed to remove debris, then immediately fixed in 2.5% gluteradehyde in 0.1 M sodium cacodylate buffer for 1 hour at room temperature. Next samples were exposed to a secondary fixation (osmium tetroxide) and dehydration and resin infiltration steps followed by sectioning and embedding samples.

Sanger sequencing

Cardiac fibroblasts were isolated for RCM patient explanted heart. Briefly, left ventricular tissue was processed by mincing tissue with scalpel. Minced tissue were plated in 10 cm tissues culture dish and incubated at 37 C in fibroblast growth medium 2 C-23020 until fibroblast are observed proliferating from tissue. Cardiac fibroblast were expanded and processed for sanger sequencing. Genomic DNA was isolated and separated on an agarose gel, the bands were then excised processed and sequenced.

Statistical analysis

Data are mean ± SD unless indicate otherwise. Statistical differences between two groups were tested with two-tailed Student's t test. Statistical differences among more than two groups were assessed using one-way ANOVA followed by tukey or bonferroni correction.

Results were considered statistically significant if the p-value was less than 0.05. Statistical analysis was performed using Graphpad Prism 6.

3.4 Results

HCM *MYH7* A663H hiPSC-CMs exhibit altered twitch Ca handling properties

The structural results of the HCM *MYH7* A663H mutation in hiPSC-CMs have been previously described including cellular hypertrophy and increased multinucleation [13]. Feng and colleagues also purpose a potential HCM *MYH7* A663H mechanism of increased Ca sensitivity (i.e., affinity) (Figure 29). I hypothesized that HCM *MYH7* A663H hiPSC-CMs exhibit distinct differences in functional phenotypes relative to control hiPSC-CMs. Here I set out to expand on the previous reports for the HCM *MYH7* A663H mutation and implement the Matrigel mattress method to perform a detailed assessment of contractile properties and Ca handling. I hypothesize that HCM *MYH7* A663H hiPSC-CMs will display altered twitch Ca transients including decreased Ca decay and kinetics (Figure 30) resulting in abnormal contractile properties at the single hiPSC-CM level. I first evaluated intracellular twitch Ca handling of HCM *MYH7* A663H hiPSC-CMs and mutation negative family member controls hiPSC-CMs (Stanford University). Although HCM *MYH7* A663H hiPSC-CMs display comparable Ca transient amplitude (Figure 30 A and B) as control, I discovered HCM *MYH7* A663H hiPSC-CMs exhibit slower Ca decay rates (Figure 30 A and B) along with prolonged Ca handling kinetics (Figure 30 A and B). These results suggest the HCM *MYH7* A663H mutation may exert an effect by modulating myofilament Ca sensitivity and hence Ca removal from the cytoplasm.

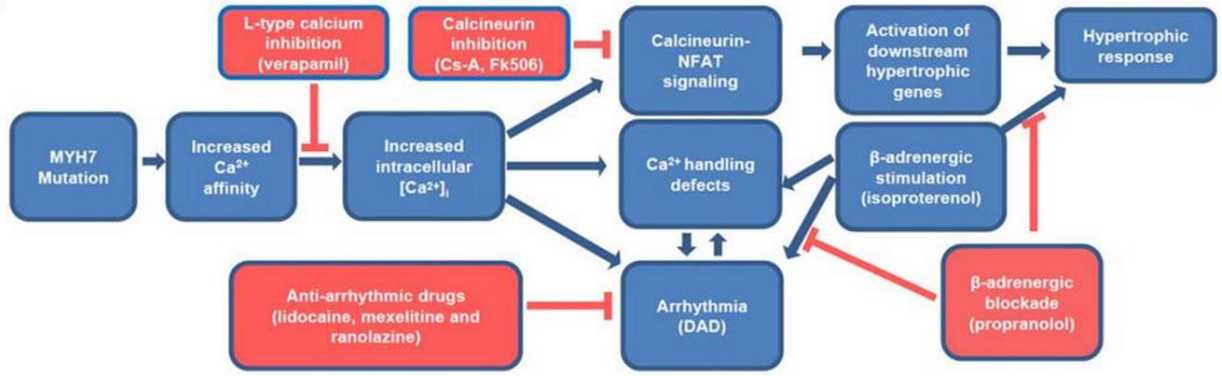

Figure 29. Proposed HCM MYH7 mechanism and nodes of intervention. Mutation in the thick filament protein β-myosin heavy chain may increase Ca affinity which in turn increases intracellular Ca concentration. This pathological increase in Ca may have consequences such as: increased calcineurin NFAT signaling, ultimately initiating a hypertrophic response. And Ca handling defects and provides an arrhythmia substrate which may be exacerbated by enhanced β- Adrenergic stimulation. Fen et al. propose therapeutic options including L-type Ca channel blockers, which may reduce the increased intracellular Ca concentration. Calcineurin NFAT signaling inhibitors, to reduce the pathological hypertrophy and β blockers to reduce arrhythmic occurrence and attenuate hypertrophy. (Feng L. et al., *Cell Stem Cell* 2013; 12, 101-103).

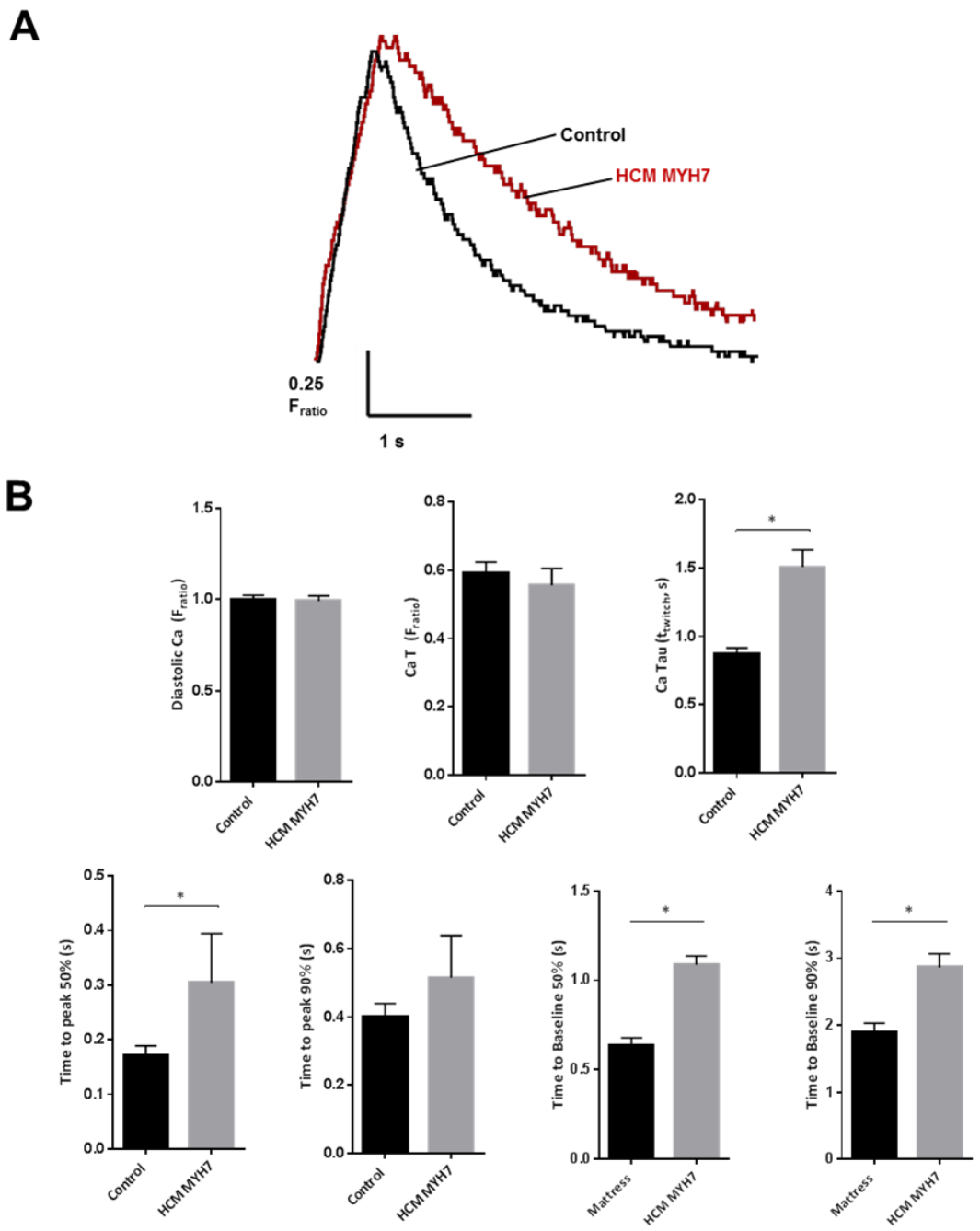

Figure 30. HCM (*MYH7* R663H mutation) hiPSC-CMs Ca handling. A, Representative twitch calcium transient from HCM (Red) and Control (Black) hiPSC-CM. B, Data are mean ± SEM (n = 6 – 35 cells per group). **P*<0.05 vs control hiPSC-CMs. Data show significate Ca handling abnormalities including decreased decay rate and prolonged kinetics.

Contractile dysfunction of HCM MYH7 A663H hiPSC-CMs

To determine if the altered twitch Ca handling properties translate to dysfunction in cellular contractions, I implement our novel culture method [24], to elucidate the contractile consequences of the HCM *MYH7* A663H mutation. I found that HCM *MYH7* A663H hiPSC-CMs display significantly increased cellular contraction (Figure 31 and table 5) relative to control hiPSC-CMs. In addition I discovered HCM *MYH7* A663H hiPSC-CMs display significantly prolonged contraction and relaxation kinetics (Figure 31 C and table 5) consistent with increased Ca affinity. Next, I use the Matrigel mattress method to simultaneously evaluate contractile properties and Ca handling properties to get a representation of the HCM *MYH7* A663H hiPSC-CM Ca sensitivity. This is done by hysteresis loop analysis (Figure 32) by plotting the cell shortening amplitude as a function of the peak Ca transient amplitude to elucidate possible alterations in the calcium-contraction relationship. When compared to control hiPSC-CM hysteresis loop I discovered that HCM *MYH7* A663H hiPSC-CMs display increased contraction at lower Ca concentrations, as indicated by the upward shift in the hysteresis loop (Figure 33), suggesting that the HCM *MYH7* A663H mutation result in increased myofilament Ca sensitively.

Since MYH7 is associated with increased risk of arrhythmia I evaluated if the HCM *MYH7* A663H mutation created a proarrhythmic substrate *in vitro* and if such effects could be assessed by differences in the HCM *MYH7* A663H hiPSC-CM contractile morphology (e.g., DAD and EAD). I found HCM *MYH7* A663H hiPSC-CM display significantly increased number of cells with irregular contractile transients (Figure 34). These data provide the first detailed assessment of twitch Ca handling and contractile properties of HCM *MYH7* A663H hiPSC-CM.

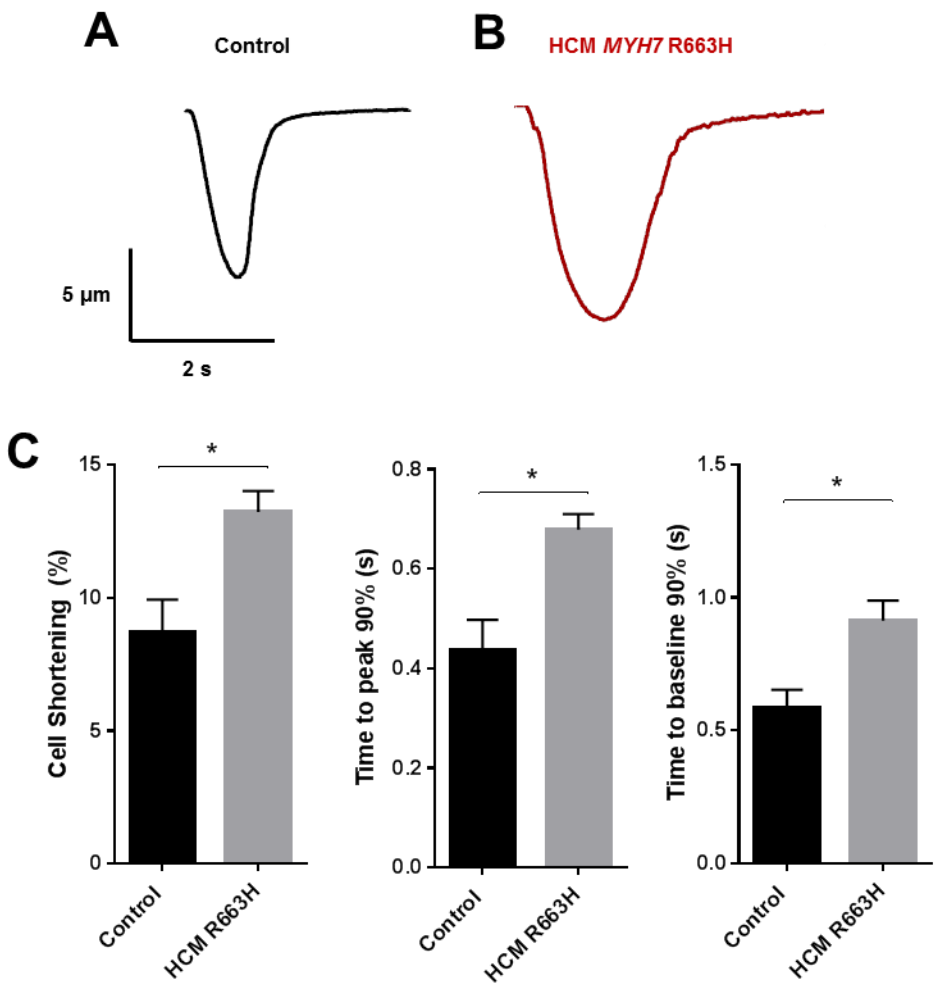

Figure 31. HCM R663H contractile assessment. A, Representative contraction trace of control (Black) and B, HCM (Red) *MYH7* R663H hiPSC-CM. C, Data are mean ± SEM (n = 5 - 29 cells per group). Data show HCM R663H hiPSC-CMs have significantly increased cell shortening % and prolonged kinetics relative to control hiPSC-CMs. *P<0.05 vs control hiPSC-CMs.

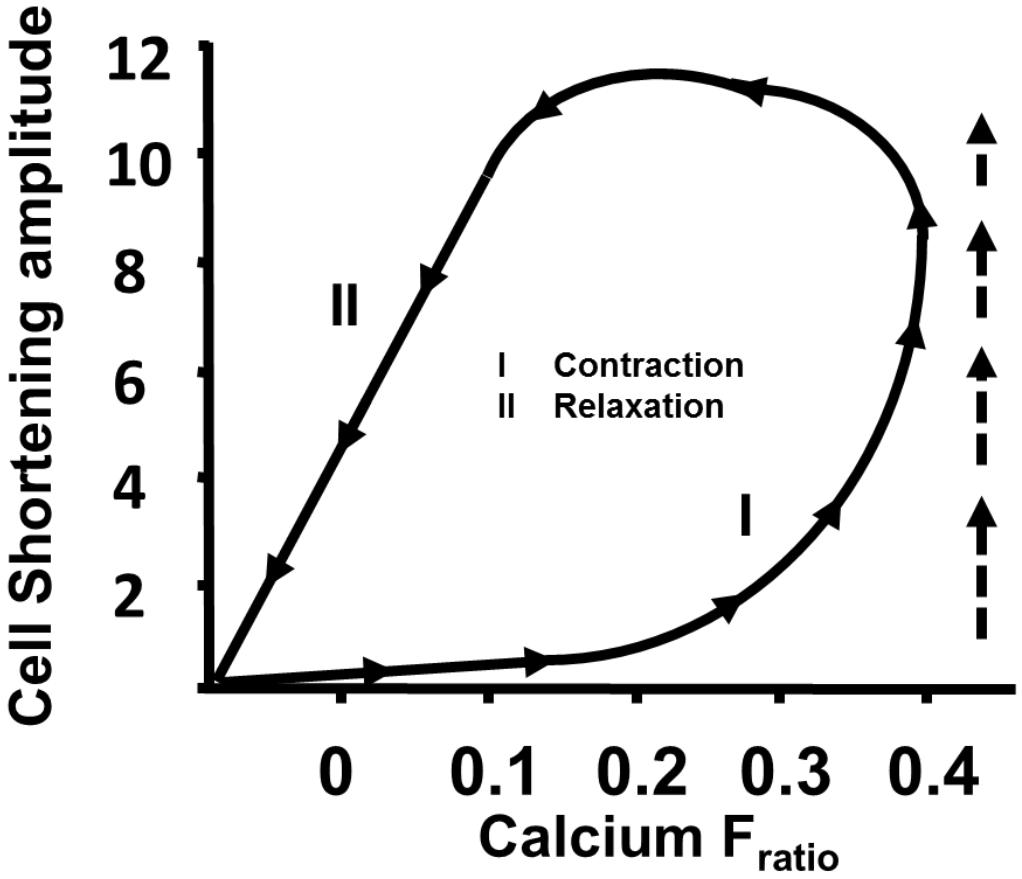

Figure 32. Hysteresis loop parameters. Graph depicts typical calcium – contraction hysteresis loop. The counterclockwise loop represents contraction (I) and relaxation (II) that ultimately converge, with the same trajectory, to baseline.

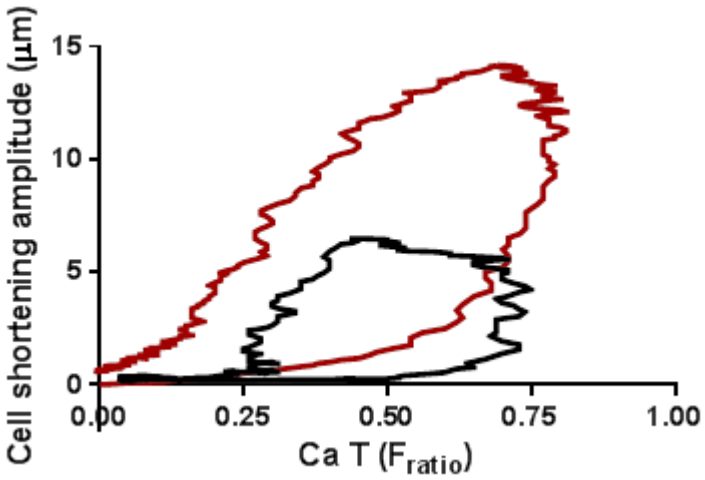

Figure 33. HCM R663H hysteresis loop. Representative HCM R663H hysteresis loop, HCM (red) and control (black). Calcium – contraction loop demonstrating hiPSC-CM carrying the HCM R663H MYH7 mutation have increased contractile performance and increased myofilament calcium sensitivity indicated by the upward shift and increased contraction at lower Ca concentrations respectively.

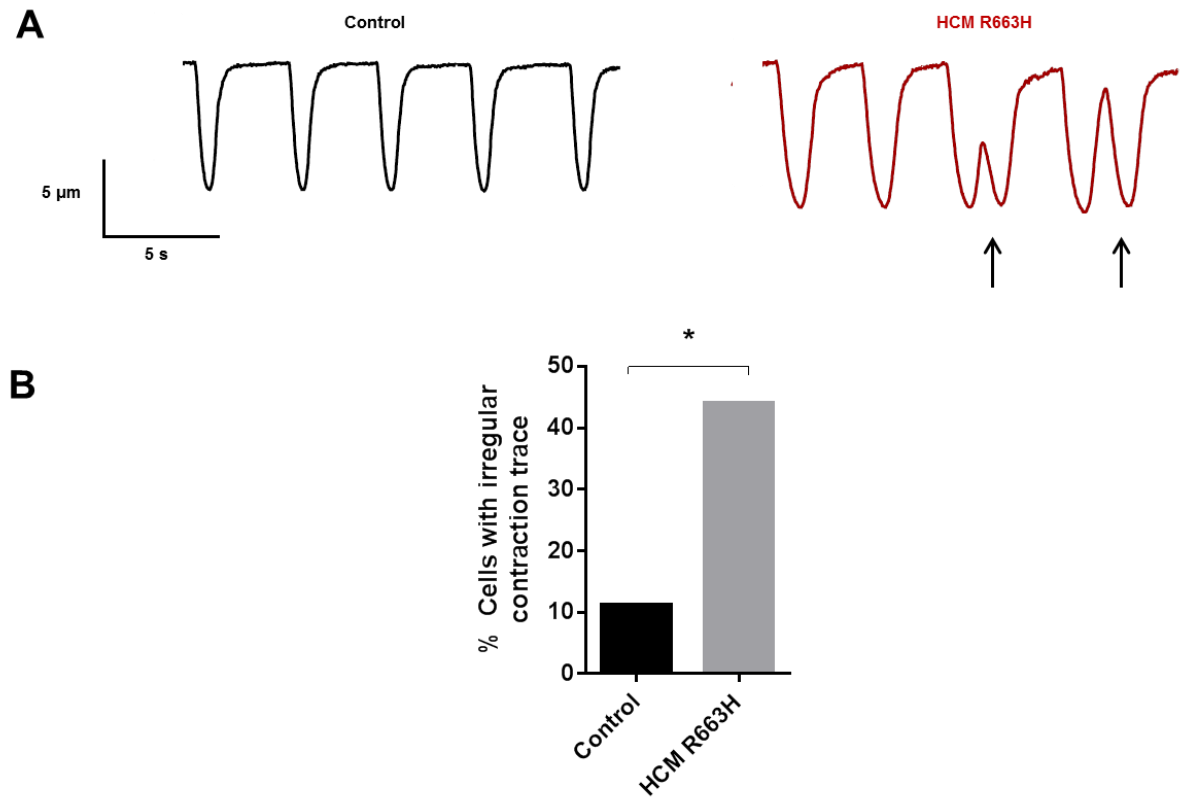

Figure 34. Contractile arrhythmia assessment. A, Representative contraction trace of control and HCM R663H hiPSC-CM, red arrows indicate irregular contraction morphology. B, Data are mean (n = 9 – 40 cells per group). Fisher exact test $P < 0.0010$.

Table 5. HCM R663C contractile assesment

Parameter	Control	HCM R663H	P-Value
Resting length (µm)	91.0 ± 11.0	68.0 ± 5.0	0.1
Cell Shortening amplitude (µm)	8.0 ± 1.4	8.6 ± 0.7	0.7
Cell Shortening (% resting length)	9.0 ± 1.3	13.2 ± 0.8*	0.03
t to peak 50% (s)	0.2 ± 0.02	0.3 ± 0.2	0.3
t to peak 90%(s)	0.4 ± 0.1	0.7 ± 0.03**	0.005
t to baseline 50% (s)	0.3 ± 0.05	0.5 ± 0.04	0.1
t to baseline 90% (s)	0.6 ± 0.1	0.9 ± 0.1*	0.02
n	5	29	

Table 5. HCM R663H contractile assessment. Data are mean ± SEM.

DCM hiPSC-CMs exhibit myofilament disarray

For these experiments patient specific hiPSC-CMs were generated from left ventricular cardiac fibroblasts obtained for explanted heart samples and reprogrammed by the plasmid-based reprogramming as described above. To determine if the DCM hiPSC-CMs display ultrastructure abnormalities I performed electron microscopy and immunofluorescence staining of the sarcomere component α-actin. I found that DCM hiPSC-CMs exhibit structural differences at the cellular level including myofilament disarray and mitochondrial defects (Figure 35).

DCM hiPSC-CMs display Ca handling dysfunction

To determine if there is a Ca handling defect I evaluated Ca handling properties in DCM and control hiPSC-CMs. I found that DCM hiPSC-CMs have normal diastolic Ca, Ca transient amplitude, and Ca decay (i.e., SERCA activity) (Figure 36). However detailed analysis of Ca kinetics and SR contribution by caffeine application revealed that DCM hiPSC-CMs display significantly prolonged Ca handling kinetics (i.e., time to peak) and significantly increased SR content (Figure 36 B and C). These data support the utility of hiPSC-CMs for disease modeling and for elucidating the consequences of a novel DCM hiPSC-CM model.

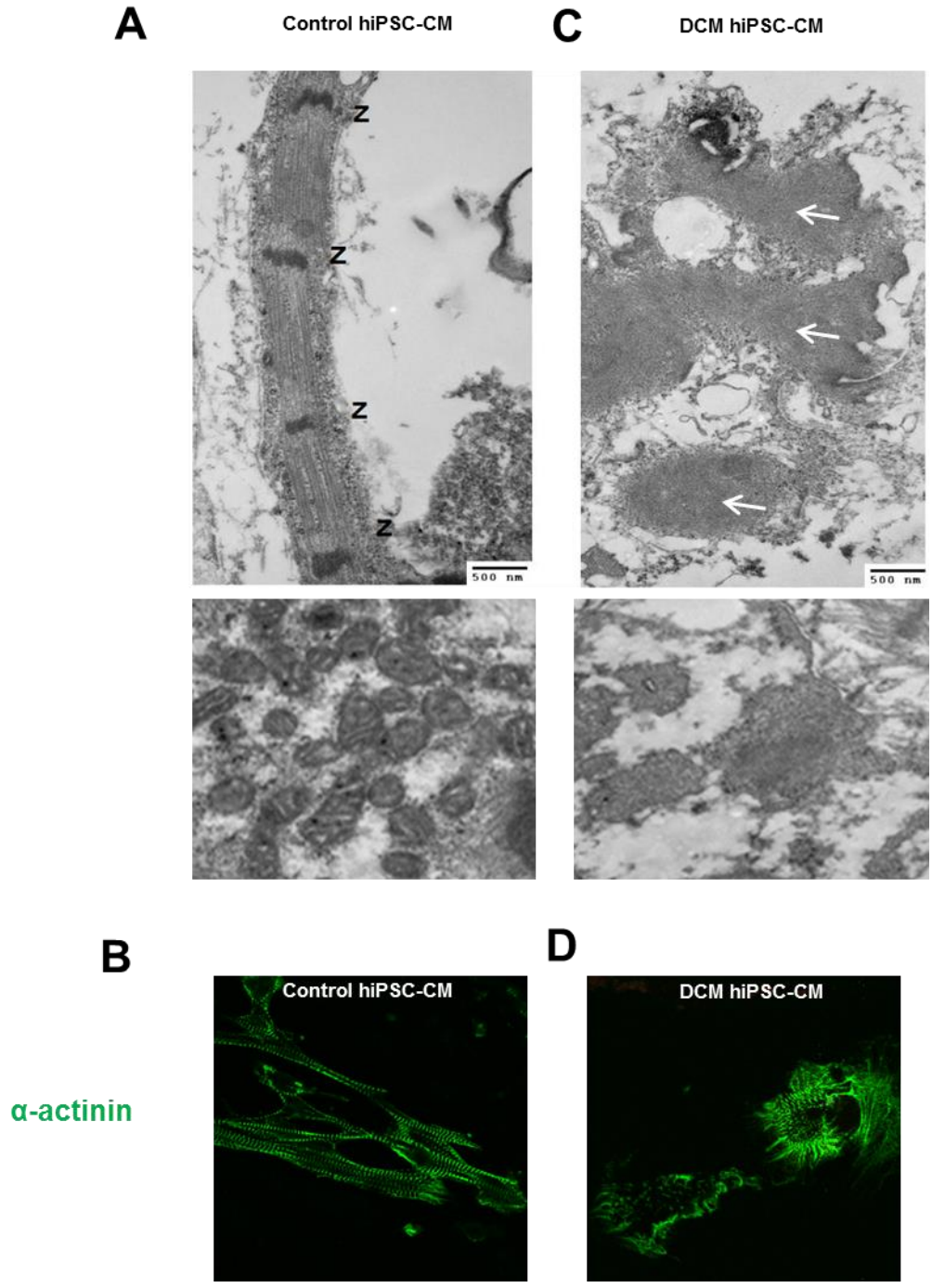

Figure 35. DCM hiPSC-CM ultrastructure. Transmission electron microscopy images and immunofluorescence staining of myofilament organization for cardiac marker α-actinin (green). A and B, control hiPSC-CM. C and D, DCM hiPSC-CM. White arrows indicate sarcomere disarray. Scale bar 10 µM. Panel B and D Courtesy of Dr. Young Wook Chun.

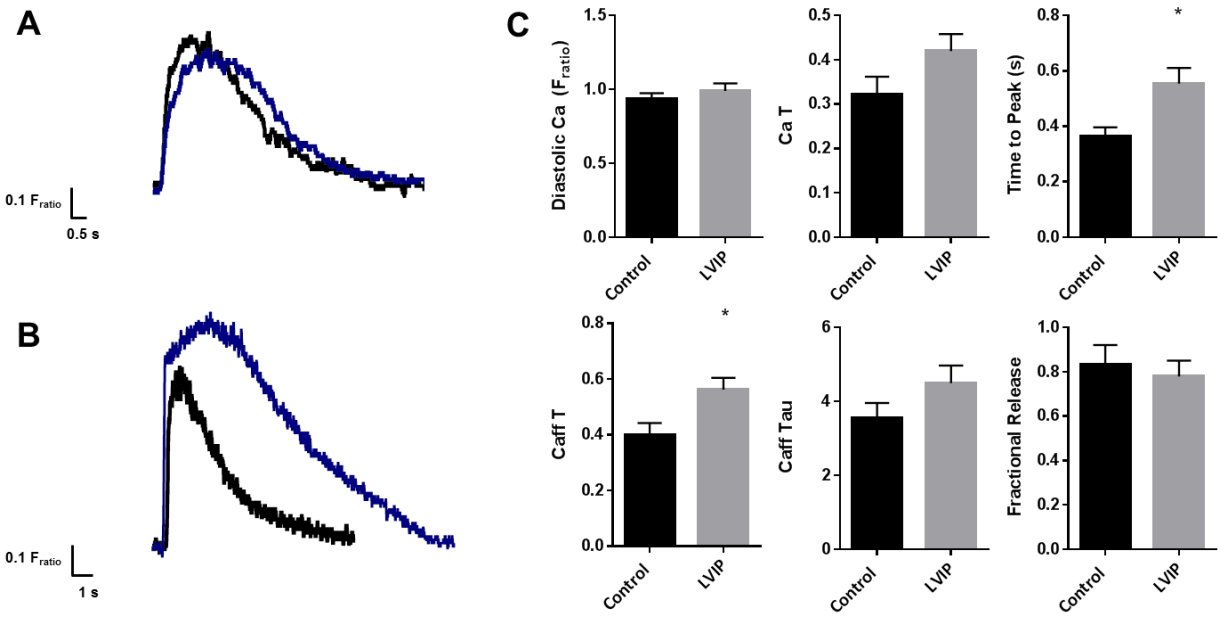

Figure 36. Calcium handling of DCM hiPSC-CMs. A, Representative Ca twitch transients, 0.2 Hz. B, Representative caffeine transients [10 mM]. C, Data are mean ± SEM (n = 5 - 29 cells per group). Control (Black) and DCM (Blue). Data show altered Ca handling properties in DCM hiPSC-CMs including prolonged kinetics and increased SR Ca content. *P<0.05 vs control hiPSC-CMs.

Assessment of RCM *TNNI3* R204C mutation

Here I set out to determine the cellular consequence of the heterozygous *de novo* arginine-to-cysteine mutation at position 204 (R204C) of the *TNNI3* gene which encodes cardiac troponin I. Since *TNNI3* is a component of the troponin complex that senses intracellular calcium Ca concentration to regulate actomyosin activity, I hypothesized that the *TNNI3* R204C mutation causes specific changes in the CM physiology, and that these perturbations will be manifested in the hiPSC-CMs through distinct differences in a wide range of cellular phenotypes, including morphology, Ca handling and contractility. As an independent confirmation of the missense mutation I performed nucleotide sequence analysis to demonstrate the *TNNI3* R204C mutation (Figure 37 B) present in the patient tissue. Subsequent evaluation of the probands parents revealed no known mutation (Figure 37 A). In addition polyphen analysis suggests that the *TNNI3* R204C mutation is damaging (Figure 37 D) and located in a highly conserved region of the protein (Figure 37 C). Here, we employ recombinant adenovirus expressing WT or mutant (R204C) *TNNI3* to determine the pathogenicity of the *TNNI3* R204C mutation by elucidating the structural and functional consequences of the *TNNI3* R204C mutation in a human CM background in hopes of identifying novel mechanistic insight.

Cardiac Troponin I expression in hiPSC-CMs

As previously shown [14] hiPSC-CMs cultured under standard conditions do not express cardiac troponin I, rather they primarily express the fetal slow skeletal troponin I isoform (Figure 38). As a first step to assess the function of mutant cardiac troponin I in hiPSC-CMs I establish the troponin I molecular signature of the hiPSC-CMs used in this study. Consistent with other reports, the hiPSC-CM used in this study primarily express the fetal slow skeletal troponin I protein relative to human control as assessed by Western blot analysis (Figure 39) and immunofluorescence staining for cardiac troponin I (Figure 39 C). Therefore to evaluate the

consequences of *TNNI3* R204C mutation in hiPSC-CMs I engineered two adenovirus constructs, one to overexpress WT and one to overexpress mutant *TNNI3* (Figure 40). As a first step in this study it is critical to demonstrate the recombinant proteins are expressed and incorporated in hiPSC-CMs.

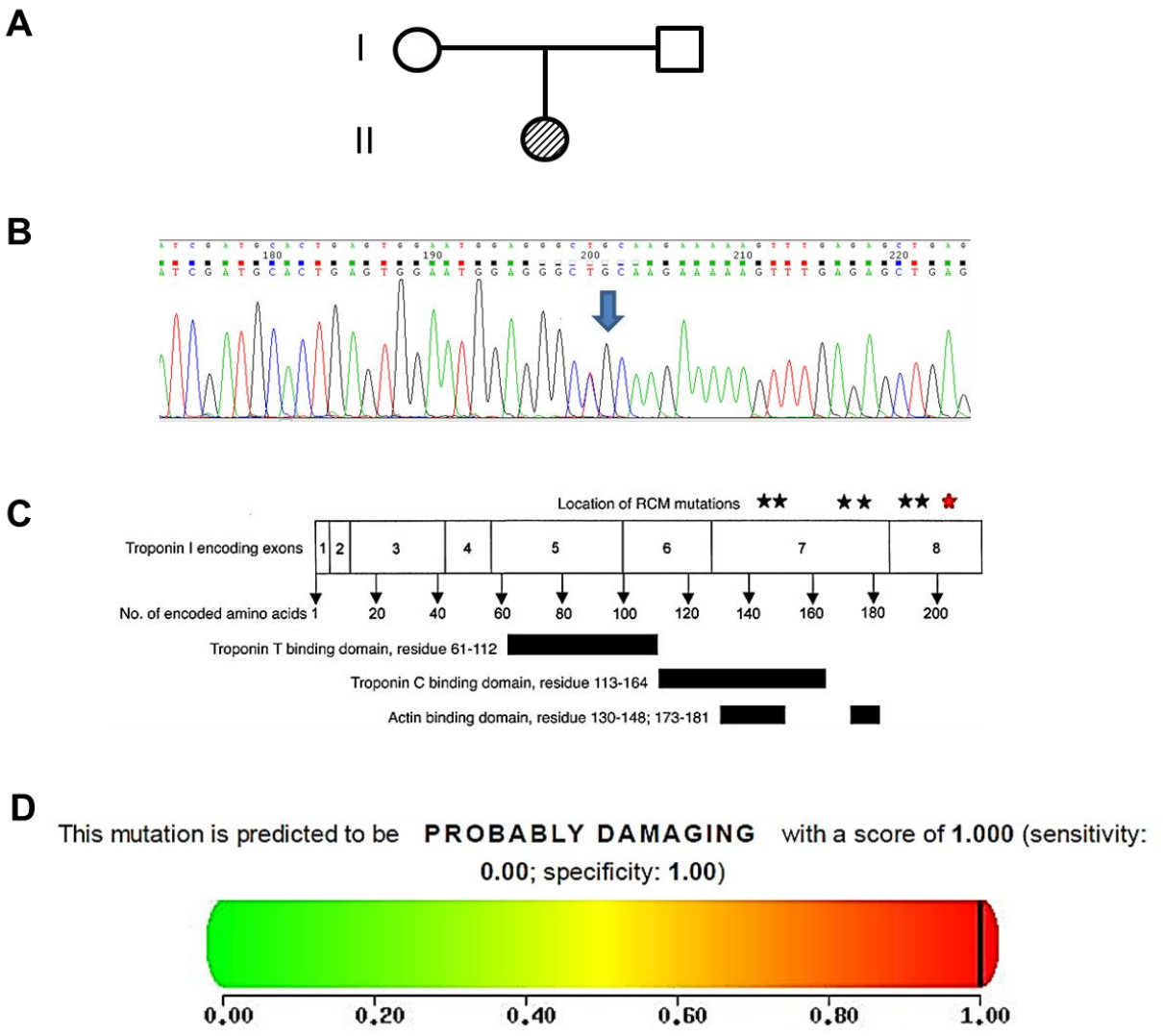

Figure 37. Validation of RCM mutation. A, Pedigree of RCM patient family indicating *de novo* mutation (Open square (male) and circle (female)). Filled in circle represents individual carrying *de novo* mutation R204C in *TNNI3* which encodes the protein cardiac troponin I. B, The R204C point mutation was confirmed in the RCM patient by PCR and sequencing analysis. C, Organization of human cardiac troponin I. The red star indicated the location of the *de novo* R204C mutation. D, Genetic analysis indicating the *TNNI3* R204C mutation is likely damaging. (Mogensen J. et al., *The Journal of Clinical Investigation* 2003; 111(2): 209–216).

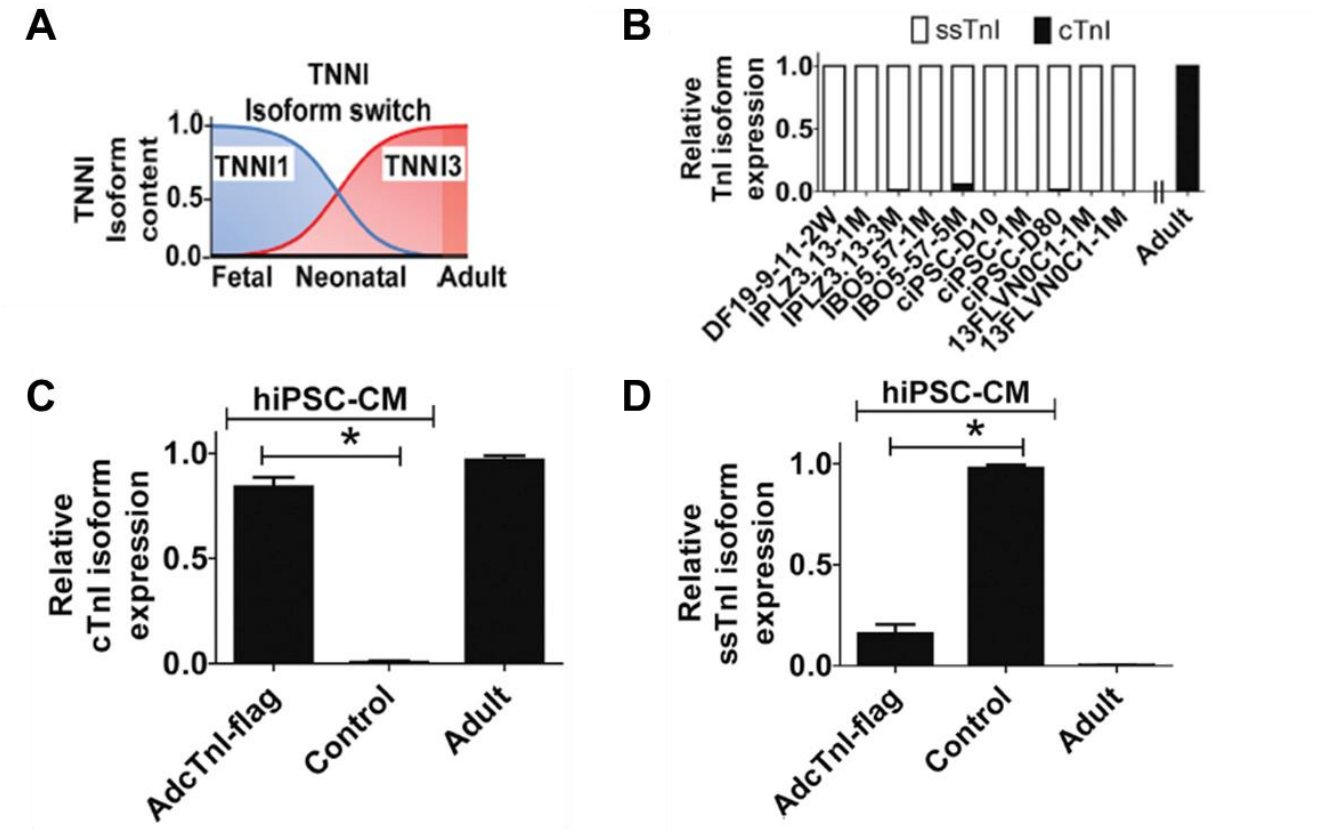

Figure 38. Cardiac troponin I isoform switch in hiPSC-CMs. A, Representation of human Troponin I isoform switch. B, hiPSC-CM relative troponin isoform expression. C, Troponin I isoform expression of Adenovirus cTnI infected hiPSC-CMs demonstrating increased cTnI expression and D, reduced fetal isoform ssTnI expression. (Bedada F. et al., *Stem Cell Reports* 2014; 3(4): 594–605).

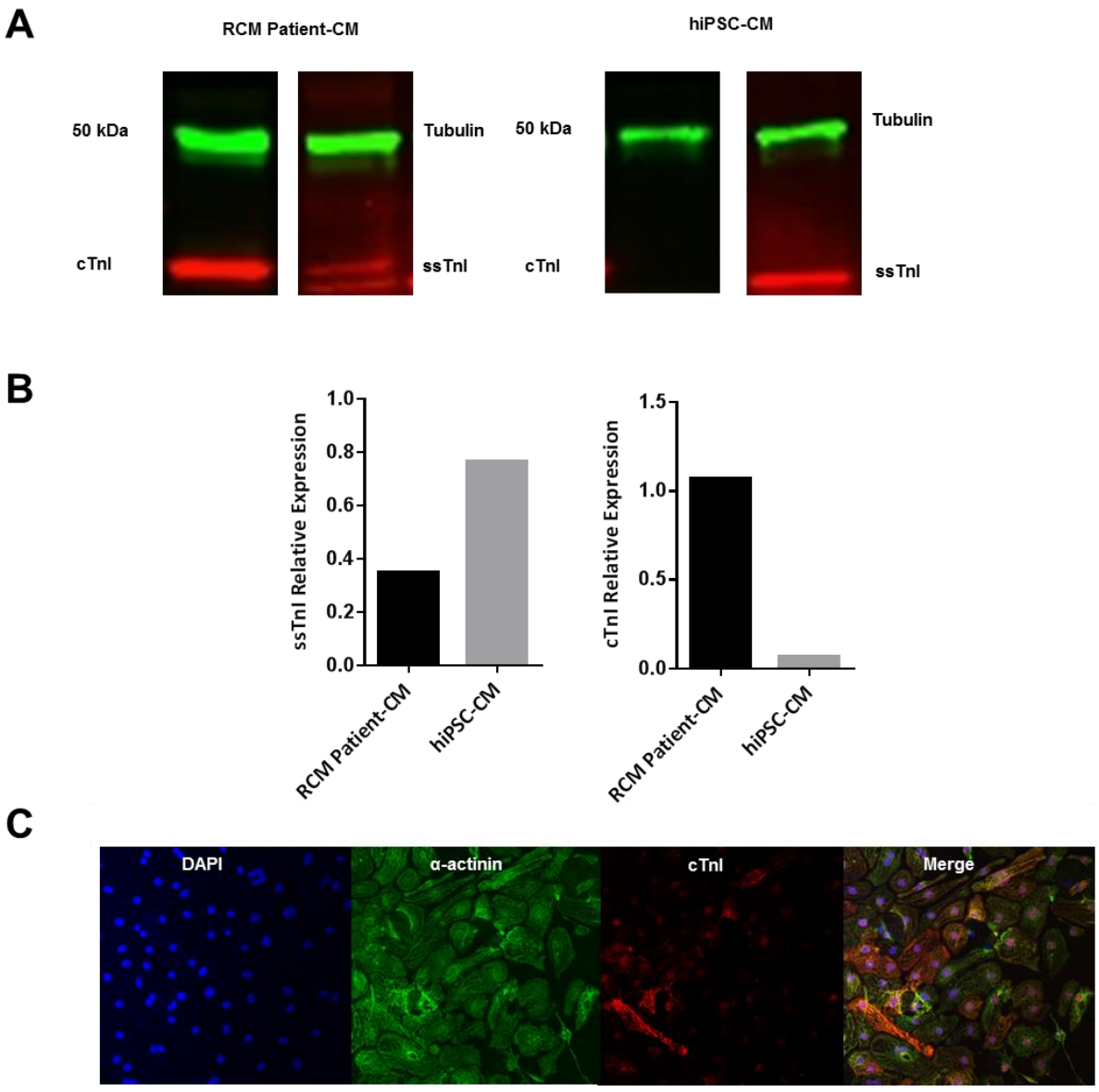

Figure 39. Troponin I isoform confirmation hiPSC-CM. A, Western blot for indicated troponin protein. Patient left ventricular tissues (left panel) and hiPSC-CMs (right panel). cTnI and ssTnI (24 kDa). B, Relative troponin protein expression ssTnI (left panel), cTnI (right panel). C, Immunofluorescence staining of hiPSC-CMs for DAPI (Blue), α-actinin (Green) and cardiac troponin I, cTnI (red). Panel C courtesy of Dr. Young Wook Chun. Data show cardiac troponin I is poorly expressed in the hiPSC-CMs used in this study. However, cardiac troponin I is robustly expressed in RCM patient left ventricular tissue.

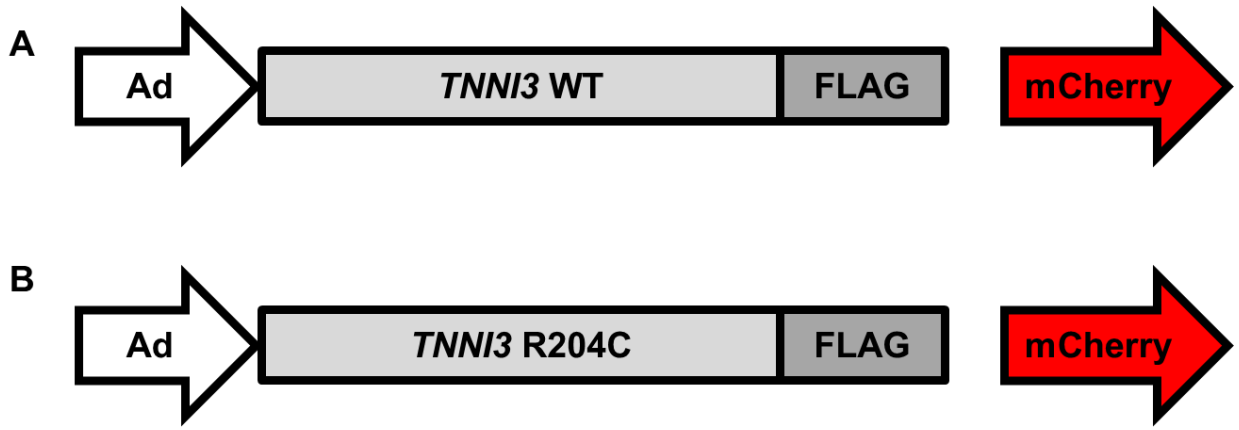

Figure 40. TNNI3 Adenovirus constructs. A, wild type (WT) *TNNI3*. B, Mutant R204C *TNNI3*. Each construct is engineered with a C-terminal flag tag and a bicistronic mCherry cassette.

Expression and sarcomeric incorporation of WT and mutant *TNNI3* in hiPSC-CMs

Adenovirus was added directly to CM culture media at a multiplicity of infection (MOI) of 200. Robust expression of mCherry was detected as early as 24 hours post transduction with greater than 90% transduction efficiency (Figure 41 A). For comparison we used freshly isolated adult rabbit-CM which displayed greater than 90% transduction efficiency (Figure 41 B). Next adenovirus transduced WT and mutant hiPSC-CMs were processed for immunofluorescence and Western blot analysis at ~36 hours post transduction (Figure 42). Each recombinant adenovirus construct was engineered with C-terminal flag tag to distinguish recombinant from any endogenous cardiac troponin I. To assess sarcomeric incorporation transduced hiPSC-CMs were immunostained with anti-flag antibody. As shown in (Figure 42 A) both WT and mutant recombinant troponin I successfully localize and incorporate into the myofilament in hiPSC-CMs. Western blot analysis confirmed adenoviral troponin I protein expression. As shown in (Figure 42 B) transduced WT and R204C mutant hiPSC-CMs exposed to anti-flag antibody display a detectable band at ~24 kDa. This band corresponds to the appropriate molecular weight of cardiac troponin I. These data are proof of feasibility for structural and functional analysis of the RCM *TNNI3* R204C mutation in hiPSC-CMs.

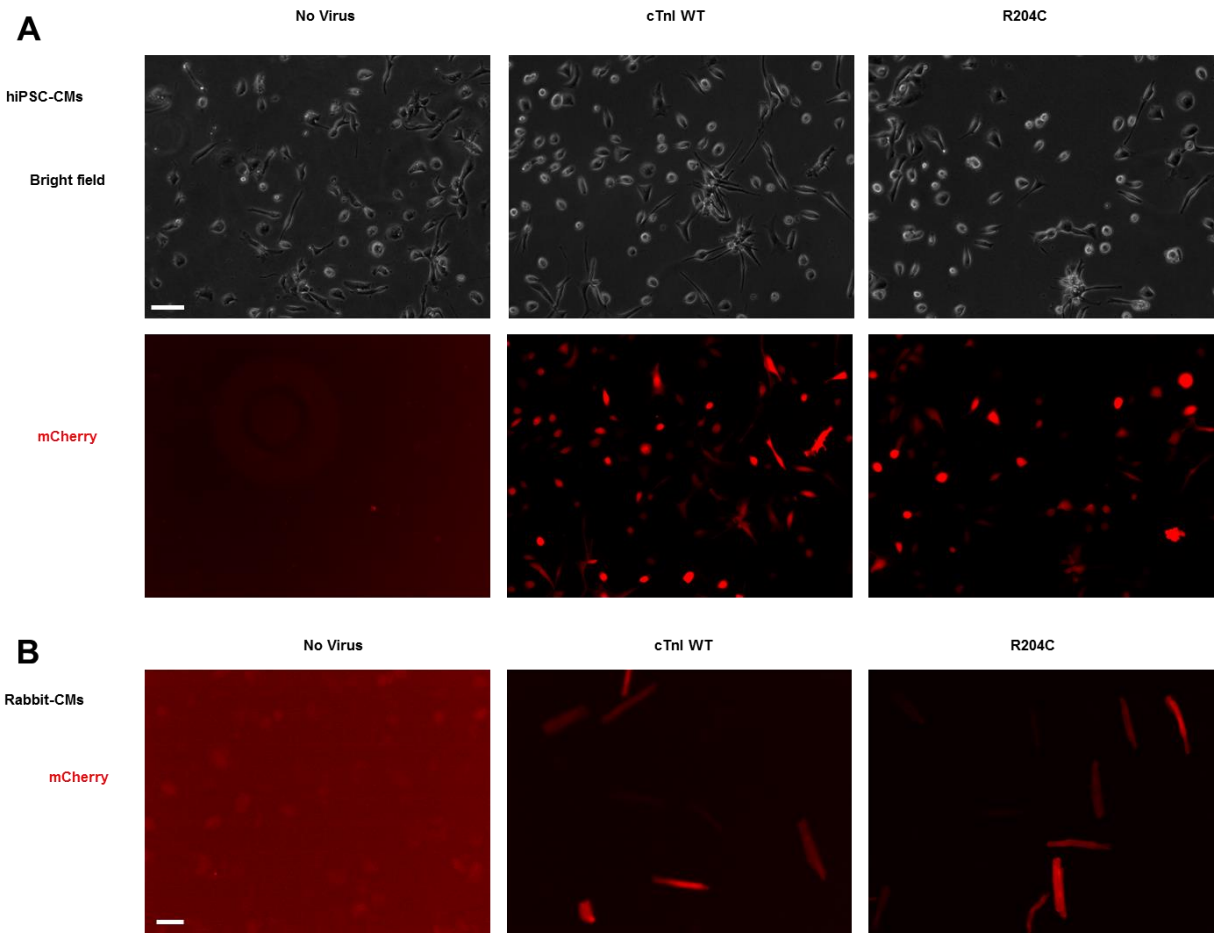

Figure 41. Adenoviral transfection efficiency. A, Bright field and immunofluorescence images of hiPSC-CMs (day 30), 72 hours post infection with WT or mutant troponin adenovirus. Scale bar, 100 µm. B, Immunofluorescence images of adult rabbit-CMs, 24 hours post infection with WT or mutant troponin adenovirus. 20X mCherry (red) MOI 200. Scale bar, 50 µm.

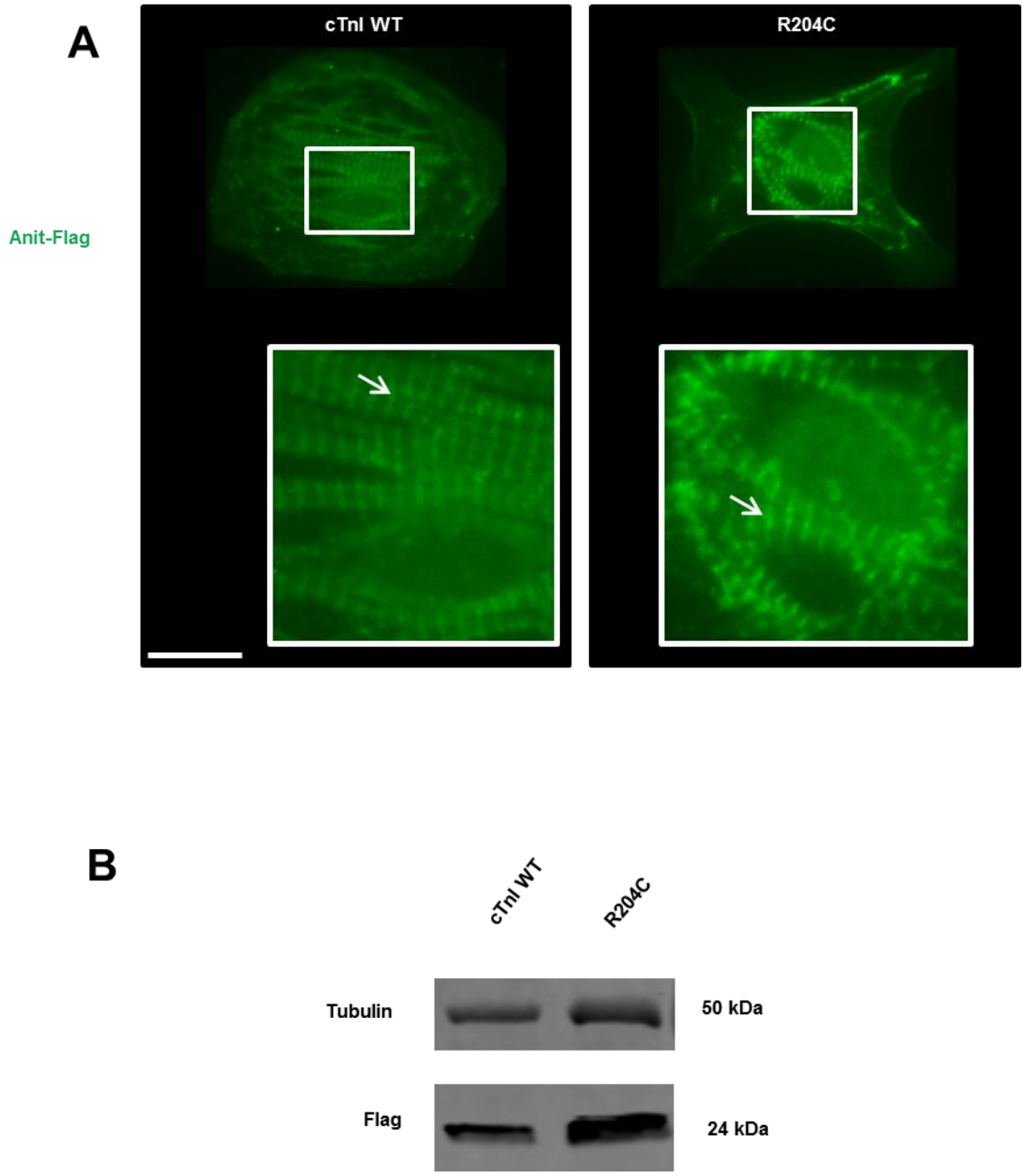

Figure 42. Ad-TNNI3 expression and incorporation. A, Immunofluorescence images of adenoviral infected hiPSC-CMs (day 30) 72 hours-post infection. Anti-flag (green) 63X. B, Western blot of protein from adenoviral infected hiPSC-CMs for anti-Flag. Scale bar, 20 µm.

3.5 Discussion

The heritable causes of sarcomeric cardiomyopathies have been elucidated. However, the mechanisms for these diseases are less clear. Previous studies of hypertrophic cardiomyopathy [13] and dilated cardiomyopathy [12] provide evidence supporting the use of hiPSC-CMs to model sarcomeric cardiomyopathies. However, these studies only peripherally evaluated Ca handling and contractility at the single hiPSC-CM level and detailed analysis have not been reported. Here, I demonstrate assessment of Ca handling and mechanical contractile properties of human cardiomyopathy. Major findings are HCM *MYH7* A663H hiPSC-CM display slower Ca decay and prolonged Ca kinetics compared to control hiPSC-CMs (Figure 30). By implementing the Matrigel mattress platform I uncover HCM *MYH7* A663H hiPSC-CMs exhibit severe contractile abnormalities at the single cell level including significantly increased contractility, diastolic dysfunction and significantly increased contractile arrhythmic events (Figure 31), consistent with clinical hallmarks of HCM. Further using hysteresis loop analysis I provided evidence supporting a myofilament Ca sensitivity mechanism (Figure 33). These data suggest the HCM *MYH7* A663H phenotype may be caused, in part, by decreased SERCA activity, as shown by decrease twitch Ca decay, and prolonged Ca kinetics. However, the Ca handling experiments assume comparable Ca buffering and flux properties, which may not be the case. Additional experiments will need to be performed to determine if the Ca buffing is altered in these cells including the Ca dissociation constant. As such, we are currently performing cytoplasmic Ca buffering and flux experiments to address the underlining mechanisms of increased myofilament Ca sensitivity and altered Ca removal regulation.

The DCM experiments reveal abnormal ultrastructure features, altered mitochondria and irregular Ca handling properties (Figure 35 and 36). These studies together with the HCM *MYH7* A663H analysis create a foundation for detailed pathophysiological studies using hiPSC-CMs. Further experiments using DCM hiPSC-CMs will need to be performed to quantify the

mitochondrial defects and determi ne if there is a direct association between the mitochondrial defects and Ca handling dysfunction. Finally it will be interesting to see if the DCM Ca handling abnormalities result in contractile dysfunction in DCM hiPSC-CMs plated on the Matrigel mattress platform.

The RCM studies used a recombinant adenovirus construct (Figure 40) to demonstrate feasibility for evaluating the functional consequences of the novel *TNNI3* R204C mutation. I show both WT and mutant construct successfully express troponin I (Figure 42 B) that is incorporated to the sarcomere (Figure 42 A) in hiPSC-CMs. A caveat for such experiments is that typical recombinant overexpression studies create a non-physiological environment. However, for the cardiac troponins excess troponin is rapidly degraded reducing the possibility of a non-physiologic sarcomere *in vitro.* From a translational perspective, these data provide a foundation for future "personalized platforms" to evaluate individuals at risk of developing heart failure, fatal arrhythmias, and to develop future targeted therapies.

Limitations

These results are specific to the *in vitro* consequences of the particular mutation for example *MYH7* A663H or *TNNI3* R204C and do sarcomeric cardiomyopathy in general. While I present significant changes in patient specific DCM hiPSC-CMs I do not present a causal mutation, this limits the utility and translatability of this characterization. However, using next generation sequencing and CRISPR/Cas9 technology studies we are actively working to determine the casual mutation in these cells.

Furthermore, the contribution of inositol triphosphate (IP3) sensitive intracellular Ca stores were not assess in control or diseases hiPSC-CMs. hESC-CMs display prominent inositol triphosphate (IP3) sensitive intracellular Ca stores. These Ca stores are not thought to play a role in healthy adult ventricular CMs physiology however they can be upregulated in

diseased CMs [47]. Future studies will determine if IP3 Ca stores are present and the effects healthy and diseased hiPSC-CMs function.

Chapter 4

hiPSC-CM DRUG SCREENING

4.1 Chapter Abstract

Drug screening and cardiotoxicity efforts are lacking greatly limiting discovery of novel HF pharmacotherapies. Here, I set out to establish the utility of hiPSC-CMs and the mattress platform for evaluation and identification of novel HF compounds, by demonstration of their pharmacological response to known compounds. Although hiPSC-CMs exhibit a modest inotropic response to adrenergic stimulation (Isoproterenol and Epinephrine ~ 4% and ~ 6% above vehicle, respectively) they do display a robust chronotropic response (Isoproterenol 75 % increase above vehicle). I further demonstrate hiPSC-CMs display a robust response to compounds that modulate nodes of EC coupling such as extracellular Ca, Verapamil and myofilament Ca sensitizers (i.e., EMD57033 and Levosimendan) , which has previously not been demonstrated in single hiPSC-CM. And with the implementation of the mattress platform I demonstrate contractile efficacy for a novel inotrope, EHF1. These experiments show hiPSC-CMs are a valuable tool for assessment of contractile function of known and novel pharmacological agents, in intact human CMs.

4.2 Introduction

Cardiac drug screening and toxicology efforts are hindered largely due to a lack of available human CMs, or a reliable surrogate, that may be used to identify novel targets and compounds without hazardous liabilities. This has led to high drug attrition rates, costly late withdrawal of toxic compounds, and even premature termination of safe compounds. HiPSC-CMs represent a strategy to address this need by enabling standardized human CMs for drug screening purposes and toxicology assessment.

To date researchers primarily use animal models to evaluate drug efficacy and safety. While useful, these models do not recapitulate certain aspect of human biology, as animals represent different genetic backgrounds, protein expression and physiological contribution of such proteins. The lack of an adequate system to asses cardiac drug response has led to poor heart failure therapeutic candidates and high and increasing prevalence of HF.

For these reasons, to obtain improved and safer drugs, the Food and Drug Administration has implemented mandatory cardiac safety requirements (i.e., ICH S7A and S7B) [48] for all compounds. This comes after cases of death or adverse drug reactions, for both drugs with cardiac and non-cardiac indications. The main assay for evaluating cardiotoxicity is the hERG channel assays, which identifies compounds that prolong the QT interval *in vitro*. These compounds could provide a proarrythmic substrate for early after-depolarization (EAD) or delayed after-depolarization (DAD) and ultimately result in Torades de Pointes (TdP) a potentially fatal arrhythmic event. However hERG channel assays are notorious for false positive (e.g., alfuzosin) and false negative (e.g., verapamil) results which limits their utility for identifying safe drugs. As such a wide appreciation has been developed for evaluation of compound effects on multiple channels and accessory proteins, simultaneously; which may better represent human biology. Moreover hiPSC-CMs have gained significant use

in this effort. However, much still needs to be learned particularly at the cellular level. The lack of simple single cell contractility methods has hindered drug screening and toxicity efforts. Currently we do not have a clear understanding of how hiPSC-CMs respond to pharmacological stimuli [49, 50] and if these cells are useful for identifying compounds and validating targets.

Here we take advantage of hiPSC technology, as well as our novel contractile method to elucidate the effects of pharmacological compounds on modulating hiPSC-CM EC coupling to better understand the utility of these cells. Next, we determine if hiPSC-CMs are capable of identifying novel inotropes with efficacy in human CMs.

4.3 Materials and methods

Primary myocyte isolation

Ventricular myocytes from mouse and rabbit were isolated by a modified collagenase/protease method as previously described [38]. All the experiments conducted in Tyrode's solution containing (in mM): $CaCl_2$, NaCl 134, KCl 5.4, $MgCl_2$ 1, glucose 10, and HEPES 10, pH adjusted to 7.4 with NaOH. Final concentration of Ca was 2 mM.

Compounds and pharmacological assay

All compounds were re-suspended based on manufactures recommendations. Briefly, EMD57033 (Sigma) was prepared in DMSO and Verapamil (Sigma) was prepared in distilled water.

Before experiments, individual hiPSC-CMs were selected based on normal contraction and morphology. HiPSC-CMs with no obvious baseline, irregular contractions or aspect ratio less than 4 were not selected for analysis. The position of suitable hiPSC-CMs was recorded. Each experiment typically measured pharmacological response for 5 to 20 hiPSC-CMs taken from independent cardiac differentiations. HiPSC-CMs were perfused with Tyrode's solution

with vehicle and allowed to equilibrate for approximately 5 minutes before experiments. The positive inotrope EMD57033 was used with external Ca concentration 1 mM Tyrode around the EC_{50}. HiPSC-CMs were exposed to increasing concentration of compound for 250 seconds or until steady state was reached [51].

Hysteresis loop analysis

Hysteresis loops were constructed as described before [46]. Briefly, select representative Ca transient and cell shortening trace, for each compound by highlighting recording in IonWizardTM software (IonOptix, Milton, MA). Both Ca transient amplitude data (F_{ratio}) and cell shortening trace data (um) were exported and pasted into Microsoft Excel. In Microsoft Excel duplicates were removed, this function is located under the data tab. Both time and length or time and ratio were highlighted and duplicates removed by selecting only the time variable. Such that for each time point there was a corresponding cell length measurement and Ca transient amplitude ratio. Next, all Ca transient amplitude values were normalized to the baseline Ca transient ratio. And all cell length measurements were normalized to the resting cell length. Transformed cell length data was multiplied by -1 to make all values positive. Normalized cell shortening values were plotted on Y-axis as a function of normalized Ca transient amplitude values on the X-axis.

Potential hysteresis loop characteristics:

- Positive inotrope, increased area and upward shift of the hysteresis loop
- Negative inotrope, decreased area and downward shift of the hysteresis loop
- Myofilament Ca sensitizer, upward leftward shift of the hysteresis loop
- Myofilament Ca desensitizer, downward rightward shift of the hysteresis loop
- Larger loop area, indicated higher contractile function

Immunohistochemistry

Immunostaining of hiPSC-CMs was carried out as before [52]**.** Briefly, day 30 hiPSC-CMs were fixed in 2% paraformaldehyde for 5 minutes at room temperature, permeabilized with 0.2% Triton X-100 (Sigma) for 10 minutes at 4 C. Samples were blocked with 1% BSA in PBS solution and incubated for 1 hour at room temperature. Primary antibody, phospho-PKA (Sigma), was added in 0.1% Triton X-100 1% BSA in PBS solution and incubated overnight at 4 C. Samples were washed with 0.2% Tween 20 in PBS, secondary antibodies specific to the primary IgG isotype were diluted (1:1000) in the same solution as the primary antibodies and incubated at room temperature for 1 hour. Samples were washed with 0.2% Tween 20 in PBS twice and mounted. Slides were examined with Olympus IX81 microscope coupled to Slidebook software.

Measurement of intracellular Ca

Myocytes were loaded with Fura-2 acetoxymethyl ester, Fura-2 AM (Molecular Probes Inc, Eugene, OR) as described previously [38]. Briefly, myocytes were incubated with 2 μM Fura 2 AM for 8 minutes at room temperature to load the indicator in the cytosol. Myocytes were washed twice for 10 minutes with Tyrode's solution containing 250 μM probenecid to retain the indicator in the cytosol. A minimum of 30 minutes was allowed for de-esterification before imaging the cells. Fura 2-AM loaded myocyte Ca transients recorded during 0.5 Hz field stimulation in 2 mM Ca Tyrode's solution for 20 second at room temperature. Then stimulation was switched off followed by application of caffeine 10 mM for 5 second to estimate SR Ca content. A subset of cells were exposed to 0Ca0Na Tyrode's solution for 10 second then caffeine 10 mM applied for 30 second to estimate non-NCX Ca extrusion. For each cell and each experimental condition, tau (τ), amplitude and baseline values were averaged from 3 consecutive Ca transients. Ca transients were recorded and analyzed using commercially

available data analysis software (IonOptix, IonWizardTM Milton, MA). All experiments were conducted at room temperature.

Video based edge detection

Video edge detection was used to assess cellular contraction (i.e., cell shortening) of contracting CMs. Briefly; CMs were visualized using Nikon Ellipse T5100 coupled to IonOptix video microscopy system (IonOptix). Spontaneous or field stimulated contraction traces were recorded in 2 mM Ca Tyrode solution. For each cell and each experimental condition typical contraction parameters including percent cell shortening (i.e., percent of resting cell length) and contractile kinetics (i.e., time to peak 90% and time to baseline 90%) values were averaged. Contraction traces were recorded and analyzed using commercially available data analysis software (IonOptix, IonWizardTM Milton, MA). Only isolated hiPSC-CMs with aspect ratio greater than or equal to 4 were used, non-shortening cells were excluded from analysis.

Statistical analysis

Data are mean ± SD unless indicate otherwise. Statistical differences between two groups were tested with two-tailed Student's t test. Statistical differences among more than two groups were assessed using one-way ANOVA followed by tukey or bonferroni correction. Results were considered statistically significant if the p-value was less than 0.05. Statistical analysis was performed using Graphpad Prism 6.

4.4 Results

Pharmacological Response

The application of hiPSC-CM contractile properties lies, for one example, in the ability to evaluate pharmacological response, for detailed analysis of hiPSC-CM EC coupling and practical applications including drug screening and preclinical cardiotoxity testing. As such, the response of myofilaments to Ca is a key element of cardiac contractile function [18]. To elucidate if hiPSC-CMs respond to changes in myofilament sensitivity, hiPSC-CMs were plated on the Matrigel mattress platform and treated with the inotrope, EMD57033, a myofilament Ca sensitizer. We found hiPSC-CMs respond to EMD57033 exhibiting a concentration-dependent increased in cellular contraction with ~ EC_{50} 2.6 µM [22] (Figure 43 A lower panel and B) along with prolonged contractile kinetics (Figure 43 A lower panel) consistent with increase Ca affinity and negligible effect on intracellular Ca transient amplitude (Figure 43 A upper panel and C). This represents the first time single hiPSC-CMs have been shown to respond to myofilament sensitization demonstrating the utility of the mattress for identifying novel myofilament Ca sensitizers.

We next assessed modulation of trans-sarcolemmal Ca by evaluating changes in extracellular Ca and application of verapamil, an L-type Ca channel blocker. Increased external Ca resulted in a concentration-dependent increase in cellular contraction with ~ EC_{50} 1.2 mM [22] (Figure 44 A lower panel and B) and intracellular Ca ~ EC_{50} 1.4 mM (Figure 44 A upper panel and C). The prototypical negative inotrope, verapamil, markedly decreased cellular contraction ~ EC_{50} 0.3 µM (Figure 45 A lower panel and B) and intracellular Ca ~ EC_{50} 1.5 µM (Figure 45 A upper panel and C).

Multiple reports have demonstrated a positive chronotropic response of single hiPSC-CMs to isoproterenol, a β-adrenergic receptor agonist (Figure 51). However, the inotropic

effects are less understood [24]. Therefore, we evaluated the effect of Isoproterenol on contraction and Ca amplitude in hiPSC-CMs (Figure 45). While we observed a modest concentration dependent increase in contraction (~ 4% above vehicle, ~EC_{50} 0.8 nM [51]) (Figure 46 A lower panel and B) there was no change in Ca transient amplitude (Figure 46 A upper panel and C) in accordance with previous hiPSC-CM reports of lack of positive inotropic Ca transient amplitude response [23] [24]. To asses if a robust inotropic response could be observed with a mixed β-adrenergic receptor agonist we treated hiPSC-CMs with Epinephrine (Figure 47) similar to Isoproterenol we found a modest concentration dependent contraction response to Epinephrine (~ 6% above vehicle, ~EC_{50} 9.3 nM [51]) (Figure 47 A lower panel and B). While or Ca transient amplitude analysis revealed a concentration dependent decrease at high test concentrations (Figure 47 A upper panel and C). Taken together these results indicate hiPSC-CMs display modest but concentration dependent inotropic response to β-adrenergic stimulation. These data confirm responses by hiPSC-CMs to pharmacological stimuli, thus validating the Matrigel mattress as a platform for detailed assessment of contractile response to novel small molecules for drug screening.

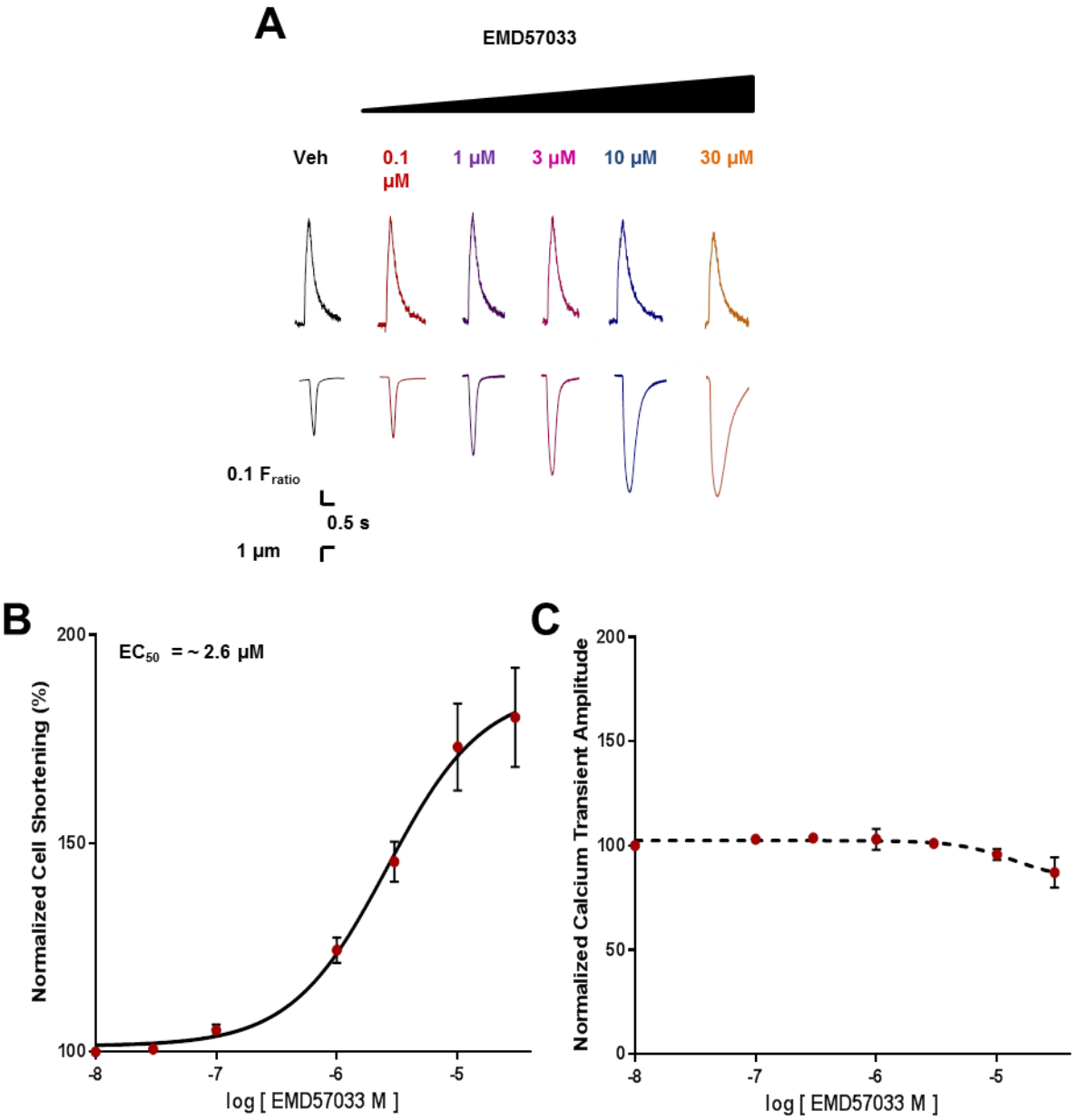

Figure 43. EMD57033 pharmacological response. A, Representative calcium transients (upper panel) and contraction traces (lower panel) for hiPSC-CMs treated with EMD57033 (myofilament Ca sensitizer). B, Contraction (Hill slope = 1.1) and C, Calcium concentration-response curves. Data show a concentration dependent increase in cell shortening % with negligible effect on Ca transient amplitude in hiPSC-CMs. EC_{50}, effective concentration 50 % of max response. Veh (vehicle). (Feaster T. et al., *Circulation Research* 2015; doi: 10.1161/CIRCRESAHA.115.307580).

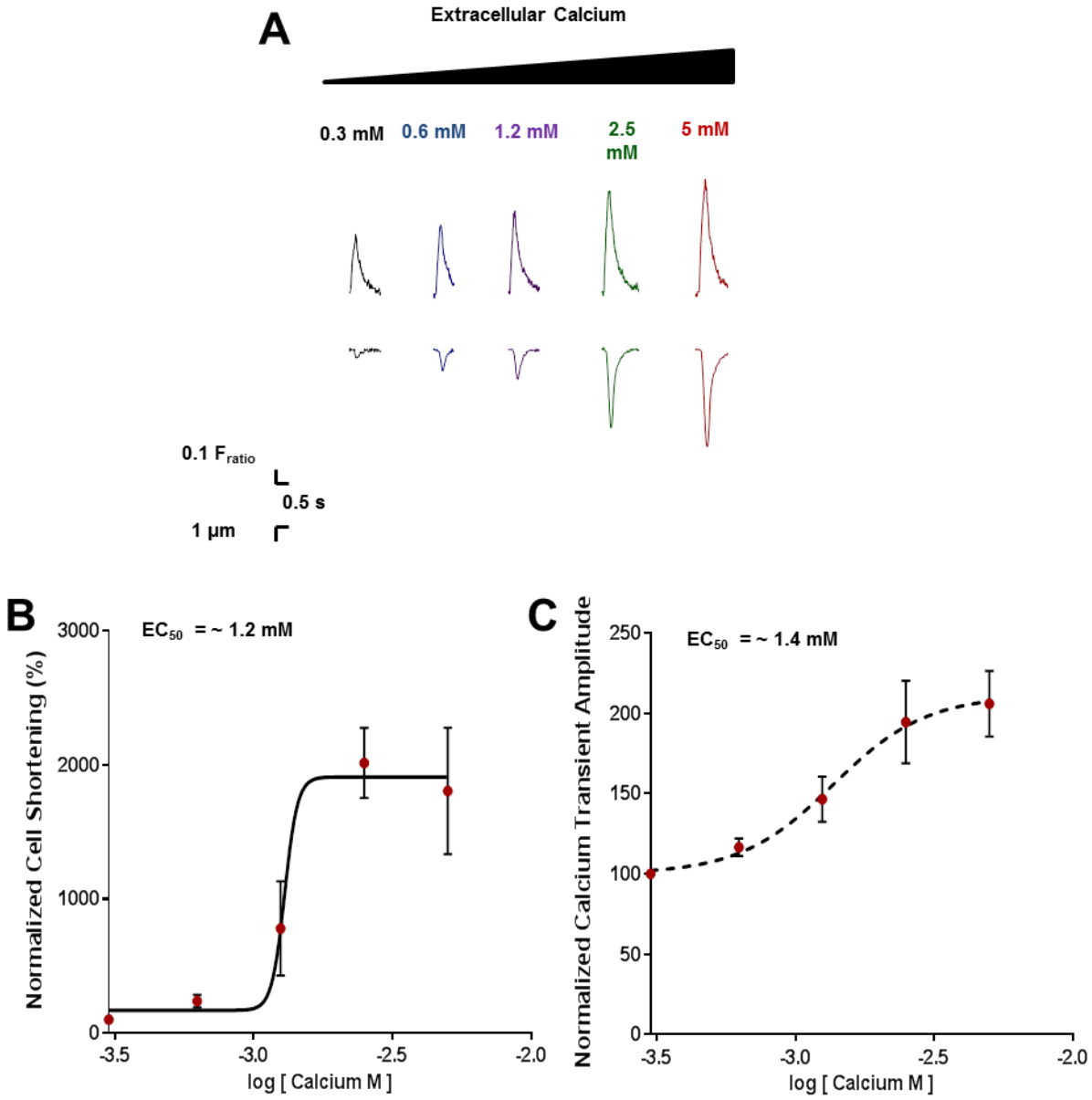

Figure 44. Extracellular calcium pharmacological response. A, Representative calcium transients (upper panel) and contraction traces (lower panel) for hiPSC-CMs treated with increasing concentration of extracellular Ca. B, Contraction and C, Calcium concentration-response curves. (Hill slope = 18.7 and 2.6 respectively). Data show a concentration dependent increase in cell shortening % and Ca transient amplitude. EC_{50}, effective concentration 50 % of max response. Veh (vehicle). (Feaster T. et al., *Circulation Research* 2015; doi: 10.1161/CIRCRESAHA.115.307580).

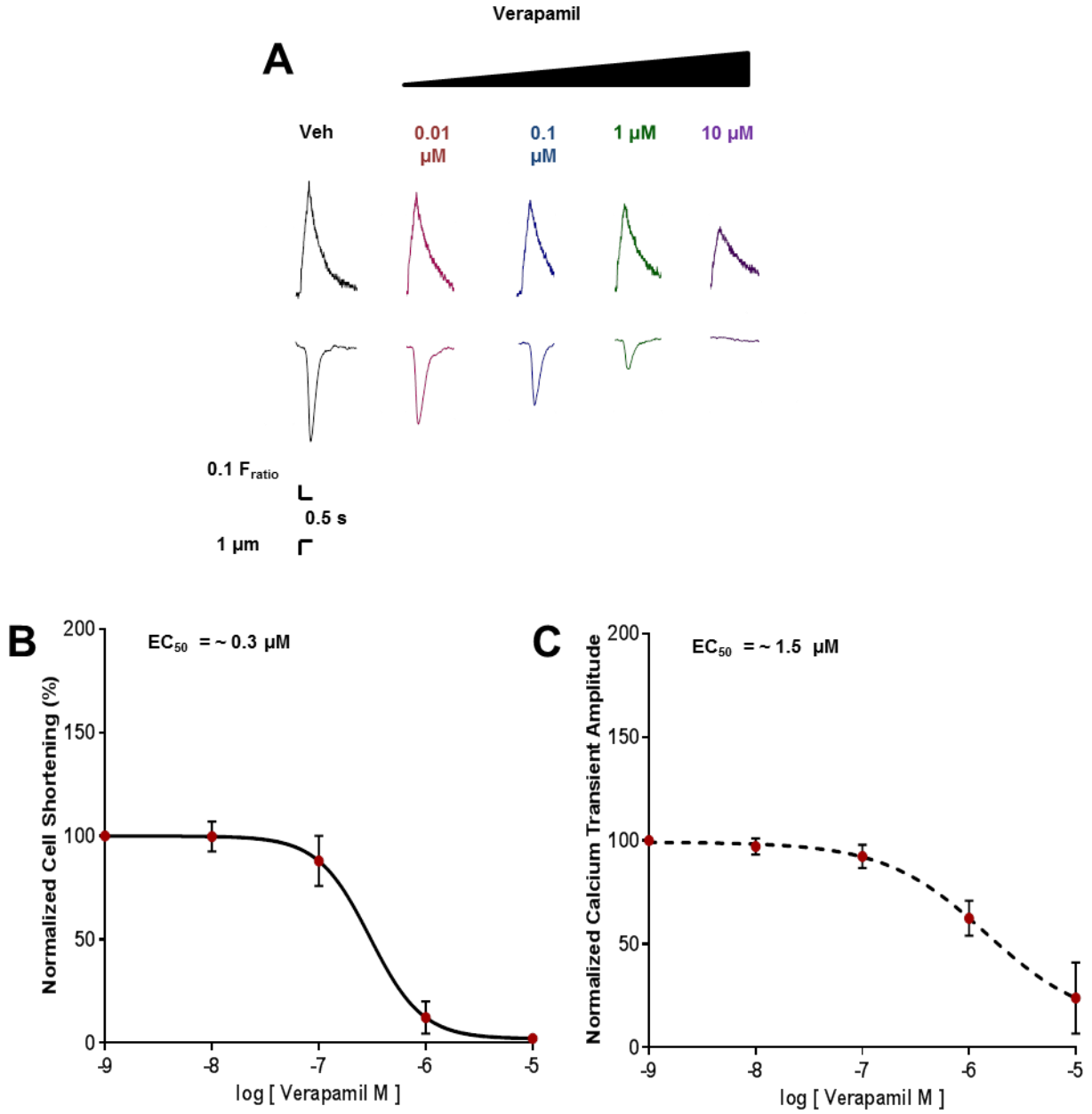

Figure 45. Verapamil pharmacological response. A, Representative calcium transients (upper panel) and contraction traces (lower panel) for hiPSC-CMs treated with Verampamil. B, Contraction and C, Calcium concentration-response curves. (Hill slope = -1.8 and -0.9 respectively). . Data show a concentration dependent decrease in cell shortening % and Ca transient amplitude in hiPSC-CMs. EC_{50}, effective concentration 50 % of max response. Veh (vehicle). (Feaster T. et al., *Circulation Research* 2015; doi: 10.1161/CIRCRESAHA.115.307580).

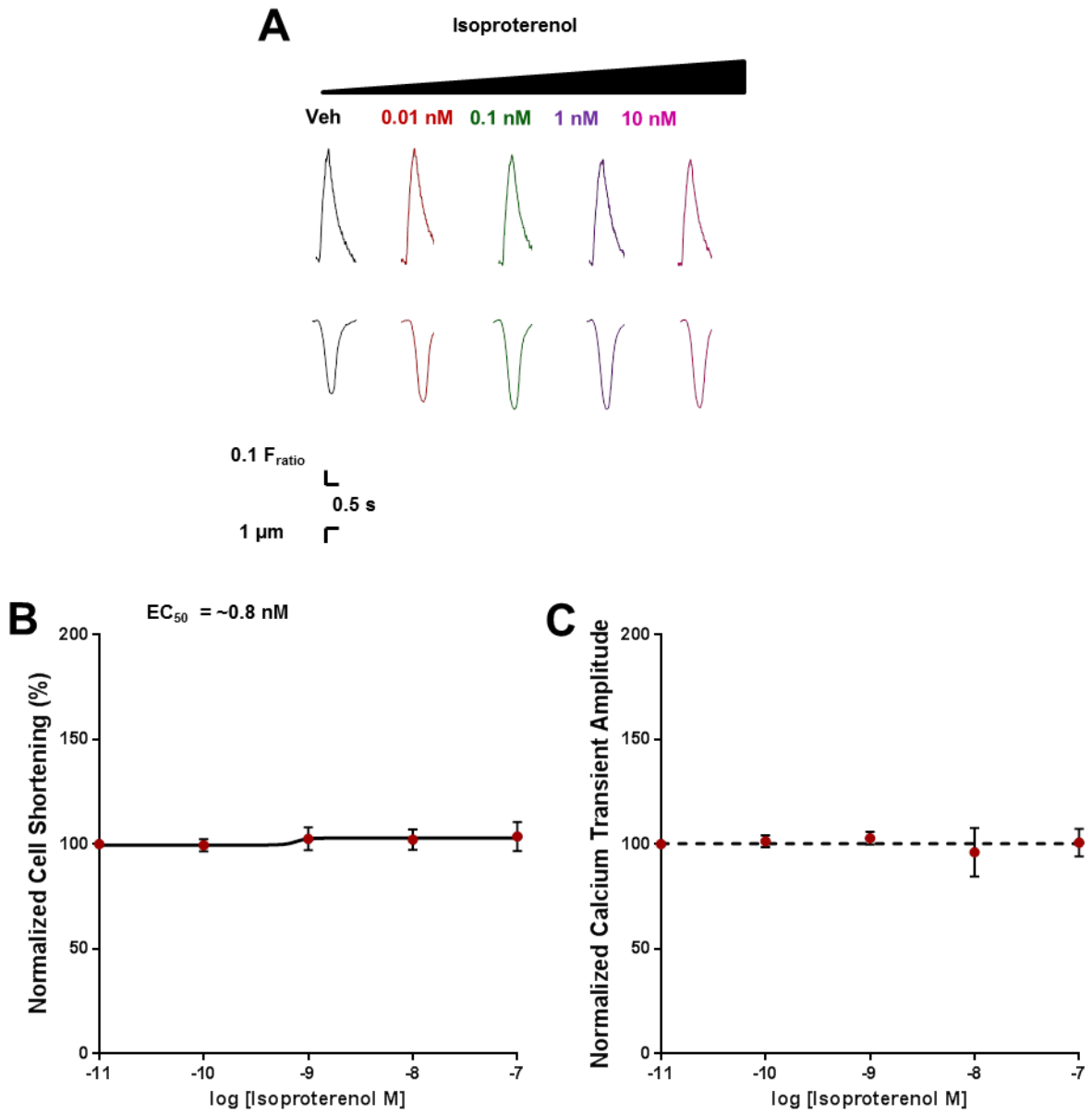

Figure 46. Isoproterenol pharmacological response. A, Representative calcium transients (upper panel) and contraction traces (lower panel) for hiPSC-CMs treated with Isoproterenol. B, Contraction (Hill slope = 8.2) and C, Calcium concentration-response curves. Isoproterenol is a β adrenergic agonist (Figure 11). Data show moderate concentration dependent increase in cell shortening % and negligible effect on Ca transient amplitude in hiPSC-CMs. EC_{50}, effective concentration 50 % of max response. Veh (vehicle).

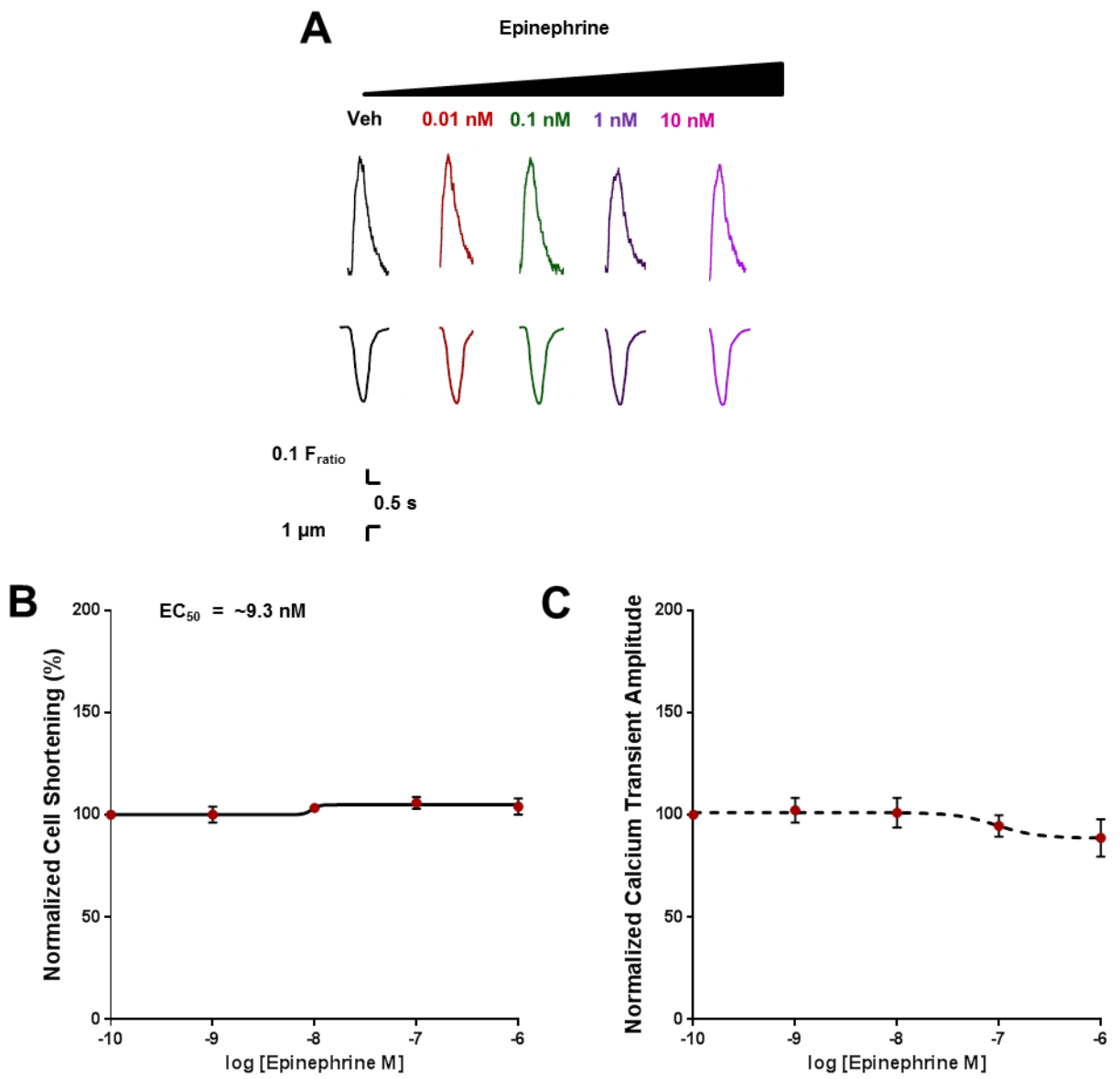

Figure 47. Epinephrine pharmacological response. A, Representative calcium transients (upper panel) and contraction traces (lower panel) for hiPSC-CMs treated with Epinephrine. B, Contraction (Hill slope = 11.3) and C, Calcium (Hill slope = -2.2) concentration-response curves. Epinephrine is a nonselective adrenergic agonist. In adult CMs Epinephrine increases Ca transient amplitude and contractile response. Data show moderate concentration dependent increase in cell shortening % and a concentration dependent decreased in Ca transient amplitude, at high test concentrations, in hiPSC-CMs. EC_{50}, effective concentration 50 % of max response. Veh (vehicle).

Hysteresis loop and contractile efficiency

To get a more detailed view of the interaction between intracellular Ca and contraction and obtain a measure of the myofilament responsiveness (i.e., Ca sensitive) we re-plotted the data obtained from our Ca handling analysis and contractility analysis [46] as hysteresis loops (Figure 48). To obtain these loops the cell shortening amplitude was normalized and plotted as a function of the normalized Ca transient amplitude. A diagram of such is depicted in (Figure 32), a contraction-Ca loops, provide yet another dimension of the EC coupling analysis in CMs. The counter-clockwise loop, similar to the pressure-volume loop relationship, can provide insight into potential mechanisms including potential compound liabilities [46]. When plotted as hysteresis loops the contractile function of pharmacological interventions or disease states can be assessed by alteration in the loop shape and location. For instance, increasing extracellular Ca (Figure 48 A) results in upward shift and increased loop area suggests improved contractile function. While treatment with Verapamil, L-type Ca channel blocker (Figure 48 C) results in downward shift and smaller loop area which suggests reduced contractile function. Treatment with the myofilament Ca sensitizer, EMD57033, results in increased loop area, and upward leftward shift suggest increased contractile function (Figure 48 B). In addition the mechanism of EMD57033 (i.e, myofilament Ca sensitizer), can be seen by the increased cell shortening at any given Ca concentrations, that is more contraction for less Ca (Figure 48 B). Treatment with the β-adrenergic receptor agonist Isoproterenol results in an upward shift and an increased loop area suggesting enhanced contractile function. These results represent the first of its kind in single hiPSC-CMs and demonstrate the utility of implementation of the Matrigel mattress and hysteresis loops analysis to provide an enhanced data set for drug screening and mechanistic assessment.

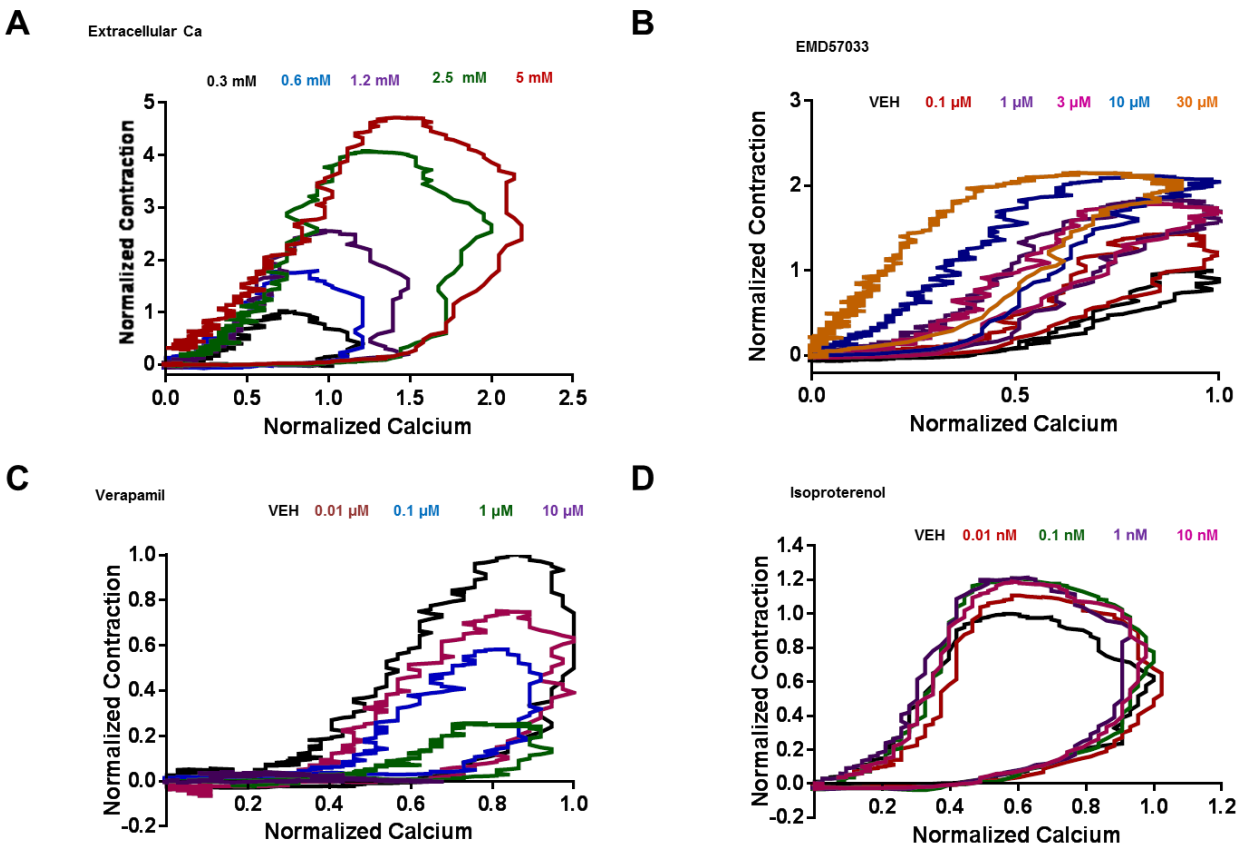

Figure 48. hiPSC-CM hysteresis loops. A, Extracellular Ca hysteresis loop, normalized peak cell shortening amplitude is plotted as a function of normalized peak Ca transient amplitude. Data show upward shift of the loop (Positive inotrope). Data are transformed from (Figure 44). B, EMD57033 hysteresis loop, normalized peak cell shortening amplitude is plotted as a function of normalized peak Ca transient amplitude. Data show upward left shift of the loop (Ca sensitizer). Data are transformed from (Figure 43). C Verapamil hysteresis loop, normalized peak cell shortening amplitude is plotted as a function of normalized peak Ca transient amplitude. Data show downward shift of the loop (Negative inotrope). Data are transformed from (Figure 45). Isoproterenol hysteresis loop, normalized peak cell shortening amplitude is plotted as a function of normalized peak Ca transient amplitude. Data show upward shift of the loop (Positive inotrope). Data are transformed from (Figure 46). Veh (Vehicle). A-D, Y-axis is set to different scale to illustrate the differences in hysteresis loop morphology.

Discovery of a novel inotrope for heart failure

EHF1 increases contractility and rates in hiPSC-CMs

EHF1 was originally identified as a potential hit in a zebrafish HTS screening assay. With the establishment of the Matrigel mattress method we assessed EHF1 inotropic potential in hiPSC-CMs. Treatment of hiPSC-CMs with EHF1 (10 µM) resulted in significantly increased contractility (i.e., cell shortening) (Figure 49 A and B) compared to vehicle treatments. In addition EHF1 results in significantly faster contraction rate and markedly increased relaxation rate (Figure 49 B). Therefore with the implementation of the mattress platform we identify a novel inotrope with efficacy in human CMs.

EHF1 has negligible effect on Ca handling in hiPSC-CMs

To determine a potential mechanism for the EHF1 inotropic effect I evaluated the effect of EHF1 on hiPSC-CM Ca handling properties. hiPSC-CMs were loaded with Fura-2 and exposed to EHF1 (10 µM) and Ca handling assessed. In contrast to the contractile response, I found EHF1 has negligible effect on hiPSC-CM Ca handling and kinetics (Figure 50) resulting in no significant change on Ca handling parameters. To investigate the chronotropic effect of EHF1 I treated hiPSC-CMs with EHF1 10 µM and evaluated beat rate. I found that EHF1 had no effect on hiPSC-CM heart rate (Figure 51) relative to vehicle treated control, in contrast to the traditional chronotrope Isoproterenol that significantly increased beat rate in hiPSC-CMs (Figure 51).

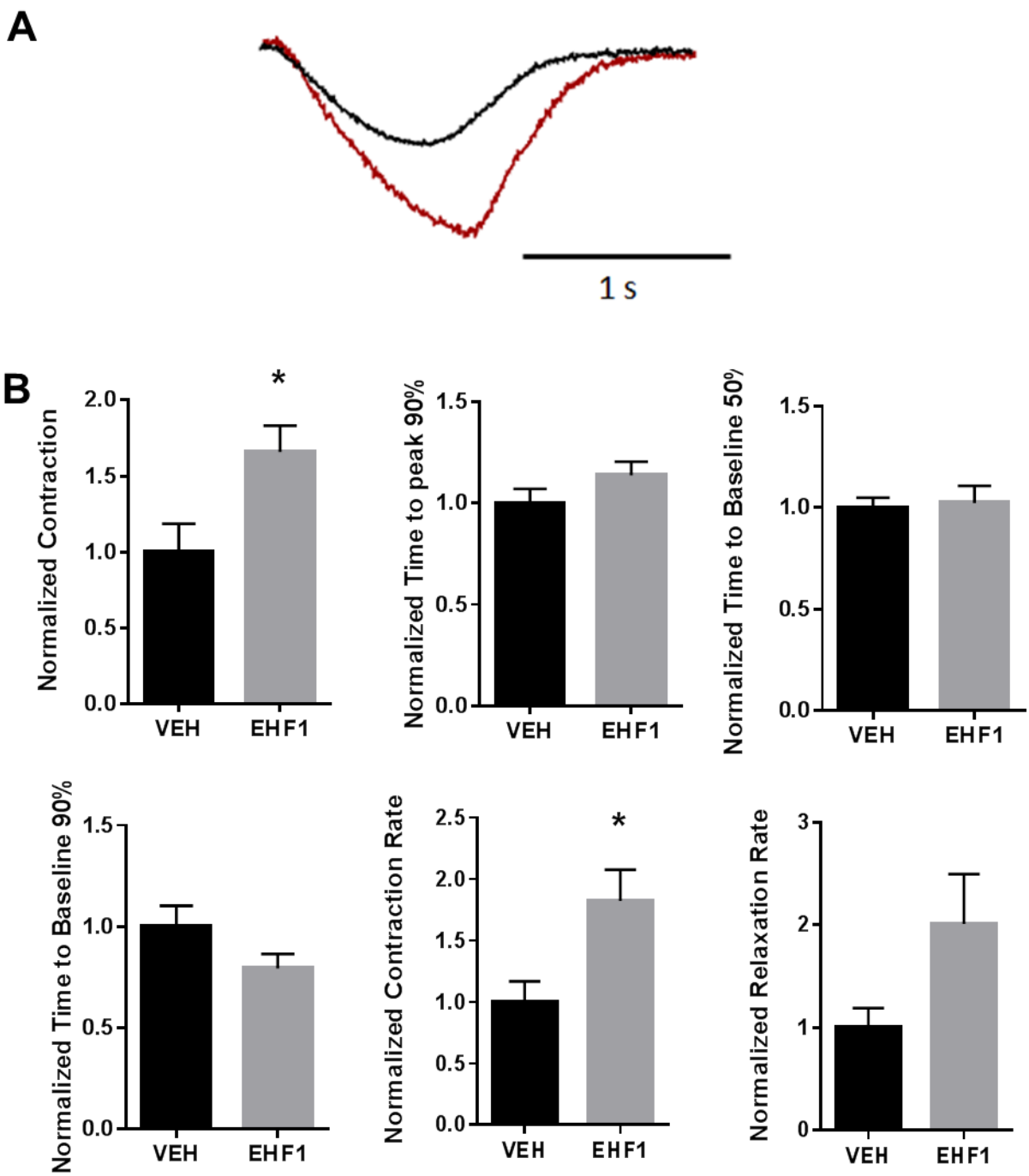

Figure 49. EHF1 contractile response. A, Representative contraction trace for hiPSC-CM treated with vehicle (black) and EHF1 (red) [10μM]. B, Data are mean ± SEM. n = 16. *P<0.05 vs vehicle (VEH). Data show EHF1 significantly increases maximum contraction and contraction rate in hiPSC-CMs.

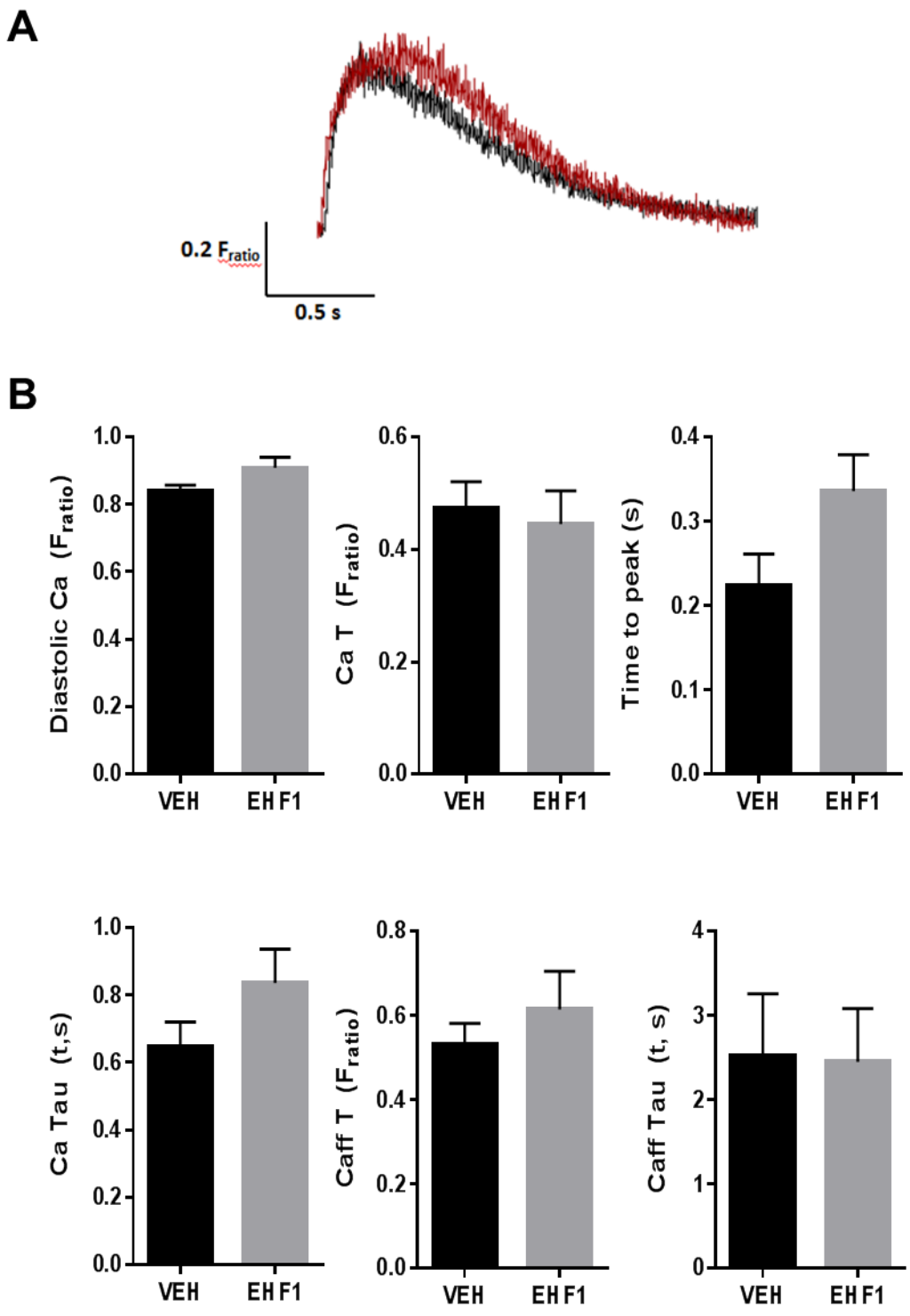

Figure 50. EHF1 Ca handling properties. A, Representative Ca twitch transients for hiPSC-CM treated with vehicle (black) and EHF1 (red) [10µM]. B, Summary data mean ± SEM. n=9 -10 per group. *P<0.05 vs vehicle (VEH). Data show EHF1 has negligible effect on hiPSC-CMs twitch Ca transient parameters.

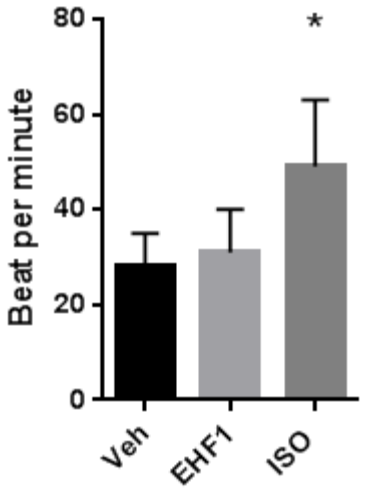

Figure 51. Chronotropic response. Beat rate analysis for hiPSC-CMs treated with EHF1 [10 µM], β-adrenergic agonist Isoproterenol (ISO) [10 µM], and vehicle (Veh). N=6 – 8 per group. **P*<0.05 vs vehicle (VEH). Graph shows EHF1 has negligible effect on beat rate in hiPSC-CMs. And the positive chronotrope, Isoproterenol, significantly increases beat rate in hiPSC-CMs.

4.5 Discussion

Despite recent medical advances, the HF prognosis remains poor with over 50% mortality within 5 years of diagnosis. Currently, apart from orthotopic heart transplantation (OHT) and mechanical left ventricular assist device (LVAD), treatment options are largely palliative. Moreover, neither OHT nor LVAD comes remotely close to meeting this unmet medical need, and both are associated with significant morbidity and mortality. To exacerbate the situation, there have been few drugs approved for treatment of systolic heart failure in the past decades, and with recent costly and spectacular failures. This is thought to be in part because of the lack of human CM for drug screening and toxicology assessment.

Here, I demonstrate hiPSC-CMs may meet this unmet need. I demonstrate hiPSC-CMs represent a valuable *in vitro* human CM source for drug screening and cardiotoxicity. Major findings are: 1) implementation of the Matrigel mattress enables simultaneous assessment of contractile and Ca response to pharmacological agents in single hiPSC-CM (Figure 44 A). 2) hiPSC-CMs respond appropriately to pharmacological stimuli and are amenable to concentration response curves and EC_{50} (Figure 45 B and C). 3) I demonstrate for the first time single hiPSC-CMs respond appropriately to myofilament Ca sensitizers; this finding would be difficult to observe on standard culture substrates (Figure 43). 4) Addition of hysteresis loop analysis enables detailed assessment of potential mechanisms in hiPSC-CMs (Figure 48). 5) We identify EHF1 as a novel inotrope using hiPC-CMs as a model (Figure 49).

In critically ill patients with end-stage heart failure, positive inotropes like milrinone and dobutamine are invaluable to augment function of failing heart in the intensive care unit setting. However, long-term administration of inotropes is limited by drug tolerance, and increased risk of arrhythmia, heart failure progression and death. The underlying mechanism is thought to be negative feedback regulation of chronic adrenergic stimulation, chronic cAMP elevation and alterations in Ca handling. Given these issues, there is presently an unmet need for novel

drugs that enhance heart function without the adverse effects of the currently available medications. These data suggest EHF1 class of compounds may be useful in this effort. Importantly, unlike adrenergic agonists, EHF1 increases contraction (Figure 49) without increasing heart rate (Figure 51). Moreover, EHF1 does not lead to alterations in intracellular Ca handling in hiPSC-CMs (Figure 50) which may alleviate abnormal pathological Ca handling properties.

Limitations

These experiments were performed in spontaneously beating hiPSC-CMs and may overlook consequences of different cycle lengths on hiPSC-CM function. Likewise, all experiments were performed at room temperature; it will be interesting to see if physiologic temperatures enhance key findings. The lack of robust inotropic contractile and Ca amplitude response to β-adrenergic receptor agonists is in contrast to expected results in adult-CMs. This suggests that while I provide evidence for maturation of key aspects of hiPSC-CMs work still needs to be done to achieve the adult phenotype.

Chapter 5

CONCLUSIONS

Although promising, the full potential of hiPSC-CMs has yet to be revealed. After the initial excitement surrounding the discovery of hiPSC-CM, researchers had begun transplanting hPSC-CM into animal models (e.g., non-human primates) post infarct, before an in-depth understanding of hiPSC-CM EC coupling properties have been established. While preliminary results from these studies appear promising as assessed by successful engraftment, re-muscularization and perfusion by host vasculature [53], there remains the looming issue of the increased arrhythmic events in these studies. For this reason the main focus in the stem cell field has been to develop strategies to generate more mature hiPSC-CMs. To model human heart *in vitro* and to also withstand proper engraftment and physiological performance for cell therapies and heart regeneration. As a first step in this effort I set out to define the EC coupling properties of normal hiPSC-CMs, providing a foundation for future applications including transplantation.

Here, I characterize the EC coupling properties of normal hiPSC-CMs **(Chapter 2)** specifically focusing on electrophysiological properties and Ca handling properties and develop a novel culture method to assess hiPSC-CM contractile properties. Our studies of normal hiPSC-CM demonstrate hiPSC-CMs exhibit relatively mature EC coupling properties which are comparable between hiPSC-CMs generated at different institutions and that of adult-CMs studied under identical experimental conditions. Of note, our results that hiPSC-CM EC coupling properties are consistent across hiPSC-CMs recovered from cryopreservation enables standardization of hiPSC-CM use for basic science and drug discovery, as well as large scale studies (i.e., > one billion hiPSC-CMs) necessary for human transplantation. To the best of our

knowledge this represents the first systematic characterization of hiPSC-CM EC coupling properties.

While I demonstrate many aspects of hiPSC-CM EC coupling are comparable to adult CMs it is important to note that these are *not* adult CM, this is demonstrated structurally by our morphological studies showing hiPSC-CMs are underdeveloped (i.e., smaller) relative to adult CMs and functionally in electrophysiological analysis by their reduced upstroke velocity and lack of the notch in the action potential morphology and in Ca handling studies by decreased Ca decay rate. Future studies will incorporate and assess EC coupling in single hiPSC-CMs generated using a combination of approaches that further increase hiPSC-CM maturity (e.g., 2D patterning [54], electrical stimulation [55] and 3D culture methods [56]). For example, Rao et al. reported a faster time to peak and improved SR function of hiPSC-CMs cultured on micropatterned substrates compared to unstructured polydimethylsiloxane membranes [54].

I further demonstrate utility of hiPSC-CMs for disease modeling **(Chapter 3)** and recapitulate previous sarcomeric cardiomyopathy findings in hiPSC-CMs, supporting the reproducibility of this model for disease modeling. In addition I provide mechanistic insight for altered function of HCM hiPSC-CMs. For example, I provide evidence that HCM hiPSC-CMs display altered twitch Ca removal and increased Ca sensitivity supporting an increased Ca affinity hypothesis. Moreover, with the implementation of the mattress culture method I elucidate previously undiscovered contractile defects, myofilament sensitivity defects and arrhythmic abnormalities of diseased hiPSC-CMs, at the single cell level. While promising, these studies do not assess the hiPSC-CM cytosolic Ca buffering properties. For instance, it is well accepted that cytoplasmic binding sites such as troponin C play a significant role in buffering cytosolic Ca. And changes in Ca buffering, or Ca affinity, may lead to alterations of twitch Ca handling properties and ultimately contractile properties resulting in pathological consequence. Future studies will assess the physiological consequences of the RCM troponin I mutation on altered Ca

sensitivity by implementation of the Matrigel mattress and hysteresis loop analysis, as above. Toward that end we are currently evaluating the Ca buffering properties of diseased hiPSC-CMs presented here.

With the addition of pharmacological analysis **(Chapter 4)** I show normal hiPSC-CMs demonstrate appropriate responses to known pharmacological compounds that modulate EC coupling, for example modulation of extracellular Ca (e.g., verapamil) as well as myofilament Ca sensitizers such as EMD57033. Future studies using our novel contractility platform will be focused on defining hiPSC-CM pharmacological responses to large panel of known agents, including EC_{50} values and compare these results to those obtained for adult animal CMs (e.g., rabbit-CM) studied under identical experimental conditions. Moreover, in their current form, I demonstrate utility of hiPSC-CMs for identifying novel inotropic compounds such as EHF1. Future studies will determine the relevant physiological target of EHF1 inotropic effect in hiPSC-CM. In addition to miniaturization of the Matrigel mattress for high throughput screening of novel cardioactive compounds.

APPENDIX

Table A-1 qRT-PCR Primers and Descriptions

Primers	Description for Primers	Primers	Description for Primers
18S-Hs99999901_s1	Eukaryotic 18S rRNA	KCNE4-Hs01851577_s1	potassium voltage-gated channel, Isk-related family, member 4
ITGA1-Hs00235006_m1	integrin, alpha 1	SCN5A-Hs00165693_m1	sodium channel, voltage-gated, type V, alpha subunit
ITGA2-Hs00158127_m1	integrin, alpha 2 (CD49B, alpha 2 subunit of VLA-2 receptor)	ATP2A2-Hs00544877_m1	ATPase, Ca++ transporting, cardiac muscle, slow twitch 2
ITGA3-Hs01076873_m1	integrin, alpha 3 (antigen CD49C, alpha 3 subunit of VLA-3 receptor)	PLN-Hs01848144_s1	phospholamban
ITGA4-Hs00168433_m1	integrin, alpha 4 (antigen CD49D, alpha 4 subunit of VLA-4 receptor)	RYR2-Hs00892883_m1	ryanodine receptor 2 (cardiac)
ITGA5-Hs01547673_m1	integrin, alpha 5 (fibronectin receptor, alpha polypeptide)	SNTA1-Hs00162045_m1	syntrophin, alpha 1
ITGA6-Hs01041011_m1	integrin, alpha 6	SGCA-Hs01033510_g1	sarcoglycan, alpha (50kDa dystrophin-associated glycoprotein)
ITGA7-Hs00174397_m1	integrin, alpha 7	NRAP-Hs00328987_m1	nebulin-related anchoring protein
ITGA8-Hs00233321_m1	integrin, alpha 8	NMRK2-Hs01043681_m1	nicotinamide riboside kinase 2
ITGA9-Hs00979865_m1	integrin, alpha 9	ITGB1BP2-Hs00183746_m1	integrin beta 1 binding protein (melusin) 2
ITGA11-Hs00201927_m1	integrin, alpha 11	DES-Hs00157258_m1	desmin
ITGAV-Hs00233790_m1	integrin, alpha V	MYOM2-Hs00187676_m1	myomesin 2
ITGB1-Hs00559595_m1	integrin, beta 1 (fibronectin receptor, beta polypeptide, antigen CD29 includes MDF2, MSK12)	MYOZ2-Hs00213216_m1	myozenin 2
ITGB3-Hs01001478_m1	integrin, beta 3 (platelet glycoprotein IIIa, antigen CD61)	CKMT2-Hs00176502_m1	creatine kinase, mitochondrial 2 (sarcomeric)
ITGB4-Hs00174009_m1	integrin, beta 4	NOS1-Hs00167223_m1	nitric oxide synthase 1 (neuronal)
ITGB5-Hs00174435_m1	integrin, beta 5	SGCG-Hs01062335_m1	sarcoglycan, gamma (35kDa dystrophin-associated glycoprotein)
TNNI3-Hs00165957_m1	troponin I type 3 (cardiac)	IRX4-Hs00212560_m1	iroquois homeobox 4
ACTN2-Hs00153809_m1	actinin, alpha 2	SLN-Hs01888464_s1	sarcolipin
MYH7-Hs01110632_m1	myosin, heavy chain 7, cardiac muscle, beta	FHL2-Hs00179935_m1	four and a half LIM domains 2
MYH6-Hs01101425_m1	myosin, heavy chain 6, cardiac muscle, alpha	HEY2-Hs00232622_m1	hairy/enhancer-of-split related with YRPW motif 2
DMD-Hs00758098_m1	dystrophin	NR2F2-Hs00819630_m1	nuclear receptor subfamily 2, group F, member 2
TNNI1-Hs00913333_m1	troponin I type 1 (skeletal, slow)	MYL7-Hs00221909_m1	myosin, light chain 7, regulatory
CASQ2-Hs00154286_m1	calsequestrin 2 (cardiac muscle)	MYL2-Hs00166405_m1	myosin, light chain 2, regulatory, cardiac, slow
KCNQ1-Hs00923522_m1	potassium voltage-gated channel, KQT-like subfamily, member 1		

Table A-1. qRT-PCR primers and descriptions. qRT-PCR primers used for Matrigel mattress molecular profiling (Figure 27 and Figure A-1).

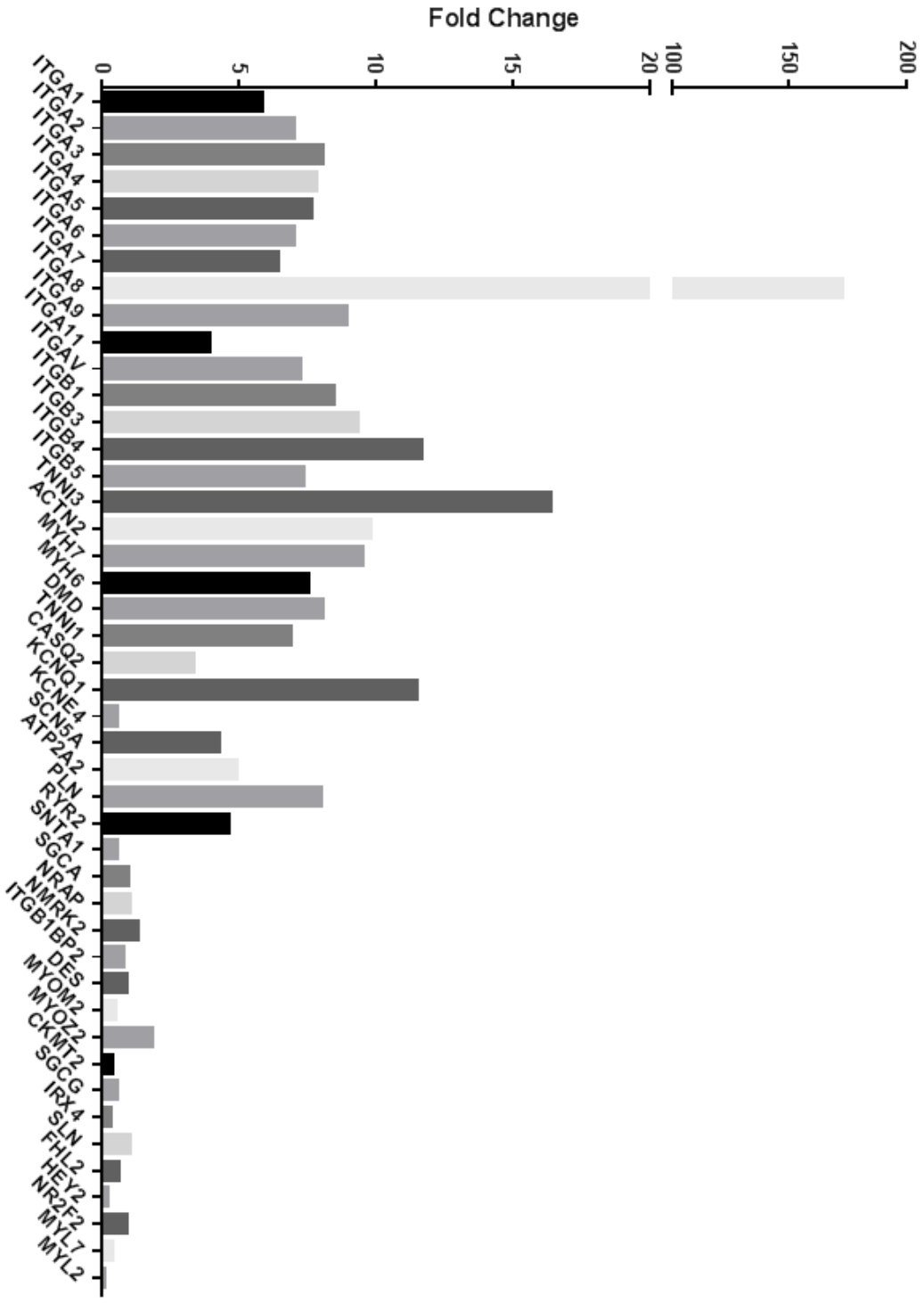

Figure A-1. Matrigel mattress qRT-PCR screen. Data are presented as fold change as above (Figure 27). Day 30-35 mattress and control hiPSC-CM transcripts were normalized to housekeeping gene 18S rRNA. Data show differential molecular profile of Matrigel mattress hiPSC-CMs after 5 days of culture on the Matrigel mattress.. Courtesy of Mr. Adrian C Gadar.

REFERENCES

[1] Jafri MS. Models of excitation-contraction coupling in cardiac ventricular myocytes. Methods Mol Biol. 2012;910:309-35.

[2] George AL. Molecular and genetic basis of sudden cardiac death. J Clin Invest. 2013;123:75-83.

[3] Bers DM. Cardiac excitation-contraction coupling. Nature. 2002;415:198-205.

[4] Fearnley CJ, Roderick HL, Bootman MD. Calcium signaling in cardiac myocytes. Cold Spring Harb Perspect Biol. 2011;3:a004242.

[5] Takahashi K, Okita K, Nakagawa M, Yamanaka S. Induction of pluripotent stem cells from fibroblast cultures. Nat Protoc. 2007;2:3081-9.

[6] Yu J, Vodyanik MA, Smuga-Otto K, Antosiewicz-Bourget J, Frane JL, Tian S, et al. Induced pluripotent stem cell lines derived from human somatic cells. Science. 2007;318:1917-20.

[7] Thomson JA, Itskovitz-Eldor J, Shapiro SS, Waknitz MA, Swiergiel JJ, Marshall VS, et al. Embryonic stem cell lines derived from human blastocysts. Science. 1998;282:1145-7.

[8] Laflamme MA, Chen KY, Naumova AV, Muskheli V, Fugate JA, Dupras SK, et al. Cardiomyocytes derived from human embryonic stem cells in pro-survival factors enhance function of infarcted rat hearts. Nat Biotechnol. 2007;25:1015-24.

[9] Zhang J, Klos M, Wilson GF, Herman AM, Lian X, Raval KK, et al. Extracellular matrix promotes highly efficient cardiac differentiation of human pluripotent stem cells: the matrix sandwich method. Circ Res. 2012;111:1125-36.

[10] Burridge PW, Matsa E, Shukla P, Lin ZC, Churko JM, Ebert AD, et al. Chemically defined generation of human cardiomyocytes. Nat Methods. 2014;11:855-60.

[11] Yang X, Pabon L, Murry CE. Engineering adolescence: maturation of human pluripotent stem cell-derived cardiomyocytes. Circ Res. 2014;114:511-23.

[12] Sun N, Yazawa M, Liu J, Han L, Sanchez-Freire V, Abilez OJ, et al. Patient-specific induced pluripotent stem cells as a model for familial dilated cardiomyopathy. Sci Transl Med. 2012;4:130ra47.

[13] Lan F, Lee AS, Liang P, Sanchez-Freire V, Nguyen PK, Wang L, et al. Abnormal calcium handling properties underlie familial hypertrophic cardiomyopathy pathology in patient-specific induced pluripotent stem cells. Cell Stem Cell. 2013;12:101-13.

[14] Bedada FB, Chan SS, Metzger SK, Zhang L, Zhang J, Garry DJ, et al. Acquisition of a quantitative, stoichiometrically conserved ratiometric marker of maturation status in stem cell-derived cardiac myocytes. Stem Cell Reports. 2014;3:594-605.

[15] Zhang GQ, Wei H, Lu J, Wong P, Shim W. Identification and characterization of calcium sparks in cardiomyocytes derived from human induced pluripotent stem cells. PLoS One. 2013;8:e55266.

[16] Liu J, Fu JD, Siu CW, Li RA. Functional sarcoplasmic reticulum for calcium handling of human embryonic stem cell-derived cardiomyocytes: insights for driven maturation. Stem Cells. 2007;25:3038-44.

[17] Dolnikov K, Shilkrut M, Zeevi-Levin N, Gerecht-Nir S, Amit M, Danon A, et al. Functional properties of human embryonic stem cell-derived cardiomyocytes: intracellular Ca2+ handling and the role of sarcoplasmic reticulum in the contraction. Stem Cells. 2006;24:236-45.

[18] Eschenhagen T, Mummery C, Knollmann BC. Modelling sarcomeric cardiomyopathies in the dish: from human heart samples to iPSC cardiomyocytes. Cardiovasc Res. 2015;105:424-38.

[19] Hayakawa T, Kunihiro T, Ando T, Kobayashi S, Matsui E, Yada H, et al. Image-based evaluation of contraction-relaxation kinetics of human-induced pluripotent stem cell-derived cardiomyocytes: Correlation and complementarity with extracellular electrophysiology. J Mol Cell Cardiol. 2014;77:178-91.

[20] Liu J, Sun N, Bruce MA, Wu JC, Butte MJ. Atomic force mechanobiology of pluripotent stem cell-derived cardiomyocytes. PLoS One. 2012;7:e37559.

[21] Ahola A, Kiviaho AL, Larsson K, Honkanen M, Aalto-Setälä K, Hyttinen J. Video image-based analysis of single human induced pluripotent stem cell derived cardiomyocyte beating dynamics using digital image correlation. Biomed Eng Online. 2014;13:39.

[22] Lundy SD, Zhu WZ, Regnier M, Laflamme MA. Structural and functional maturation of cardiomyocytes derived from human pluripotent stem cells. Stem Cells Dev. 2013;22:1991-2002.

[23] Hwang HS, Kryshtal DO, Feaster TK, Sánchez-Freire V, Zhang J, Kamp TJ, et al. Comparable calcium handling of human iPSC-derived cardiomyocytes generated by multiple laboratories. J Mol Cell Cardiol. 2015;85:79-88.

[24] Feaster TK, Cadar AG, Wang L, Williams CH, Chun YW, Hempel J, et al. Matrigel Mattress: A Method for the Generation of Single Contracting Human-Induced Pluripotent Stem Cell-Derived Cardiomyocytes. Circ Res. 2015.

[25] Takahashi K, Yamanaka S. Induction of pluripotent stem cells from mouse embryonic and adult fibroblast cultures by defined factors. Cell. 2006;126:663-76.

[26] Knollmann BC. Induced pluripotent stem cell-derived cardiomyocytes: boutique science or valuable arrhythmia model? Circulation research. 2013;112:969-76; discussion 76.

[27] Yamanaka S. Strategies and new developments in the generation of patient-specific pluripotent stem cells. Cell Stem Cell. 2007;1:39-49.

[28] Lee YK, Ng KM, Lai WH, Chan YC, Lau YM, Lian Q, et al. Calcium homeostasis in human induced pluripotent stem cell-derived cardiomyocytes. Stem Cell Rev. 2011;7:976-86.

[29] O'Rourke B, Kass DA, Tomaselli GF, Kääb S, Tunin R, Marbán E. Mechanisms of altered excitation-contraction coupling in canine tachycardia-induced heart failure, I: experimental studies. Circ Res. 1999;84:562-70.

[30] Pogwizd SM, Qi M, Yuan W, Samarel AM, Bers DM. Upregulation of Na(+)/Ca(2+) exchanger expression and function in an arrhythmogenic rabbit model of heart failure. Circ Res. 1999;85:1009-19.

[31] Itzhaki I, Rapoport S, Huber I, Mizrahi I, Zwi-Dantsis L, Arbel G, et al. Calcium handling in human induced pluripotent stem cell derived cardiomyocytes. PLoS One. 2011;6:e18037.

[32] Liang P, Lan F, Lee AS, Gong T, Sanchez-Freire V, Wang Y, et al. Drug screening using a library of human induced pluripotent stem cell-derived cardiomyocytes reveals disease-specific patterns of cardiotoxicity. Circulation. 2013;127:1677-91.

[33] Sharma A, Marceau C, Hamaguchi R, Burridge PW, Rajarajan K, Churko JM, et al. Human induced pluripotent stem cell-derived cardiomyocytes as an in vitro model for coxsackievirus B3-induced myocarditis and antiviral drug screening platform. Circ Res. 2014;115:556-66.

[34] Yang T, Chun YW, Stroud DM, Mosley JD, Knollmann BC, Hong C, et al. Screening for Acute IKr Block Is Insufficient to Detect Torsades de Pointes Liability: Role of Late Sodium Current. Circulation. 2014;130:224-34.

[35] Yu J, Hu K, Smuga-Otto K, Tian S, Stewart R, Slukvin II, et al. Human induced pluripotent stem cells free of vector and transgene sequences. Science. 2009;324:797-801.

[36] Okita K, Matsumura Y, Sato Y, Okada A, Morizane A, Okamoto S, et al. A more efficient method to generate integration-free human iPS cells. Nat Methods. 2011;8:409-12.

[37] Sanchez-Freire V, Lee AS, Hu S, Abilez OJ, Liang P, Lan F, et al. Effect of human donor cell source on differentiation and function of cardiac induced pluripotent stem cells. J Am Coll Cardiol. 2014;64:436-48.

[38] Knollmann BC, Chopra N, Hlaing T, Akin B, Yang T, Ettensohn K, et al. Casq2 deletion causes sarcoplasmic reticulum volume increase, premature Ca2+ release, and catecholaminergic polymorphic ventricular tachycardia. The Journal of clinical investigation. 2006;116:2510-20.

[39] Chun YW, Balikov DA, Feaster TK, Williams CH, Sheng CC, Lee JB, et al. Combinatorial polymer matrices enhance in vitro maturation of human induced pluripotent stem cell-derived cardiomyocytes. Biomaterials. 2015;67:52-64.

[40] Knollmann BC, Knollmann-Ritschel BE, Weissman NJ, Jones LR, Morad M. Remodelling of ionic currents in hypertrophied and failing hearts of transgenic mice overexpressing calsequestrin. J Physiol. 2000;525 Pt 2:483-98.

[41] Hazeltine LB, Simmons CS, Salick MR, Lian X, Badur MG, Han W, et al. Effects of substrate mechanics on contractility of cardiomyocytes generated from human pluripotent stem cells. Int J Cell Biol. 2012;2012:508294.

[42] Himmel HM. Drug-induced functional cardiotoxicity screening in stem cell-derived human and mouse cardiomyocytes: effects of reference compounds. J Pharmacol Toxicol Methods. 2013;68:97-111.

[43] Li X, Tsai P, Wieder ED, Kribben A, Van Putten V, Schrier RW, et al. Vascular smooth muscle cells grown on Matrigel. A model of the contractile phenotype with decreased activation of mitogen-activated protein kinase. J Biol Chem. 1994;269:19653-8.

[44] Ribeiro MC, Tertoolen LG, Guadix JA, Bellin M, Kosmidis G, D'Aniello C, et al. Functional maturation of human pluripotent stem cell derived cardiomyocytes in vitro--correlation between contraction force and electrophysiology. Biomaterials. 2015;51:138-50.

[45] Westfall MV, Albayya FP, Metzger JM. Functional analysis of troponin I regulatory domains in the intact myofilament of adult single cardiac myocytes. J Biol Chem. 1999;274:22508-16.

[46] Butler L, Cros C, Oldman KL, Harmer AR, Pointon A, Pollard CE, et al. Enhanced characterization of contractility in cardiomyocytes during early drug safety assessment. Toxicol Sci. 2015;145:396-406.

[47] Roderick HL, Knollmann BC. Inositol 1,4,5-trisphosphate receptors: "exciting" players in cardiac excitation-contraction coupling? Circulation. 2013;128:1273-5.

[48] Pugsley MK, Curtis MJ. Safety pharmacology in focus: new methods developed in the light of the ICH S7B guidance document. J Pharmacol Toxicol Methods. 2006;54:94-8.

[49] Chen G, Li S, Karakikes I, Ren L, Chow MZ, Chopra A, et al. Phospholamban as a crucial determinant of the inotropic response of human pluripotent stem cell-derived ventricular cardiomyocytes and engineered 3-dimensional tissue constructs. Circ Arrhythm Electrophysiol. 2015;8:193-202.

[50] Wu H, Lee J, Vincent LG, Wang Q, Gu M, Lan F, et al. Epigenetic Regulation of Phosphodiesterases 2A and 3A Underlies Compromised β-Adrenergic Signaling in an iPSC Model of Dilated Cardiomyopathy. Cell Stem Cell. 2015;17:89-100.

[51] Harmer AR, Abi-Gerges N, Morton MJ, Pullen GF, Valentin JP, Pollard CE. Validation of an in vitro contractility assay using canine ventricular myocytes. Toxicol Appl Pharmacol. 2012;260:162-72.

[52] Williams CH, Hempel JE, Hao J, Frist AY, Williams MM, Fleming JT, et al. An in vivo chemical genetic screen identifies phosphodiesterase 4 as a pharmacological target for hedgehog signaling inhibition. Cell Rep. 2015;11:43-50.

[53] Chong JJ, Yang X, Don CW, Minami E, Liu YW, Weyers JJ, et al. Human embryonic-stem-cell-derived cardiomyocytes regenerate non-human primate hearts. Nature. 2014;510:273-7.

[54] Rao C, Prodromakis T, Kolker L, Chaudhry UA, Trantidou T, Sridhar A, et al. The effect of microgrooved culture substrates on calcium cycling of cardiac myocytes derived from human induced pluripotent stem cells. Biomaterials. 2013;34:2399-411.

[55] Chan YC, Ting S, Lee YK, Ng KM, Zhang J, Chen Z, et al. Electrical stimulation promotes maturation of cardiomyocytes derived from human embryonic stem cells. J Cardiovasc Transl Res. 2013;6:989-99.

[56] Eschenhagen T, Fink C, Remmers U, Scholz H, Wattchow J, Weil J, et al. Three-dimensional reconstitution of embryonic cardiomyocytes in a collagen matrix: a new heart muscle model system. FASEB J. 1997;11:683-94.